MULTI-PROXY ~8500 YEAR PALEOENVIRONMENTAL RECONSTRUCTION OF BAIE DES BARADÈRES, HAITI

Thesis submitted in partial fulfilment of the requirements for the degree of

Master of Science in Physical Geography

Sydney Moser, B.Sc.

Supervisors:

Dr. Matthew Peros and Dr. André Viau

Committee members:

Dr. Konrad Gajewski and Dr. Michael Sawada

Laboratory for Climate Change Research (LCC)

Department of Geography, Environment and Geomatics

Faculty of Arts

University of Ottawa

Abstract

In the Circum-Caribbean, long timescale paleoenvironmental records, which are used to establish important baseline data for climatological phenomena such as droughts, floods, and hurricanes, are rare. This project uses geological and geochemical proxies (X-Ray fluorescence core scanning data, grain-size analysis, loss on ignition) from a nine-meter-long sediment core from a coastal karst basin near Haiti's southwestern peninsula to reconstruct Holocene environmental and climatic changes in a region that is both understudied and highly sensitive to the effects of storms, sea level change, tectonics, and anthropogenic impacts. The chronology of the core is established with 4 AMS dates from terrestrial organic matter and shows continuous sedimentation from ~8500 cal BP to the present, with an abrupt increase in sedimentation rate at ~2900 cal BP. High values of Ti and Ti/Ca are associated with finer sediments in the core and indicate relatively humid conditions at ~6500 cal BP, followed by a gradual drying trend. This is consistent with data from elsewhere in the Caribbean that reflects a southward migration of the ITCZ during the early Holocene. After 2500 cal BP, a series of large and abrupt increases in Ti and Ti/Ca are associated with an influx of finer, terrestrially-derived sediment into the bay due to enhanced discharge from the nearby Baradères River, possibly as a result of short-duration shifts to wetter climate conditions, hurricane-induced precipitation, and/or prehistoric-era human settlement. Variations in silicate input (*e.g.*, K/Ti), marine productivity (*e.g.*, Ca/Ti), and redox conditions (*e.g.*, Mn/Fe) are linked to local climate changes and resulting changes in the depositional environment, while peaks in Rb/Sr and Ti/Ca could be signals for erosion related to events such as hurricanes and/or land use changes. Finally, high values of silt and clay, in conjunction with enhanced organics, Ti, Fe, K and P over the last couple centuries reflect historic-era deforestation and erosion. This study presents an excellent opportunity to further our understanding of the diverse relationships between ecosystem dymanics, climate, and anthropogenic forcings and adds to the growing inventory of paleoclimatological records in the Caribbean, improving the spatial distribution of such studies, and ultimately improving our understanding of the driving forces of both short- and long-term climate variability.

Résumé

Dans les Caraïbes, les enregistrements paléoenvironnemntales à longue échelle de temps sont utilisés pour établir des archives environnementales de base dans l'etude des phénomènes climatologiques tels que les sécheresses, les inondations et les ouragans. Cette thèse utilise des donnees indirectes (proxies) géologiques et géochimiques (e.g. données de balayage de carottes sedimentaires par fluorescence a rayon-X, analyse de la taille des grains, perte au feu) à partir d'une carotte de sédiments de neuf mètres de longueure prélevée dans un bassin karstique de la péninsule sud-ouest d'Haïti pour reconstituer les changements environnementaux et climatiques de l'Holocène. Cette region est à la fois peu étudiée et très sensible aux effets des tempêtes tropicales, aux changements du niveau de la mer, à la tectonique et aux impacts anthropiques. La chronologie est établie avec 4 dates AMS de matière organique terrestre et montre une sédimentation continue de ~8500 cal BP à présent, avec une augmentation abrupte du taux de sédimentation à ~2900 cal BP. Des valeurs élevées de Ti et Ti/Ca sont associées à des sédiments plus fins indiquent des conditions relativement humides vers ~6500 cal BP, suivies d'une tendance graduelle à l'assèchement. Ceci est cohérent avec les données provenant d'autres régions des Caraïbes qui reflètent une migration de la ZCIT vers une position plus au sud. Suivant 2500 cal BP, une série d'augmentation abruptes de Ti et Ti/Ca est associée à un influx de sédiments plus fins, d'origine terrestre, en raison d'une augmentation du débit de la rivière Baradères a proximité, suivant un changement de courte durée vers des conditions climatiques plus humides, des précipitations provoquées par des ouragans, et/ou d'un peuplement humain de l'ère préhistorique. Les variations de l'apport en silicates (K/Ti), de la productivité (Ca/Ti) et des conditions redox (Mn/Fe) sont liées aux changements climatiques locaux, tandis que les pics de Rb/Sr et Ti/Ca pourraient être des signaux d'érosion liés à des événements tels que des ouragans et/ou des changements d'utilisation des terres. Enfin, les valeurs élevées de limon et d'argile, associées à une augmentation des matières organiques, Ti, Fe, K et P au cours des deux dernières siècles, reflètent la déforestation et l'érosion de l'ère historique. Cette étude offre une excellente opportunité pour approfondir notre compréhension des diverses relations entre la dynamique des écosystèmes, le climat et les forçages anthropiques. Elle s'insere à l'inventaire croissant des enregistrements paléoclimatologiques dans les Caraïbes, améliorant la distribution spatiale ainsi que notre compréhension des forces motrices de la variabilité climatique à court et à long terme.

Acknowledgements

The work presented here would not have been possible without the support of many people. First and foremost, I am extremely grateful to my supervisors Dr. Matthew Peros and Dr. André Viau for their guidance, patience, and encouragement. Completing this thesis is my greatest accomplishment thus far and the most challenging experience I have faced, and I truly could not have done it without your advice and support. Matt, thank you for introducing me to this field which I now love, and for being both an amazing teacher, and mentor. André, thank you for being so present and reassuring through every step of this degree. I must also thank my committee members Dr. Konrad Gajewski and Dr. Michael Sawada for their thorough and insightful comments and feedback throughout the evaluation process and thesis defence.

To our research partners- Dr. Andrea Hawkes, Dr. Pete van Hengstrum, Dr. Jon Woodruff, Dr. Chris Maio, Dr. Lizzie Wallace, Dr. Jeffrey Donnelly, and the crew aboard the R/V Alucia- thank you for providing me with this opportunity to work on such important and fascinating research. Thank you especially to Jeff for meeting with us on Zoom, for coordinating and funding our radiocarbon dating, and for your advice. Thank you to Simon Pendleton and Nicole D'Entremont at NOSAMS for their support in processing samples and providing figures, photos, field notes, and contact from their lab. Thank you to Tanya O'Reilly at Bishop's University for her lab contribution to this project. This field work was funded by the U.S. National Science Foundation.

Thank you to my lab mates and colleagues, including the GGSA exec team and the many outstanding professors and support staff in the GEG department, without whose assistance and kindness I would not have been able to persevere through my degree during a global pandemic. A special thank you to Marie-Lore Beaudry, Michelle Briere, Paige Cincio, Kethra Campbell-Heaton, Hannah Ackerman, and Yulun Wu for their compassion, camaraderie, and willingness to help, whether it be with Excel, R, ArcGIS, statistics, or simply what the heck I should be doing at any given time.

Finally, thank you to friends and family who have supported and uplifted me throughout moments of uncertainty, doubt, stress, and anxiety. Shannon, Sam, my Bishop's girls, and many others, your unwavering support means to world to me. To Chris and Mina, thank you for being my rocks. And of course, to my mom and dad, Klara and Lionel, благодаря ти за всичко което направи за мен. I cannot put into words how grateful I am to have such supportive and devoted parents, who fostered my interest in science at an early age, and who always have the best advice. I'm so lucky to have this support system.

-Demi

Table of Contents

List of Figures

List of Tables

List of Acronyms

AMM	Atlantic Meridional Mode
AMO	Atlantic Multidecadal Oscillation
AMS	Accelerator Mass Spectrometry
BP	Before Present
Cal BP	Calibrated Years Before Present
CE	Common Era
CKB	Coastal Karst Basin
ENSO	El Niño–Southern Oscillation
EPGF	Enriquillo–Plantain Garden fault
GHG	Greenhouse Gas
GIA	Glacial Isostatic Adjustment
ITCZ	Intertropical Convergence Zone
kyr	1000 years
LIA	Little Ice Age
LOI	Loss on Ignition
MDR	Main Development Region
Mw	moment magnitude
MWP	Medieval Warm Period
NAO	North Atlantic Oscillation
NOSAMS	National Ocean Sciences Accelerator Mass Spectrometry
OM	Organic matter
PCA	Principal Component Analysis
RSL	Relative Sea Level
SF	Septentrional fault
SST	Sea Surface Temperature
TC	Tropical Cyclone
XRF	X-Ray Fluorescence
WHOI	Woods Hole Oceanographic Institution

CHAPTER 1:

Introduction

1.1. Thesis Format

This thesis is presented in five chapters. The first is an introduction which briefly describes the relevance of the project and presents the project research objectives. The second chapter provides an in-depth literature review summarizing the relevant published articles relating to the different components affecting the project study site. Chapter three discusses the methodology used in this project in detail, including the field methods, study site selection and appropriateness, laboratory methods, analytical and statistical methods, and a short summary of how this methodology has been applied to similar studies in the literature. The fourth chapter is a draft manuscript for a journal article. This article should be read with the caveat that this is the preliminary study of sediment core HATC1 and is based on an age-depth model of only four radiocarbon dates. It is therefore not intended to be published in its current form, but rather, will be re-drafted with additional radiocarbon dates and input from our research partners in upcoming months, before being submitted to a peer-reviewed journal. The fifth and final chapter is a summary of my research contribution to the advancement of science in the field of Paleoclimatology including conclusions, limitations, and recommendations for future work. At the end of the thesis there is a bibliography and five appendices containing supplemental data and figures.

1.2. Context and Background

Throughout the Holocene, island ecosystems in the Circum-Caribbean have faced various levels of stress relating to human population dynamics, climatological forcings and their variability, and sea level changes (Castilla-Beltrán et al., 2020). These ecosystems and their inhabitants (especially those in coastal settings) face increasing risk in upcoming decades and centuries due to global warming, sea level rise, and landscape transformations resulting in habitat loss (Rick et al., 2013). Haiti is highly vulnerable to numerous environmental threats including droughts, floods, tropical cyclones (hurricanes), earthquakes, and landslides. Using paleoenvironmental and palaeoclimatological data to assess pre-observational environmental variation is key to understanding how these climate factors will change as a result of modern climate change. Despite this, high temporal resolution paleorecords spanning long (millennial) timescales are rare. Specifically, on the island of Hispaniola, there exist few paleoclimatological study sites, and to our knowledge, only one paleotempestological (hurricane) study site (Leblanc et al., 2017), despite that the island falls within the North Atlantic Basin's hurricane belt.

Paleoenvironmental records from small islands, which, in the past, have largely been excluded from the study of the Anthropocene[1] epoch (Chandler & Pugh, 2021), can also provide evidence and context for this proposed geological time unit and defining when it may have begun (Rick et al., 2013). Anthropogenic activities have been a driving force of Caribbean island landscape transformations since initial settlement thousands of years ago. These transformations included significant burning and landscape changes that tended to accelerate as populations grew and human

[1] The Anthropocene is a disputed epoch of geologic time that is differentiated from the Holocene by rapid environmental change in recent history prompted by the industrial revolution and other human activities resulting in dramatic increases is GHG's.

activities intensified (Rick et al., 2013). Plants and animals were part of this transformation, including migration disruption, evolution of fire-tolerant flora and fauna, and direct and indirect extinction of mammals and birds, followed by soil erosion, and strong influences on marine and fluvial ecosystems (Rick et al., 2013).

Haiti is one of the poorest and most food-insecure countries in the world, with one of the major contributing factors being soil infertility (Bargout & Raizada, 2013). In Haiti, 40% of the population lives in urban areas, including slums, located in coastal plains prone to flooding (Lozano-Gracia & Garcia Lozano, 2017). Furthermore, the metropolitan region, Porte-au-Prince, lies directly along the boundary of two tectonic plates, and the countries relationship with the Intertropical Convergence Zone (ITCZ) means that it is potentially sensitive to droughts and changes in hydrological regimes. Moreover, hurricanes are among the most catastrophic and costly environmental phenomena along Atlantic coasts, but the factors that control their patterns over millennial timescales are poorly understood. This project aims to reduce this knowledge gap by using geological and geochemical proxies (x-ray fluorescence (XRF) core scanning data, grain-size analysis, and loss on ignition) to identify long timescale climate trends in southwestern Haiti.

1.3. Research Objectives

Very few paleoenvironmental studies have been conducted in Haiti and those that exist are limited to one study site: Lake Miragoâne (*e.g.*, Brenner & Binford, 1988; Curtis & Hodell, 1993; Higuera-Gundy et al., 1999; Hodell et al., 1991), which is approximately 60 km from the Baradères Bay. Because high-resolution data used to test climate modeling studies are scarce, our ability to understand how tropical climates will respond to present and future warming is hindered. This project adds to the growing inventory of Caribbean climate reconstructions in the Holocene that will help to model and understand such scenarios. Filling this knowledge gap may also help answer important questions regarding local versus basin-wide controls on climate variability.

<u>This thesis aims to answer the following research questions:</u>

1) Does the site record sedimentary and/or geochemical evidence of climate variability and/or human activity during the Holocene and if so, what is the nature of this variability?
2) What long- and short-timescale climate factors best account for this variability?
3) How does this compare to other paleoclimatological work in the region?

To address these questions, this project analyzes a continuous, marine ~9-meter sediment core collected from a karst hole in Baie des Baradères, Haiti, using a multiproxy paleoenvironmental approach.

CHAPTER 2:

Literature Review

2.1. Overview of Caribbean Paleoenvironment in the Holocene

At the end of the Pleistocene (~11,900 cal BP), the Caribbean climate was dry, and lake levels were low. Sea and lake levels rose at the end of the last deglaciation reflecting wetter conditions in the early Holocene (Hodell et al., 1991). Humid conditions between 8000 and 6000 cal BP have been validated by several proxies including micropaleontological indicators from a sinkhole in the Bahamas (van Hengstum et al., 2018) and oxygen isotopes from Lake Miragoâne, Haiti (Hodell et al., 1991). Short-duration fluctuations within this time include an abrupt dry period known as the "8.2 kyr event" which has been recorded by numerous proxies, including a sediment core from a sinkhole in Cuba, which was characterized by abrupt peaks in Cl and Br between ~8120 and ~8275 cal BP (Peros et al., 2017). This moist period was followed by an overall drying pattern over the last ~5000 years (Fensterer et al., 2013; Haug et al., 2001; Higuera-Gundy et al., 1999; Hodell et al., 1991), with lake levels declining gradually though the middle Holocene, and accelerating abruptly at ~3200-3400 cal BP (Curtis & Hodell, 1993; Hodell et al., 1991; Kennedy et al., 2006). Following ~3400 cal BP, moist-forest taxa diminished, and lake levels remained low until the present, with only brief returns to moister conditions (ie. ~1600-900 cal BP) (Curtis & Hodell, 1993; Higuera-Gundy et al., 1999; Hodell et al., 1991; Kennedy et al., 2006).

Superimposed upon this long-term trend, the Caribbean has experienced multiple centennial-, decadal-, and annual-scale droughts whose impacts have varied on the regional scale. For example, between 2013 and 2016, the Caribbean experienced one of the most severe droughts of the last 50 years, which was likely due to a strong El Niño event in conjunction with regional warming related to anthropogenic activities, and which resulted in widescale agricultural crop loss and food insecurity (Herrera et al., 2018).

2.1.1. Tectonic and Seismic Activity in Southwestern Hispaniola

Given that the region of study is directly in contact with several plate boundaries, it is likely that the site was influenced to some degree by tectonic movement. The island of Hispaniola is tectonically dynamic, as it lies upon and close to several active faults and folds (Hashimoto et al., 2011). For instance, there is immense crustal strain caused by the oblique collision of the Caribbean and North American tectonic plates, which are currently converging in an east-northeast to west-southwest direction at approximately 20 mm/year (Hashimoto et al., 2011).

Recent GPS-based studies indicate that today, over two-thirds of the relative plate motion in southwestern Hispaniola is accommodated by two faults: the Septentrional fault (SF) (~9 mm/year), and the Enriquillo–Plantain Garden fault (EPGF) (~7 mm/year) (P. Mann et al., 2002). The SF is the boundary between the Gonave microplate and the North American plate, and the EPGF is the boundary between the Gonave microplate and the Caribbean plate. As thrust and fold structures exist in this region, it is possible that other faults may be activated by changing stress, which could cause changes in the nearby sediment (Hashimoto et al., 2011). This suggests a need to consider tectonic movements as a factor in energy changes, element ratios, and particle size changes that occur in this core analysis.

Historical records suggest frequent seismic activity along the north-east Caribbean plate boundary in the past 500 years, particularly on the island of Hispaniola (Bakun et al., 2012; Moreau de Saint-Méry, 1796, 1798). Paleoseismic studies on the SF zone indicate a Holocene slip rate of

6-12 mm/year, and show that the most recent surface rupturing earthquake on the SF occurred more than 800 years ago, demonstrating an ongoing seismic hazard (Prentice et al., 2010). Few paleoseismic studies have been done of the EPGF, but historical records show that Haiti's southern peninsula experienced significant earthquakes in 1701 CE (249 cal BP), 1751 (199 cal BP), 1770 CE (180 cal BP), and 1860 CE (90 cal BP) (Bakun et al., 2012; Scherer, 1912), that may have occurred on the EPFG (Prentice et al., 2010). As an example, figure 2.1, shows that the Baradères Bay was likely an aftershock intensity centre in the 1860 CE earthquake.

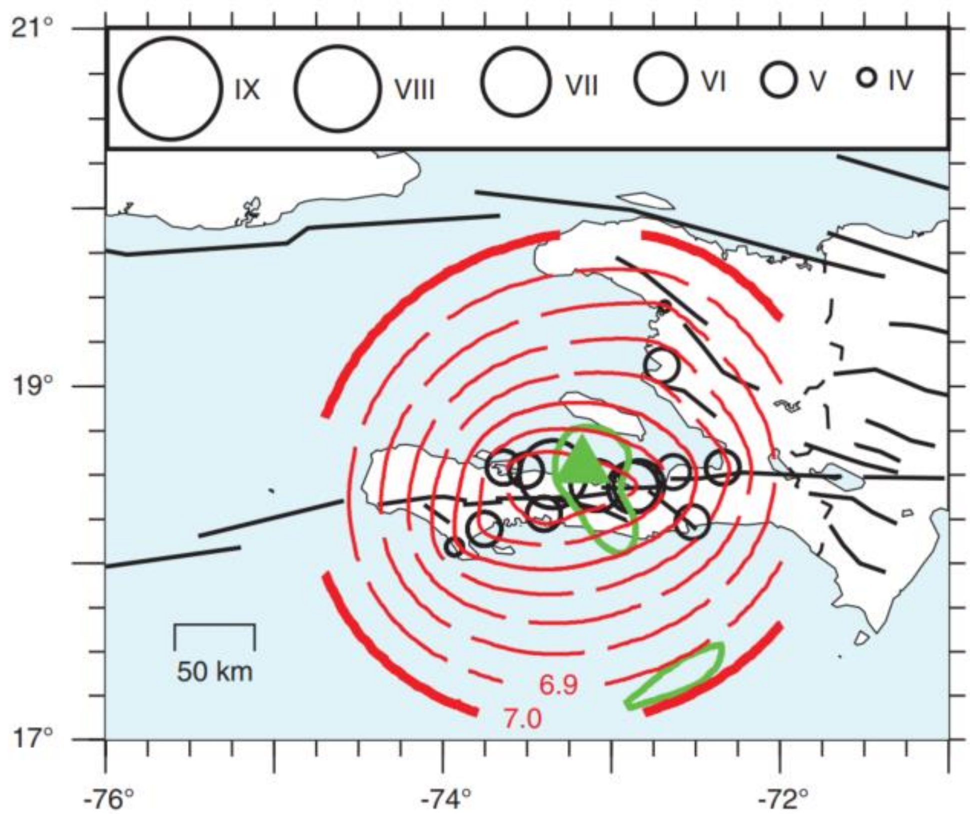

Figure 2.1: From Bakun et al. (2012). The 8 April 1860 earthquake with the preferred intensity assignments. The black circles are sites with modified Mercally intensity (MMI) assignments with symbol size increasing with intensity. Black lines are active fault traces and dashed red lines are contours of MI. The intensity center is a green triangle.

There are no reports of earthquakes in southwestern Hispaniola before 1700 CE, although there are sufficient "felt reports" in 1562 CE to estimate the size and location of an earthquake in

Northern Hispaniola, indicating that an earthquake of such a size would have been detected in southern Hispaniola at this time (Bakun et al., 2012). It was also in the financial interest of communities to report earthquake damage to the Spanish king in order to receive recuperation funds (Bakun et al., 2012). However, there is no reason to suppose that small earthquakes were not occurring prior to this year. Rather, the detection threshold of small earthquakes has increased with time.

The role of the EPGF on earthquake risk in southwestern Haiti is considered to be very important, but poorly understood (Prentice et al., 2010). For example, in 2010, southern Haiti experienced an Mw 7.0 earthquake that caused severe damage in cities including Port-au-Prince and Baradères, more than 220,000 fatalities reported, and between 8 to 14 billion dollars in damages (Hashimoto et al., 2011; Hayes et al., 2010). It was originally hypothesized that the EPGF was responsible for this earthquake, but this theory was quickly disproven as the primary geologic signature of this earthquake involved coastal uplift and generated no significant surface rupture along the EPFG (Hashimoto et al., 2011; Hayes et al., 2010; Prentice et al., 2010).

Hayes et al (2010) explains that "together with the predominance of shallow off-fault thrusting, the lack of surface deformation implies that remaining shallow shear strain will be released in future surface-rupturing earthquakes on the EPGF fault zone, as occurred in inferred Holocene and probable historic events". These findings indicate that such earthquakes involving broad warping and coastal vertical deformation rather than surface-rupture will not be easily recognized by modern paleoseismic methods, and therefore similarly complex seismic activity is likely missing from our prehistoric record (Hayes et al., 2010). Furthermore, some studies (McHugh et al., 2011; McHugh et al., 2014) attribute this earthquake and subsequent tsunami to nearshore sediment deformation and failures for paleoenvironmental studies.

2.1.2. Sea Level

Circum-Caribbean sea level rise throughout the Holocene has been documented through fossil coral records and peat deposits (Toscano & Macintyre, 2003). Mangroves that grow along sheltered tropical and subtropical coastlines in the intertidal zone generally accumulate peat at a rate relative to that of sea level rise (Tomlinson, 1986), and are therefore sometimes used in corroboration with corals as an indicator of sea level rise. The Holocene is of particular interest with respect to sea level as it includes the end of the last glacial–interglacial transition, during which the North American and Eurasian ice sheets melted while the Greenland and Antarctic ice sheets underwent a primary deglaciation phase, eventually reaching a stage of quasi-equilibrium which resulted in relatively stable sea levels during the mid-to-late Holocene (Milne & Peros, 2013). This is now considered an ideal period with which to compare modern rates of sea level rise in order to assess the impacts of today's warming on sea level and to distinguish to what degree human activities are impacting the rate of change (Milne & Peros, 2013).

Sea-level change following the last glacial maximum was dominated by the transfer of water from land ice to oceans. According to Milne et al. (2005), the monotonic rise of mid-to-late Holocene relative sea level (RSL) in the Circum-Caribbean was strongly driven by the isostatic deformation from the continuous melting of the North American ice sheet. This indicates strong regional variability in sea level rise that can be influenced by local factors such as tectonics and glacial isostatic adjustment (GIA) (Milne et al., 2005; Milne & Peros, 2013). For example, models predicting RSL minus the eustatic value[2] at 10,000 cal BP and again at 5000 cal BP from Milne &

[2] The eustatic sea level is the distance from the center of the earth to the sea surface, thus the eustatic component relates to changes in sea level caused by changes in volume of glacial ice or changes in sea water volume caused by tectonic processes.

Peros (2013) demonstrated that spatial variability in the insular Caribbean has changed significantly during the Holocene (Figure 2.2).

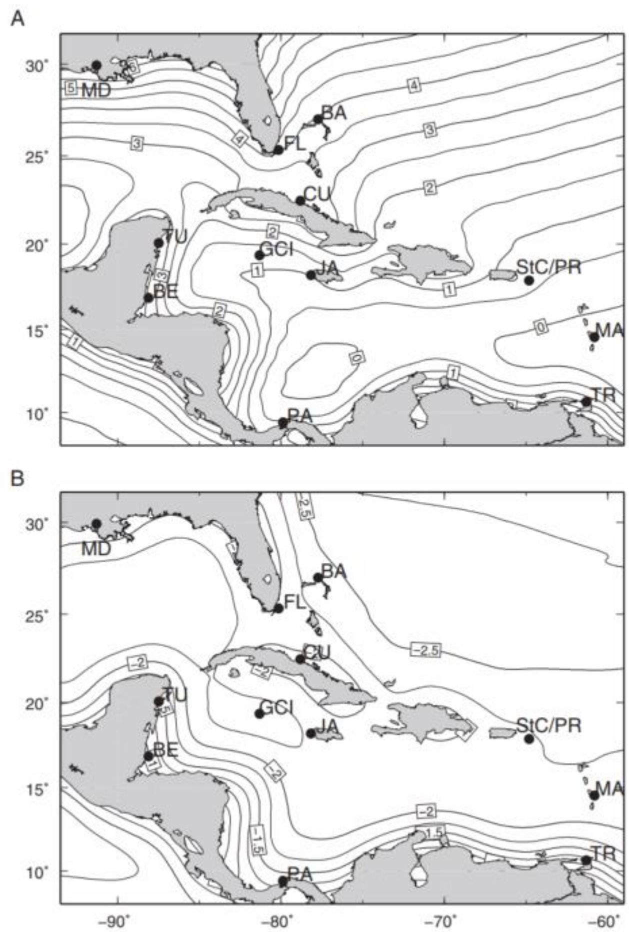

Figure 2.2: From Milne & Peros (2013). Predicted RSL minus the model eustatic value at 10 cal kyr BP (A) and 5 cal kyr BP (B). The model eustatic values are -24.6 and -1.3 m at 10 and 5 cal kyr B.P., respectively.

During early Holocene, sea level in the North Atlantic was significantly lower than today (Moore, 1991; Schwartz, 1982). In this condition, Moore (1991) speculated that there may have been two separate land bridges connecting the island of La Gonave to Porte-au-Prince, with a large freshwater lake or lagoon in what is now Port-au-Prince Bay (Moore, 1991). This freshwater marsh environment would have been an ideal habitat for local marine animals and reptiles as well as migrating species. The earliest settlers in Haiti could have been drawn here from the mainland by following the migrating sea mammals, which would have to move through narrow channels to get between open sea and the large lagoon or lake, where they would be most easily captured by early populations (Moore, 1991). The theory of a sunken lake in the Port-au-Prince Bay requires further exploration and evidence, but it is possible that similar connections may have existed between Baradères and La Gonave Island at this time.

Milne & Peros (2013) predicted RSL from a site in Cuba that showed some of the component GIA curves (Figure 2.3). Their results indicated that since ~9000 cal BP the local sea level changes in this region were dominated by ice-loading effects, and that by ~8000 cal BP, the steady collapse of the peripheral bulge associated with North American deglaciation caused land subsidence and enhanced local sea level rise (Milne & Peros, 2013). They estimated that in the Circum-Caribbean, there was about 3-4 m of land ice melt from ~7000 cal BP to ~3000-2000 cal BP (Milne & Peros, 2013).

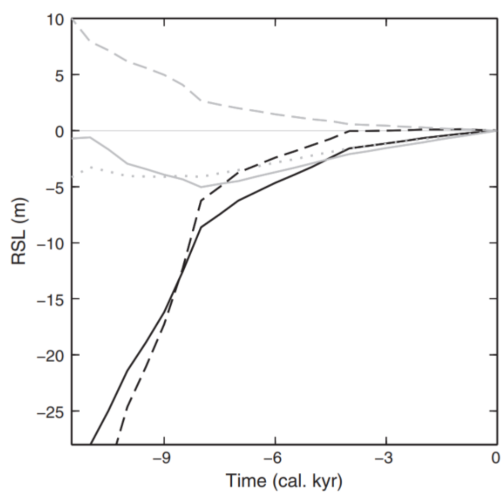

Figure 2.3: From Milne & Peros (2013). RSL in Cuba from the best-fitting GIA model. Solid black line represents total RSL change and differs from the model eustatic signal (dashed black line) due to a globally uniform shift in mean sea-surface height (dashed grey line) and local changes in RSL due to ice-ocean mass redistribution and rotational effects (solid grey line). Dotted grey line represents ice-loading effects.

2.1.3. El Niño–Southern Oscillation (ENSO), Atlantic Multidecadal Oscillation (AMO) and North Atlantic Oscillation (NAO)

Three important natural components of climate change in the Caribbean are the ENSO (Li et al., 2013), the AMO (Gray et al., 2004), and the NAO (Trouet et al., 2009). Changes in, and teleconnections between, these atmospheric phenomena throughout the Holocene have played an important role on hydrological regimes, including the frequency of droughts and intense hurricanes (Goldenberg et al., 2001; Muller et al., 2017). The ENSO describes an interdecadal-centennial ocean-atmospheric circulation mechanism that has important implications on SST patterns, tropospheric vertical wind shear dynamics, strength of the trade wind system, and tropical cyclone (TC) activity (Schmitt et al., 2020). For example, intervals of fewer strong El Niño (warm phase) events during the late Holocene resulted in less vertical wind shear over the tropical North Atlantic and more favorable conditions for intense hurricane development (Donnelly & Woodruff, 2007). Moreover, ENSO variance was low in the early LIA, and much higher in the 20th century, with unprecedented variability in recent decades in response to increased anthropogenic radiative forcing (Li et al., 2013).

The AMO is a major oceanographic phenomenon of climate variability which is known to modulate both Atlantic and Caribbean SST patterns, which in turn may impact the development of intense hurricanes (Schmitt et al., 2020). The AMO has been linked to multi-year precipitation anomalies and appears to modulate ENSO teleconnections over large portions of the Northern Hemisphere (Enfield et al., 2001). Over the instrumental record (1856 CE to present), the AMO has exhibited a 65–80-year cycle with a 0.4°C range, with warm phases between 1860-1880 and 1930-1996 and cold phases between 1905-1925 and 1970-1990 (Gray et al., 2004).

The NAO is an important component of climate variability over the whole Atlantic region, which has a strong influence on ocean-atmospheric interactions including precipitation and storms, temperature, and both marine and terrestrial ecosystem dynamics (Marshall et al., 2001). There is evidence of a positive phase of the NAO as a dominant driver during the Medieval Warm Period (MWP), as well as a clear shift to a negative phase of the NAO during the Little Ice Age (LIA) (Trouet et al., 2009). More recently, the tropical North Atlantic response to a positive phase of the NAO is an increase in trade wind strength in the Northern Hemisphere and a feedback through the Hadley circulation causing cooler average SSTs in the tropics and subtropics (Marshall et al., 2001).

2.1.4. Sea Surface Temperature (SST)

Although there is a lack of comprehensive and continuous sea surface temperature records during the Holocene, it has been suggested that the modulation of SST in the Common Era likely operates on two levels: (1) Solar- and volcanic activity-triggered climate changes which induce responses from the AMO, the NAO and the ENSO, and result in a change in SST; and (2) SST modulation controlled by AMO phase change (Schmitt et al., 2020). Most tropical Atlantic SST records come from sclerosponges (Haase-Schramm et al., 2003), foraminifera (Black et al., 2007) and corals (DeLong et al., 2014; Kilbourne et al., 2008; Tierney et al., 2015). Unfortunately, most records span only centennial timescales, and longer paleo SST reconstructions are largely synthesis approaches combining several shorter regional records (*e.g.*, Mann et al., 2008; Rosenthal et al., 2017).

Recently, Schmitt et al. (2020) provided the longest and only continuous annually-resolved tropical SST and AMO variability reconstruction - which extends through the last 2000 years (Figure 2.4). Their results show that early in the common era (100-500 CE) the climate was characterized by a warm interval (known as the Roman Warm Period), with a corresponding positive anomaly in SST. Subsequently, the following time interval of 500-900 CE was characterized by global cooling, known as the Dark Ages Cold Period, with fewer positive SST anomalies globally and regionally. The Medieval Warm Period (900-1400 CE) was the most recent past warm climate interval, with SST anomalies surpassing present-day temperatures (Schmitt et al., 2020). The Little Ice Age from ~1400-1850 CE, was the most recent cold interval that correlates with significant negative global and regional SST anomalies with surface ocean temperatures decidedly below present conditions (Black et al., 2007; Kilbourne et al., 2008; Schmitt et al., 2020). In recent decades and centuries there has been an increase in global and relative SST, with the increase in Atlantic SST being greater than in the tropics (Black et al., 2007; Ramsay & Sobel, 2011).

Warm local SSTs are necessary for the formation and intensification of TCs (Camargo et al., 2013). For this reason, multidecadal variations in major hurricanes have been attributed to changes in Atlantic SST, specifically within the "main development region" (MDR) (Denommee et al., 2014; Lane et al., 2011; Mann et al., 2009). It has been proposed that in recent decades, increases in SST related to anthropogenically-triggered climate warming have caused an increase in the frequency of intense hurricanes (Emanuel, 2005). However, given the apparent increase of intense hurricane landfalls during the later half of the LIA (Donnelly & Woodruff, 2007), tropical SSTs as warm as at present are evidently not a required condition for increased intense hurricane activity (Winter et al., 2000). Furthermore, according to Donnelly & Woodruff (2007), the Caribbean experienced a relatively active interval of intense hurricanes for more than a millennium when local SSTs were on average cooler than present. Thus, although ENSO appears to be a primary control on Atlantic SST fluctuations and hurricane intensity, climate controls independent of ENSO such as the West African Monsoon may also have played an important part in modulating hurricane activity during the Holocene (Donnelly & Woodruff, 2007).

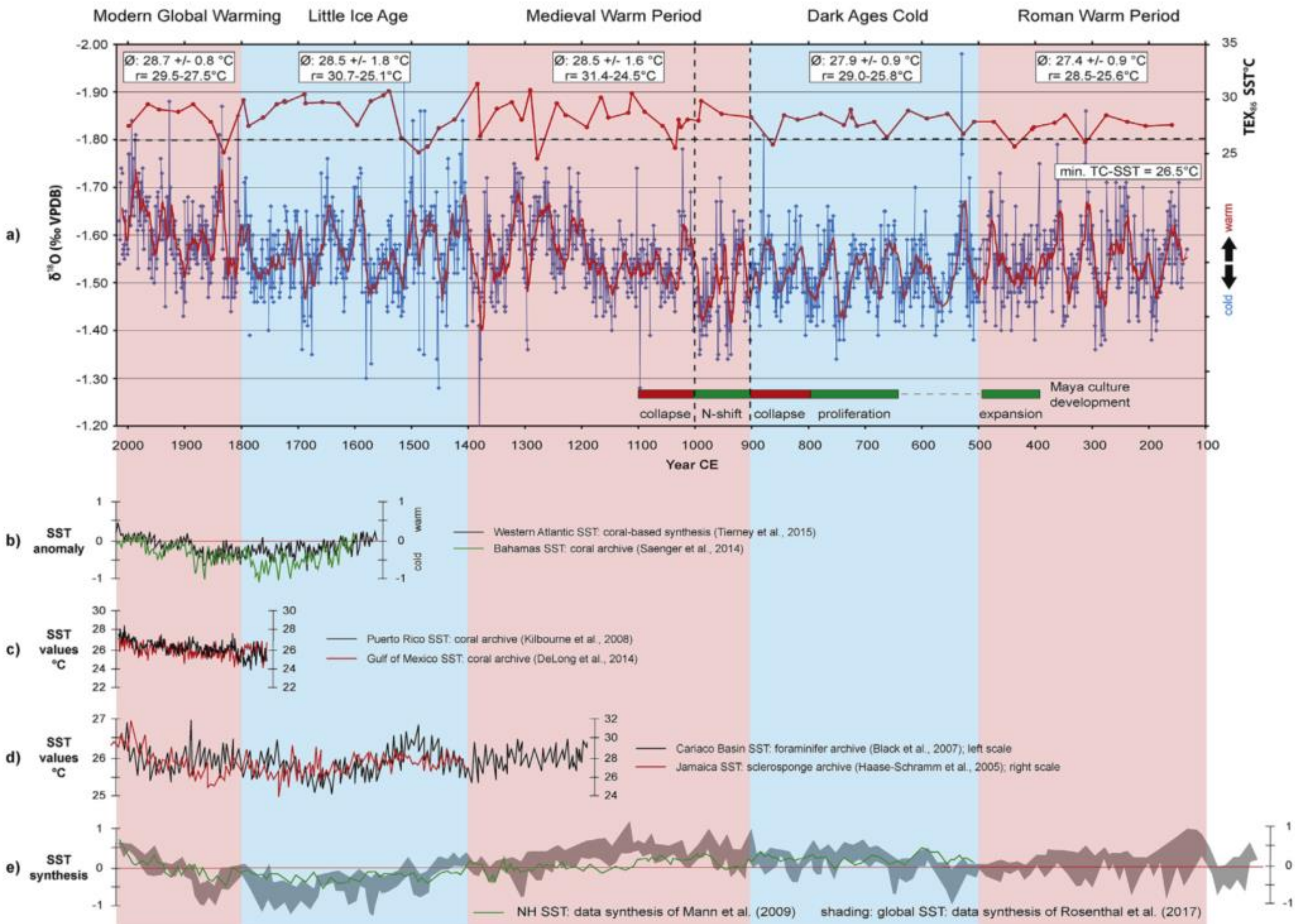

Figure 2.4: From Schmitt et al., 2020. a) d18O (relative SST curve) and TEX86 (absolute SST curve) time series. Horizontal dashed black line indicates the boundary of 26.5 C, which is relevant for TC formation. Timing of Maya culture development is based on the study of Kennett et al. (2012). b) Coral-based relative reconstructions of tropical Atlantic SST patterns. c) Absolute SST reconstruction from coral archives from Puerto Rico and Florida/Gulf of Mexico. d) Absolute SST reconstruction from a foraminifer archive from the Cariaco Basin and a sclerosponge archive from Jamaica. e) Northern Hemisphere SST reconstruction by synthesis approach.

2.1.5. Hydroclimate Variability and the Intertropical Convergence Zone (ITCZ)

The dry conditions of the late Pleistocene were followed by a general trend toward increasing water levels in the tropics, marking the switch to humid conditions in the early Holocene with increased precipitation levels (Hodell et al., 1991). The transition was not smooth and includes an abrupt minimum in δ18O at around 8.1kyr BP (~9000 cal BP)[3], indicating a relatively dry climate (Hodell et al., 1991). Lake levels on Hispaniola were high during the middle Holocene, which corresponds to a moister period, and remained relatively high until ~3.2 kyr BP (~3400 cal BP). Meanwhile, since the middle Holocene (~5400 years ago), there has been an overall trend toward dryer conditions in the Caribbean (Haug et al., 2001). There is lack of uniformity among paleoclimate records after ~3000 cal BP in the Circum-Caribbean mainly due to greater inter and intra-regional variability and human disturbances. However, most records agree that between ~3400 and ~2500 cal BP there was an abrupt shift to drier conditions (van Hengstum et al., 2018), and after ~3400 cal BP, moist-forest taxa diminished, and lake levels remained low until the present, with only brief returns to moister conditions (ie. ~1200-900 cal BP) (Curtis & Hodell, 1993; Higuera-Gundy et al., 1999; Hodell et al., 1991; Kennedy et al., 2006).

The ITCZ is a zone of deep convection and heavy precipitation that is generated by convergence of the trade winds, migrates between 9°N and 2°N in response to seasonal SST warming, and largely affects variations in regional hydrological cycles (Schneider et al., 2014). Climatic variations such as the trend toward dryer condition since ~5.4 BP (~6300 cal BP) and the high-amplitude fluctuations and precipitation minima between ~2.8 to 3.8 kyr BP are best explained by changes in the average latitude of the ITCZ (Haug et al., 2001; Van Hengstum et al.,

[3] Uncalibrated dates from Hodell et al. (1991) have been calibrated with OxCal 4.4

2016). Oxygen isotope records from sediment obtained from a small mid-elevation lake in the Dominican Republic indicate that during the LIA the ITCZ shifted southward, which produced more arid conditions, and which highlights the overall sensitivity of the Caribbean to the relative location of the ITCZ (Lane et al., 2011).

Throughout the Holocene, changes in solar insolation (related to changes in Milankovitch orbital forcing) caused migration in the average position of the ITCZ (Haug et al., 2001; Hodell et al., 1991). The early Holocene was characterized by intense summer insolation which resulted in warming of the Northern Hemisphere and northward movement of the ITCZ (Poore et al., 2004). This, in turn, enhanced southeasterly winds, which resulted in increased precipitation recorded by runoff records in the Cariaco Basin, off the coast of Venezuela (Haug et al., 2001), and in lake-level records at Lac Miragoâne, Haiti (Hodell et al., 1991). After ~5 kyr, decreasing summer insolation in the Northern Hemisphere caused a southward migration of the ITCZ, which caused a decline in southeasterly winds, and thus a decline in precipitation in Haiti and along the coast of Venezuela (Haug et al., 2001; Hodell et al., 1991). Figure 2.5 shows a relationship between solar insolation at 10° N and Oxygen isotopes from Lake Miragoâne, Haiti throughout the Holocene, with a congruent peak at around 6500 BP.

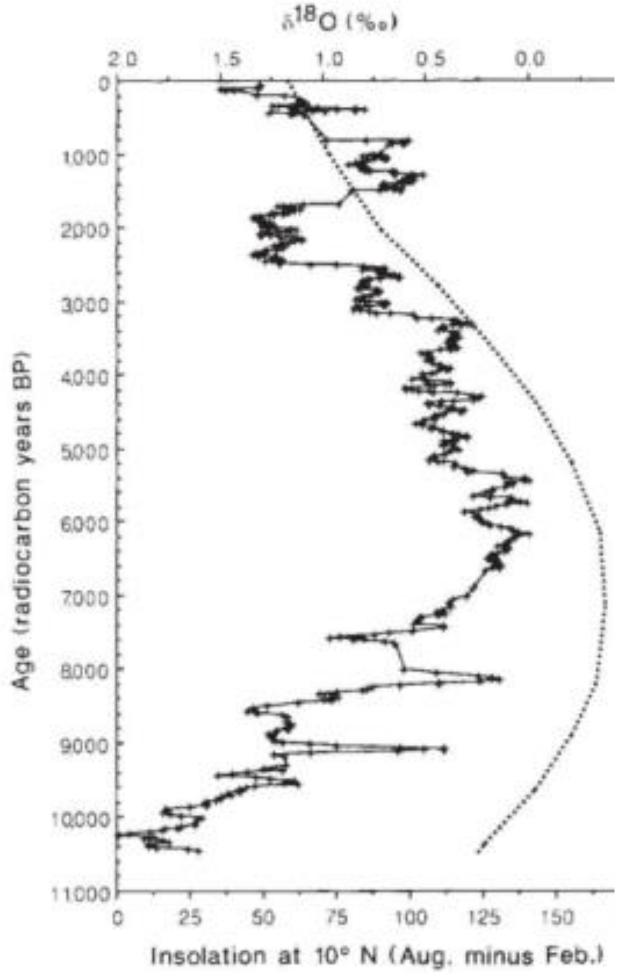

Figure 2.5: From Hodell et al. (1991). Solar Insolation at 10°N (Aug. – Sept.), and stable oxygen isotope data from a single ostracod species from lake Miragoâne, Haiti. The ratio of evaporation to precipitation is high to the left and low to the right. Note that ages are not calibrated.

There is evidence of an abrupt shift to dry conditions in the Caribbean (also referred to as a megadrought) from ~3.3 to 2.5 kyr BP (Berman & Pearsall, 2000), which has been attributed to a southern shift in the ITCZ (van Hengstum et al., 2018). Further evidence of this dry period in the Caribbean comes from an abrupt cessation of speleothem growth in Cuba, most likely related to a decrease in regional precipitation (Fensterer et al., 2013), and shallow coastal lagoon drying indicators (*e.g.*, gypsum deposition) in Cuba (Gregory et al., 2015).

Moreover, most Atlantic hurricanes develop from easterly waves propagating westward along the Northern edge of the ITCZ (Goldenberg et al., 2001). This location is often referred to as the "main development region" (MDR) because nearly all major hurricanes develop here, and thus hurricane development is quite sensitive to climatic fluctuations in the tropics. In the tropical North Atlantic, the Atlantic Meridional Mode (AMM) is the dominant mode of ocean-atmospheric interaction. A positive phase of the AMM is associated with a strong meridional SST gradient, a northward shift in the ITCZ, and therefore deceased vertical wind shear (van Hengstum et al., 2016). For this reason, research has suggested that meridional shifts in the ITCZ position on geological timescales may modulate hurricane activity in the tropical North Atlantic Basin. For example, Wallace et al. (2019) indicates that multi-decadal shifts in the ITCZ and volcanic activity have modulated hurricane patterns in the Bahamas, and van Hengstrum et al. (2016) confirmed that the ITCZ has to some extent modulated hurricanes on millennial to centennial scales in the western North Atlantic margin.

Many studies have suggested that in upcoming decades and centuries, decreased precipitation and increased aridity and freshwater stress in the Caribbean resulting from anthropogenic climate change will cause alterations to hydrological regimes and drastic increases in drought risk (Herrera et al., 2018; Karnauskas et al., 2018; Lehner et al., 2017). As Haiti is severely deforested and mountainous, the hydrological cycle is critically important, with topsoil removed by erosion hampering successful agriculture and increasing runoff and weathering (McGillis et al., 2015).

2.1.6. Hurricanes in the North Atlantic Basin

TCs, including tropical storms and hurricanes, are among the world's most catastrophic and costly atmospheric phenomena, increasingly resulting in landscape and infrastructural damage, fatality, and injury (Emanuel, 2005). Haiti lies within the North Atlantic hurricane belt and is therefore at risk of TCs during annual hurricane season. Human deaths from TCs in Haiti are primarily due to severe flash floods and landslides in eroded watersheds that flow through densely populated poor riverine/coastal communities such as Baradères and Port-au-Prince (Smucker et al., 2007). Understanding climatic controls on TC patterns is of great importance, but records of TC strikes spanning millennia with high temporal resolution are rare (Denommee et al., 2014). Due to this lack of baseline information, the factors that control hurricane variability on millennial timescales are poorly understood, and this limits our ability to predict and attenuate changes to their patterns of frequency and intensity related to anthropogenic global warming.

Paleotempestology is the relatively new study of paleo-storm activity by means of geological proxies (overwash deposits preserved in sediments of coastal lakes, bays, bogs, etc.) and historical documentary records, with the aim of understanding how hurricane frequency and intensity has varied over the past decades, centuries, and millennia. For example, Mann et al. (2009) proposed that there may have been enhanced TC activity during the MWP (900-1200 CE/1050-750 BP) in the North Atlantic, which could have been caused by climate patterns similar to the current warming in this region (Rhein et al., 2013). To understand the impacts that future hurricanes will have on growing coastal populations, we must first develop a better understanding of the relationships between TC's and climate forcing variables at different timescales (Muller et al., 2017).

There is no debate that in recent decades, global economic damages from TCs have significantly increased. However, there remains disagreement in the paleotempestological community about the short and long-timescale trends of hurricanes. Although some studies suggest that extreme Atlantic cyclones have increased in frequency and intensity over the last 100 years (*e.g.,* Emanuel, 2005; Lehmann et al., 2011; Paciorek et al., 2002), others have argued that there have been no significant TC trends over this time period (*e.g.*, Klotzbach, 2006; Knutson et al., 2010; Weinkle et al., 2012) and that increases in economic damage from TCs can be explained entirely by societal changes such as increasing wealth, infrastructure, and population in locations with high TC risk. Additionally, some scientists credit our improved capability to detect intense hurricanes (*e.g.*, Klotzbach & Landsea, 2015; Landsea et al., 2006), and the fact that intense hurricanes rarely last long or make landfall at their peak speeds, making them less easily detectable in the past (*e.g.*, Fitzpatrick, 2006), with causing a bias which results in the apparent increase of intense hurricanes in recent decades and centuries.

In recent decades, the North Atlantic Basin has experienced an average of 12 named TCs per year (Wallace et al., 2019), while exhibiting substantial interannual and interdecadal variability. Since at least the mid-Holocene, periods of greater activity ("active periods") or lesser activity ("inactive periods") are correlated with variations in climatic conditions, and last anywhere from several centuries to a few thousand years (Denommee et al., 2014; Donnelly et al., 2001, 2015; Donnelly & Woodruff, 2007; Gischler et al., 2008; P. Lane et al., 2011; Liu & Fearn, 2000; McCloskey & Liu, 2013; Metcalfe et al., 2016; van Hengstum et al., 2016, 2014; Wallace et al., 2019). Notably, Lane et al. (2011) recorded several periods of intense hurricanes, with the most active interval between 2800 and 2300 cal BP. Additionally, van Henstrum et al. (2016) noted that from 2500 to 1000 cal BP the North Atlantic Basin experienced an "active interval" of intense hurricanes related to a more northern ITCZ position relative to present, yet not as far north as its position in the middle Holocene. This was the beginning of a period of Caribbean aridity relative to the middle Holocene, with the shift of ITCZ position favouring cyclogeneses in the MDR, reducing vertical wind shear, and increasing hurricane activity. At ~1000 cal BP, intense hurricane activity decreased in the western North Atlantic, in conjunction with a southward movement of the ITCZ leading to decreased cyclogenesis in the MDR (van Hengstum et al., 2016).

Overall, the North Atlantic Basin, and specifically the Caribbean, has shown dramatic multidecadal variations in hurricane activity in the Holocene. These changes show the enhancement of Caribbean hurricane activity during warmer periods, probably including the present anthropogenically enhanced warming period (Goldenberg et al., 2001). Thus, the general consensus among the climate modeling community is that climate change is likely increasing the frequency of the most powerful hurricanes in the North Atlantic Basin, but not necessarily the total number of storms (Paciorek et al., 2002).

2.2. History of Human Impact and Land Use Changes on Hispaniola

Land-use activities including deforestation (clear-cutting), practicing subsidence agriculture, mining, and urban expansion have far-reaching effects on global systems such as atmospheric dynamics, the global carbon cycle, nutrient inputs into ecosystems and the hydrologic cycle (Foley et al., 2005). Islands with long histories of human settlement such as Hispaniola require temporal and spatial reconstructions of anthropogenic changes to the environment and subsequent responses to improve our understanding of the driving mechanisms that affect Caribbean ecosystems, and our ability to predict and attenuate costly damages to human and natural environments (Nogué et al., 2017). In the centuries after Columbus landed in the insular Caribbean in 1492, Haiti and it's surrounding islands have undergone significant landscape transformations. That being said, there is still very little information on the degree and extent of pre-Columbian human impacts in this region (Castilla-Beltran et al., 2020).

2.2.1. Archaeological Evidence

Archeologists recognize four waves of settlement in the Circum-Caribbean region: Lithic (~7000-4000 cal BP), Archaic (~5000-2000 cal BP), Ceramic (~2500 cal BP in some areas, somewhat later in others), and Historic (since 1492 CE, i.e. ~500 cal BP) (Cooke et al., 2017). All ceramic, archaic and lithic sites on Hispaniola have been greatly disturbed/depleted due to exposure to natural elements and human activities, with resource overexploitation and land-use practices leaving sites exposed to increased erosion (Moore, 1991). The environmental impact and subsequent effect on terrestrial and coastal landscapes increased with each successive migration wave. In fact, some pre-columbian societies practiced sustainable farming practices such as constructing terraces on sloped agricultural landscapes to prevent soil and nutrient loss and reduce the speed of water drainage (Bargout & Raizada, 2013). Such practices have not been upheld in modern Haitian farming activities.

The first Caribbean settlers were unique in that they were the only settlers in the Americas who travelled hundreds or thousands of kilometers through open sea using dugout canoes to reach uninhabited islands (Fitzpatrick, 2013). However, the timing of arrival and pace of dispersion of these settlement waves are still debated, with major disagreement concerning when, from where, and in what order the Caribbean archipelago islands were first inhabited by humans (Napolitano et al., 2019). During the Holocene, the insular Caribbean has experienced more mammalian extinction than any other global region (Turvey, 2009). While this was in part due to habitat loss induced by sea level rise (Cooke et al., 2017; Dávalos & Turvey, 2012), most postglacial species extinctions in the Holocene occurred on islands and have been associated with the regional arrival of prehistoric settlers (Cooke et al., 2017; Turvey, 2009).

Archaeological studies on Hispaniola indicate that during the Lithic period, settlements were often abandoned and recolonized, suggesting non-linear population growth, and making it challenging to infer regional population dynamics (Rick et al., 2013). Early lithic groups in Hispaniola used flint material such as knives, scrapers, cores, and chips (Moore, 1991), but likely left negligible environmental footprints on vegetational patterns (although shifts in environments influenced how and to what extent different regions were exploited). It is worth noting that most lithic sites on Hispaniola were located on Miocene limestone and alluvial deposits, while the large deposits of Eocene limestone which compose the southern peninsula of Haiti apparently did not yield the type of flint desired by the first settlers (Moore, 1991). Consequent Ceramic and Archaic groups did, however, utilise this type of limestone.

Archaic sites are identified on Hispaniola as early as ~5.2 kyr BP (~5900 cal BP), mostly on shorelines suggesting seasonal occupation, but with evidence of increasing land management, establishment of horticultural and agricultural practices, and fire-use to bring natural landscapes into production (Keegan, 1994). Sedimentary records from Hispaniola display regional fire regimes reflecting anthropogenic fires from the Archaic period (Cooke et al., 2017). Archaic people introduced crops such as avocado, wild fig, primrose, and wild beans to Hispaniola and other Caribbean islands between 3-4 kyr BP (Fitzpatrick, 2015). Furthermore, while Archaic shell mounds on the southwestern peninsula of Haiti are often found near shorelines, mostly in the vicinity of mangrove swamps, shell refuse indicates that food gathering at this time was oriented more toward shallow bays and open water (Rouse & Moore, 1984).

Ceramic sites were usually located further inland at higher elevations or on hilltops (Moore, 1991). It has been established that Ceramic-age peoples at the western coast of Hispaniola made daily trips to eastern Puerto Rico, due to similarities between archaeological records on both coasts

(Rouse & Moore, 1984). Similar records have established regular passage between Ceramic-age peoples at the southern and western tips of southwestern Haiti's peninsula and Jamaica's eastern coast, and between Haiti and eastern Cuba via the Windward Passage (Rouse & Moore, 1984). The Ceramic peoples introduced dogs, guinea pigs, and other mammals to several Caribbean islands and systematically practiced horticulture and agriculture, introducing a variety of crops including beans, tobacco, chilis, peanuts, and guava (Cooke et al., 2017; Rick et al., 2013). This wave of settlement was the first to establish sedentary villages, often along rivers, and has been linked to drastic habitat changes, unprecedented in scale, with long-lasting effects on biotic ecosystems (Rick et al., 2013).

Hispaniola was rapidly colonized by Spain after 1492, and this instigated drastic ecological resource transformations relating to the introduction of non-native plant and animal species, and the rapid spread of diseases affecting indigenous communities (Castilla-Beltrán et al., 2020; Koch et al., 2019). It is estimated that within 12 years of European arrival, more than 99% of the indigenous Taino people died from enslavement, violence, and disease (Watts, 1987). Europeans repopulated the island with African slaves and transformed the island to plantation-style sugar-cane farming, forgetting many of the sustainable farming practices of the Taino (Bargout & Raizada, 2013). After being effectively deserted by the Spanish by 1606 following the discovery of gold in Mexico and Peru, the western third of Hispaniola was populated largely by French, Dutch, and English pirates throughout the 17^{th} century. In 1697 CE, the colony that would later become Haiti (in 1791 CE) officially became a French possession (Bakun et al., 2012), and was relatively prosperous until the beginning of the twentieth century (Hazard, 1873).

2.2.2. Fire History and Deforestation

The tropics have the highest rates of deforestation and land conversion in the world (Brown, 1996). In Haiti, land degradation by deforestation and consequent soil erosion are serious problems in the drainage systems (Brenner & Binford, 1988). With the continued soil erosion, the soil-moisture storage potential has also been affected (Lewis & Coffey, 1985). Haiti has experienced one of the most severe deforestation episodes historically and globally since the arrival of Europeans about 500 years ago (Stevenson, 1989). Historical arboreal cover, however, is largely disputed as until recent availability of high-resolution, remotely sensed satellite imagery, estimations relied exclusively on field site visits and qualitative assessments from aerial flyovers- often following similar flight paths and therefore producing geographically limited data (Tarter, 2016). Assessing the effects of deforestation on river discharges in Haiti has also been challenging since no continuous and accurate data on river flows exists.

Deforestation, land management, and the burning of waste have significantly altered most catchments in the tropics, including the alteration of carbon speciation as it is transported from land to ocean (Houghton et al., 2000; Mayorga et al., 2005; Moyer et al., 2013). In the Caribbean, the longest fire records come from Lake Miragoâne, Haiti (Higuera-Gundy et al., 1999), Laguna Totuguero, Puerto Rico (Burney et al., 1994), and Laguna Saladilla, Dominican Republic (Caffrey & Horn, 2015). These studies have yielded different interpretations by different investigators. In Haiti, it was interpreted that the fire record was primarily driven by climate (specifically shifts in the intensity of the seasonal and annual solar insolation cycles), whereas in Puerto Rico, the record was thought to be representative of human activity.

Higuera-Gundy et al. (1999) reported an increase in charcoal and fire-resistant pollen during the mid-Holocene, starting sharply at 5050 cal BP, which was interpreted as a time of generally wetter climate. Incidentally, on Puerto Rice, Burney et al. (1994) had previously reported a coinciding increase in charcoal values that had been attributed to anthropogenic influences, but Higuera-Gundy et al. (1999) rejected this idea and instead hypothesized that the fires were caused by lightning and a greater forest cover due to greater summer moisture. The exception to their theory was the period after 1030 cal BP, when the indigenous group *Taino*, and later Europeans are known to have deforested the region. Caffrey and Horn (2015) found a layer of shells at around 5000 cal BP that prevented them from acquiring high resolution charcoal data at this exact time, but a sample from 5230 cal BP showed a sharp charcoal influx. They also found another major increase at 3600 cal BP, as well as a smaller peak at 7960 BP. Burney et al. (1994) reported a sharp increase in charcoal at ~5200 cal BP, which they attributed to human presence because they found no evidence of a shift in climate in regional paleoclimate records that could otherwise explain this influx of charcoal. If this is correct, then this would become the earliest known human presence in Puerto Rico, whose archaeological record places the earliest humans ~3200 cal BP (date calibrated from Rouse, 1992).

All ecosystems on Hispaniola have suffered degradation through deforestation and land-use changes during the last ~220 years which has lead to today's fragmented landscapes (Castilla-Beltrán et al., 2020). Climate reconstructions from Caribbean islands systematically show an influx in charcoal values during the late Holocene (Caffrey & Horn, 2015). Moreover, Hedges et al. (2018) discovered that primary forest cover in Haiti declined from 4.4 percent in 1988 to 0.32 percent in 2016, which is less than 1 percent of its original primary forest. They reported that 42 of Haiti's 50 largest mountains have lost the entirety of their primary forests and that the country is presently undergoing mass extinction of its biodiversity due to habitat loss (Hedges et al., 2018). According to Lewis & Coffey (1985), the Baradères river basin was completely deforested by 1985.

CHAPTER 3:

Detailed Methodology

3.1. Study Site

Caribbean coasts are characterized by prominent features of classic karst landscapes such as cockpits, towers, dry valleys, sinkholes, blue holes, caves, and under water caves (Kueny & Day, 1998). Human impacts on these karst ecosystems have been significant, and protected karst areas have increasingly become designated at both local and international levels (Kueny & Day, 1998). Present research suggests that the Caribbean climate is currently becoming dryer, and this trend is likely to present major repercussions for the populations living in the region, especially those within close proximity to coastlines (Herrera et al., 2018). Climate models project that the Caribbean is expected to develop more frequent and severe droughts from reduced precipitation and increased evaporation related to anthropogenically-enhanced global warming (IPCC, 2014).

The study site for this research is in Baie des Baradères, Haiti. The Baradères Bay covers ~7 km^2 and has a maximum water depth of 29 m. The core was collected from a coastal karst basin (CKB) with vertical depth of approximately 11.5 m, at coordinates 18.514571° N, 73.628903° W, approximately a kilometer away from the Baradères River delta (Figure 3.1, 3.2). The Baradères River crosses the town of Baradères, whose population was 47,060 in 2015 (IHSI 2015). The river is deeply embedded into the local economy, as it is used by locals and tourists alike for transportation and trade (Bertrand, 2017). Subsidence farming and trade are the main economic activities in the region, as well as coffee production (Bertrand, 2017). The initial interest in this location was due to its proximity to the delta, which provides abundant sediment and is therefore likely to preserve terrestrial land use changes as well as high energy flooding events such as hurricanes and tsunamis.

Haiti is a small country of about 28,000 km^2 which shares the island of Hispaniola with the Dominical Republic. Haiti occupies the western third of the island, with the Dominican Republic to its east, and Cuba approximately 80 km to its west. The island is shaped like a horseshoe, with prominent north and south capes along a coastline of approximately 1,771 km (Figure 3.2). Haiti is mountainous, with mountain ranges separated by fertile but overpopulated lowlands, which are susceptible to flooding (Hadden & Minson, 2010). The coast is mostly rocky, rimmed with cliffs, and surrounded by waters dominated by coral reefs. The humid, tropical climate of the region controls the intensity and frequency of periodic droughts and hurricanes (Hadden & Minson, 2010). Northeast trade winds drive the wet season, and because the country lies within the North Atlantic "hurricane belt", it is subject to tropical storms from June to October. Haiti's average annual rainfall is 140 to 200 cm, with the heaviest rain occurring in the northern plains and mountains, and in the southern peninsula (Hadden & Minson, 2010).

Hispaniola's major plant communities are tropical lowland dry forests, highland mesic and pine forests, and coastal mangrove swamps (Holdridge, 1945). The only pine species on Hispaniola is a predominantly high-elevation tree, *Pinus occidentalis,* but it can occasionally be found in ravines and at low elevations (Higuera-Gundy et al., 1999). Haiti's southern peninsula is characterized by tropical dry forests on coastal lowlands and mesic plant and pine forests in the Massifs (Judd, 1987). Natural burning of Hispaniola's drier lowland communities has occurred historically during winter dry season (Holdridge, 1945) but it is possible that at some time, lower temperatures and infrequent fires may have allowed fire-intolerant taxa to colonize at lower-than-modern elevation ranges (Higuera-Gundy et al., 1999).

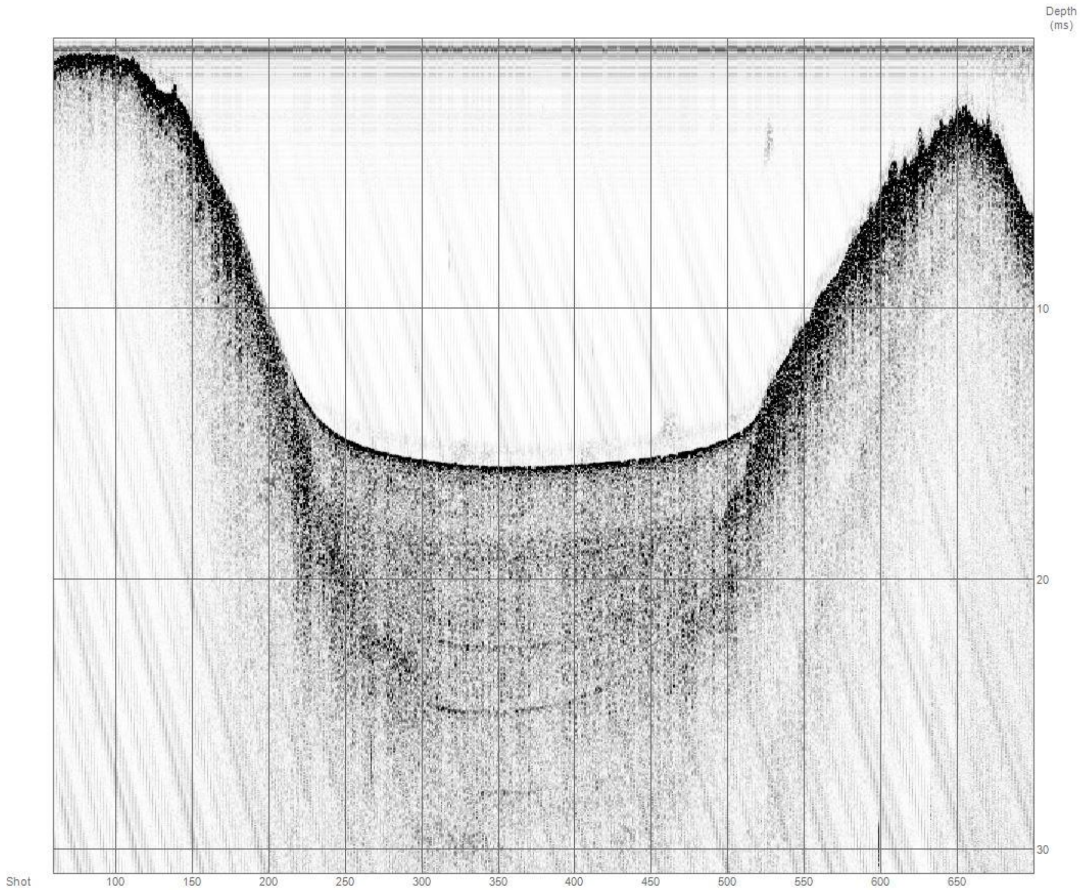

Figure 3.1: Cross section of blue hole from which sediment core was extracted. Vertical depth below water surface, and sediment/water interface is visible. Image courtesy of Nicole D'Entremont (WHOI).

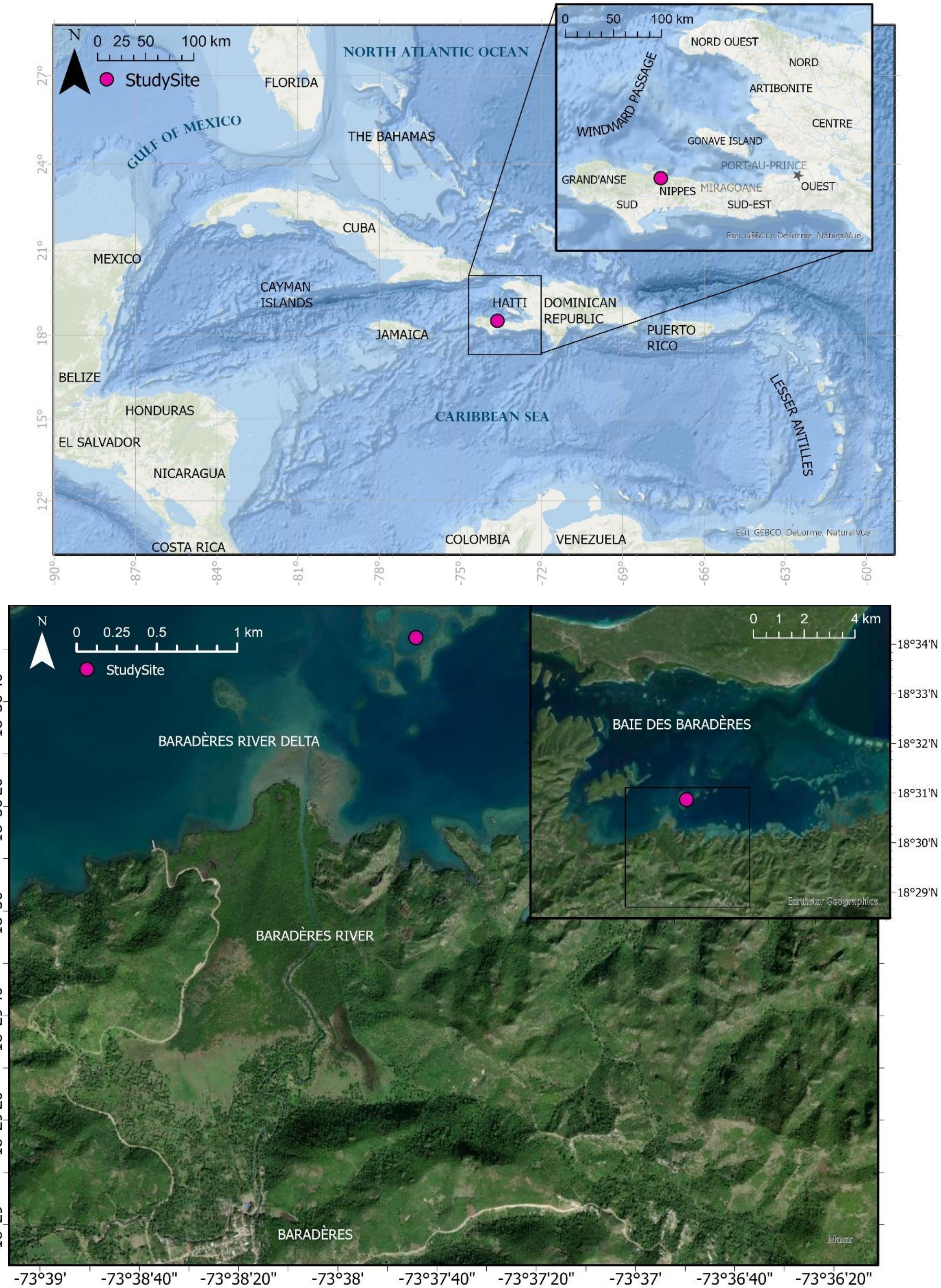

Figure 3.2: Coring site within the Caribbean (above), and relative to the Baradères River Delta, the Baradères River, and the town of Baradères (below). Maps created with ArcGIS.

3.1.1. Climate Proxies from Sediment Cores

The most common climate proxies come from ice cores, tree rings, sub-fossil pollen, boreholes, corals, carbonate speleothems, and lake and marine sediments (Oliva et al., 2017). Common proxy techniques from sediment cores include grain size analysis, loss on ignition (LOI), and foraminiferal, pollen, and charcoal assemblages, while in recent decades, researchers have begun employing more advanced geochemical techniques, such as tree cellulose/speleothem isotopic analysis, stable isotopic geochemistry and X-ray fluorescence (XRF) core scanning. Many paleo-studies employ a multi-proxy technique on marine and lacustrine sediment cores to create reconstructions of Holocene climates (Denommee et al., 2014; Donnelly et al., 2015; Gischler et al., 2008; C. S. Lane et al., 2011; Liu & Fearn, 2000; Peros et al., 2007; van Hengstum et al., 2014, 2016; Wallace et al., 2019). In this study, we use grain-size analysis, LOI, and XRF core scanning data analysis to create a multi-proxy paleoenvironmental reconstruction.

3.1.2. Suitability of Blue Holes for Paleo study site

To successfully reconstruct a paleoclimate record in a marine setting, it is important to choose a study site behind barrier islands or other low energy environments, ideal for tempestite (storm overwash layer) deposits, and varved sediment formation (Donnelly et al., 2004). In the Greater Antilles, karst is developed in a wide variety of carbonates, ranging from deep to shallow water facies with some reef-type structures. Tectonic activity in this region causes stress which can result in vertical dissolution (Kueny & Day, 1998). For example, elongated caves are often formed via tectonic movement circulating freshwater through subaerial exposure on faults and folds (Gischler, 2011). Coastal Kast Basins (CKBs) such as sinkholes, blue holes, and underwater caves are common on carbonate bedrock and often contain important sedimentary data that is generally not preserved well in these landscapes (van Hengstum et al., 2014).

Blue holes are CKB's located in shallow waters that are usually visually distinguishable from above due to the contrast between the dark blue sinkhole opening and the light blue surrounding sea floor. Blue holes develop from the cave development and subsequent ceiling collapse of carbonate platforms. In recent decades, blue holes have generated environmental and climatological records spanning the last Glacial Maximum until present (Grimm et al., 1993; Steadman et al., 2007; van Hengstum et al., 2020), including Holocene aquifer hydrodynamics (van Hengstum et al., 2011) and paleotempestological records (Brandon et al., 2014; Donnelly et al., 2015; P. Lane et al., 2011; van Hengstum et al., 2014, 2016). A famous example is the blue hole in the lagoon of the Lighthouse Reef Atoll in Belize, which has been used in several high-resolution Holocene climate reconstructions (*e.g.,* Denommee et al., 2014; Gischler et al., 2008; Schmitt et al., 2020).

Our coring site is in a CKB that falls within the category of "blue hole" as it can be easily viewed via arial imagery, in a small bay off the northern coast of Haiti's southwestern peninsula (Figure 3.2). CKBs are ideal for paleoclimatological research because after deposition, low benthic energy limits bioturbation and protects sediments from surface wave action (Gischler et al., 2008). Furthermore, adjacent reefs, beaches, and deltas provide abundant sediment supply (Wallace et al., 2019). In this case, the CKB is protected from oceanic wave action by the Baradères Bay, and is in close proximity to the Baradères River delta, which has impacted the rate of sedimentation during and since its formation.

The abundant accommodation space of relatively deep CKBs often results in depositional environments with exceptionally high sedimentation rates with high-level fine-grained sediment flows (Wallace et al., 2019). Typical sedimentation rates in North Atlantic deep ocean basins are about 2-3 cm per 1000 years (Keigwin & Jones, 1989), but at this site, the overall sedimentation rate is ~105 cm per 1000 years (based on our core of length 896 cm and maximum age of ~8500 years).

3.1.3. Field methods

The field program during which the sediment cores were obtained took place as part of a scientific cruise aboard the R/V Alucia (Figure 3.3) in May 2016 by Dr. Jeffrey Donnelly (Woods Hole Oceanographic Institution), Dr. Andrea Hawkes (University of North Carolina Wilmington), Dr. Pete van Hengstrum (Texas A&M University at Galveston), Dr. Jonathan Woodruff (University of Massachusetts Amherst), Dr. Elizabeth Wallace (Rice University), and Dr. Chris Maio (University of Alaska Fairbanks). Once in the bay, the coring was accomplished from a 20-foot pontoon boat, the R/V Arenaria (Figure 3.4). A CHIRP transect was performed across the widest section of the bay, and the bathymetry was studied using a sub-bottom profiler. Sediment cores HATCD1 and D2 were collected using a Rossfelder vibracorer- the former in a 3-inch polytube, the latter a 3-inch Aluminum tube. The continuous cores were then sectioned for transportation and split. One half of each section was sent to Dr. Donnelly's Coastal Systems Laboratory at the WHOI in Woods Hole, Massachusetts, and stored as a control. The other half was sent to Dr. Peros' Climate Change Research Laboratory at Bishop's University in Lennoxville, Quebec. This is the core which was used for this project.

Figure 3.3: The research vessel R/V Alucia, Woods Hole Oceanographic Institution (https://www.whoi.edu/website/alucia/).

Figure 3.4: Coring in Baradères Bay, Haiti. Our research partners can be seen on the R/V Arenaria surrounded by curious locals. Picture supplied by colleagues at WHOI.

3.2 Laboratory Methods

3.2.1. Grain-Size Analysis and Loss on Ignition (LOI)

The properties of sediment including grain size and grain shape are important for identifying changes in a depositional environment. Grain-size analysis is widely used within earth and archaeological sciences to reveal indications of past environmental changes, particularly within the context of energy transport conditions (Donnelly & Woodruff, 2007; Liu, 2004; Oliva et al, 2017). Many sedimentary properties including colour, texture, density, permeability, and wetness are directly influenced by particle grain size, shape, orientation, and grain-to-grain relation (López, 2016). For example, darker sediment usually relates to silt and clay richness whereas lighter sediment is generally rich in biogenic silica and carbonate (Haug et al., 2001).

Changes in composition and concentrations of river-suspended sediment offer information on the rate and volume of erosion and transport of organic and inorganic terrestrial materials from a landscape, which may result from ecosystem processes and/or human disturbance (Warrick & Rubin, 2007). Water runoff in southwestern Haiti is generally exposed to calcium carbonate rock. Calcite weathering is particularly pronounced on small Caribbean islands with significant land use (Rad et al., 2006, 2011) and tropical storms (Rad et al., 2013). Weathering is enhanced in the study area by two major factors; firstly, the warm climate accelerates chemical reactions, and secondly, the steep slopes of mountainous limestone rivers are likely to have exposed bedrock (McGillis et al., 2015).

Furthermore, when high energy events occur, such as hurricanes, sediment is transported into coastal basins with much higher energy than under "normal" sedimentation. Thus, the composition of sediment changes during these events. Using the NOAA best track dataset (NOAA, 2009), event beds in modern sections of sediment cores can be attributed to well-documented storms that passed close to a site, which can then be used to interpret the signal for storm surges at a specific site. This interpretation can often be applied to large portions of (or up to the entire) core length.

The most common method for grain-size analysis is a quantitative method of sieving specified portions of sediment at a high-resolution (usually 1 cm) to separate particles into size fractions (usually the cut-off between sand and silt is considered to be 63 µm). This way, we can establish the percent sand (>63 µm) versus percent silt (<63 µm) in each subsample, which can be interpreted in terms of energy transport conditions throughout time (Brandon et al., 2014; McCloskey & Liu, 2013). For example, sudden peaks in the fraction of silt versus sand within layers of the core can be indicative of abrupt sediment transport caused by flash floods and overwash deposits into coastal water systems, especially ones with small mountainous rivers through low-lying plains such as the Baradères river.

Before performing grain-size procedure, core sections were inspected visually, making notes of any changes in colour and texture, with reference to the Munsell Soil Color Chart. The core was sub-sampled at 1 cm intervals, with approximately 2 grams of wet sediment collected, weighed, and dried in crucibles. A standard 4 decimal place lab scale was used to weigh the crucibles. Crucibles with wet sediment were dried in an oven at 110 degrees Celsius overnight, or until completely dry. The next day, crucibles were reweighed with the dry sediment in them. This allowed us to calculate the water loss, and thus use percent water as additional proxy. Next, the sub-samples were sieved through a 63 µm sieve so that only sand remained. The material that did not pass through the sieve was collected, replaced into its respective crucible, and dried again overnight or until fully dry. Finally, the crucibles were reweighed, along with the remaining dried sand, carefully removing any rocks or shells greater than half a centimeter in diameter. The weight of these rocks and shells was noted to use as an additional proxy. Using this data, the weight of the sand was subtracted from the original material and crucible to calculate the percent sand in each subsample, which was used as a proxy for changes in sediment influx.

Loss-on-ignition (LOI) was performed at 3 cm intervals throughout the core, in a similar manner to grain-size analysis but with the aim of quantifying organic matter, carbonate, and silicate content as a function of dry sediment weight. This involved drying in an oven at 105°C, followed by combustion in a high-temperature furnace at 550°C, and then 950°C, followed by weighing the residue to estimate mass lost at each step. Organic matter can act as a proxy for several things including hurricane-induced flooding, although the signal may be different at different sites, and throughout cores. In our core, increased periods or organic matter might indicate increased river discharge from flooded plains bringing increased OM through the river system into the delta. Similarly, abrupt peaks in % sand may indicate large amounts of discharge from the river into the basin through storm-related flooding.

3.2.2. XRF Core Scanning

Within the last couple decades, X-Ray Fluorescence (XRF) core scanning has become increasingly prominent in the analysis of marine sediments (De Boer et al., 2014). An XRF scanner is a computer-controlled carriage that slides sediment cores past a camera and X-ray source, capturing images of the sediment at a very high resolution. Each element releases radiation with a distinguishable wavelength that can be identified by the XRF in the unit of counts per second, or cps. The Cox Analytical Systems ITRAX XRF core scanning system is commonly used (Boldt et al., 2010; Donnelly & Woodruff, 2007; Toomey et al., 2013) as it provides sub-mm scale resolution of up to 62 elements, in addition to core x-radiography.

XRF data enables us to support grain-size data, especially in cases where visual evidence is not distinguishable (Toomey et al., 2013). For example, several researchers (McCloskey & Liu, 2013; Naquin et al., 2014) interpreted decreases in terrestrially-derived elements (Ti, Fe, and Zn) as indicators of TC overwash in the Atlantic Basin and used this to support LOI and grain size data previously generated for their cores. Peros et al. (2017) provided high-resolution evidence of the 8.2 kyr event in the Caribbean by identifying peaks in Cl and Br which are attributed to increased evaporation due to regional drying. XRF data has also been used as a method of detection of a change in element composition linked to past human land-use or industrial activities (Boldt et al., 2010). However, while this approach is often effective in locations such as northeastern United States (*e.g.,* Donnelly et al., 2015) where human impacts have been continuous and well documented, it is somewhat more challenging in areas such as the Circum-Caribbean, where land-use history is not well known.

Generally speaking, iron (Fe), titanium (Ti), and Silicon (Si) as well as alkali metals such as rubidium (Rb), and potassium (K) are prominent in clay minerals whereas elements such as copper (Cu), zinc (Zn), lead (Pb), chromium (Cr), nickel (Ni) and cadmium (Cd) characterize anthropogenic imprints (Schreiber et al., 2014). Calcium (Ca) can be used as a salinity indicator as it is strongly marine driven and could indicate occurrence of carbonate precipitation in the sediment column (Schreiber et al., 2014). Influxes in K and Ti have been corelated to higher terrestrial discharge into basins through either higher precipitation/runoff or through high coastal erosion due to storm surges and currents (Rothwell & Croudace, 2015b). Similarly, ratios of Ti/Ca and Fe/Ca have been used in marine environments as indicators of terrestrial input (Gregory et al., 2015). Mn/Fe is used as an assessment of redox conditions, as Mn is mobile under sub-oxic conditions and is separated from Fe during diagenesis (Marsh et al., 2007), while K/Ti and Rb/Sr have been used to demonstrate changes in weathering regimes (Yang et al., 2020). Additionally, the ratio of Sr/Ca has been used as a proxy for temperature history validating the Little Ice Age and other SST anomalies in the Caribbean (Flannery & Poore, 2013; Haase-Schramm et al., 2003; Kilbourne et al., 2008).

The most important feature of XRF scanning on the advancement of paleoclimatological research is that it does not damage the core whatsoever, meaning that other researchers can sample the same sediment to pursue other proxies to further their research. This can increase the interpretability and utility of long timescale cores and increase their cost efficiency. Moreover, with this recent technology we are now able to generate high-quality, high-resolution geochemical records very quickly, which can greatly advance the speed and spatial resolution with which upcoming research can be produced (Rothwell & Croudace, 2015b).

The use of XRF element indicators for this study lies of the assumption that they could represent variations due to long-term and shorter timescale climate change and provide evidence of element compositions representing environmental variations to support grain size data. There is also the potential that they could represent TC-driven precipitation events (Oliva et al., 2017) and anthropogenic activities. For this sediment core, our research partners at the WHOI have produced 1-mm resolution XRF data using an ITRAX™ system. The elemental and grain-size data were analyzed using principal component analysis (PCA), using the "FactoMineR" package v.2.0 (Lê et al., 2008) and visualized using the "factoextra" package v.3.6.3 (Kassambara & Mundt, 2020).

3.3. Analytical Methods

3.3.1. Age-Depth Modeling

Within a vertical sediment core, proxies are treated as estimates of environmental and climatological conditions at the time that the sediment of those depths was deposited. It is therefore essential to establish reliable relationships between these depths and their ages. Age-depth models are created using the exponential radioactive decay (half-life) of radioactive isotopes to estimate how much time has passed since the death of organic material. A curve is then fitted to the radiocarbon data and interpolated to estimate an age for every depth of the core. Radiocarbon (C-14) is produced in the upper atmosphere and assimilated into plants and animals through photosynthesis and respiration. The concentration of C-14 in an organism is in equilibrium with the atmosphere, because as old cells die, they are replaced. When organisms die, replacement of the dead C-14 cells stops, and the C-14 begins to decay as a function of time. Materials containing organic matter such as wood, twigs/plant matter, seeds, bivalve shells, and corals can be used to date layers of sediment (Blaauw & Christen, 2011; De Boer et al., 2014; Gregory et al., 2015; Reimer et al., 2013). If no suitable organic matter of terrestrial origin is discovered in the core, marine specimens or bulk sediment may be used for dating (Peros et al., 2007). We used Bacon v2.5.6 (Blaauw et al., 2021; Blaauw & Christen, 2011) to generate the age-depth model for Baradères Bay.

C-14 years do not directly equate to calendar years because atmospheric C-14 concentration varies through time due to changes in the production rate, caused by geomagnetic and solar modulation of the cosmic-ray flux, and the carbon cycle (Reimer et al., 2013). Radiocarbon is continually being formed in the atmosphere, and in theory, its concentration in the atmosphere, biosphere, and oceans should be equivalent. However, due to the marine reservoir effect, the C-14 concentration is not the same in terrestrial and marine organisms. Terrestrial organisms primarily get carbon from atmospheric carbon dioxide, while marine organisms uptake carbon that has already undergone radioactive decay during long periods in the deep ocean (Ulm, 2006). This means that two organisms could have the same age yet produce different radiocarbon dates (organisms from marine environments usually exhibit older apparent ages).

The marine reservoir effect varies globally as it depends on local and regional factors, but these effects can be particularly powerful in regions like the Caribbean where there is a lot of carbonate, and in estuarine environments where there is interaction and mixing between terrestrial and marine reservoirs, and where 'old' carbonates from the deep ocean can circulate upward (Ulm, 2006). Hence, a calibration is required, which, to be accurate, should be based on an absolutely dated record that has carbon incorporated directly from the atmosphere at the time of formation. The IntCal20 and Marine20 calibration curves represent a hypothetical "global" marine reservoir, which serves as a baseline for regional oceanic variations. We used the IntCal20 (Reimer et al., 2020) dataset to calibrate the radiocarbon dates for the age-depth model used in this study, and we will use the Marine20 calibration (Heaton et al., 2020) to incorporate marine macrofossils into future studies of core HATC1 as additional data becomes available.

3.3.2. Statistical Analysis

PCA is a multivariate linear transformation used on large datasets to reduce dimensionality and identify correlated variables, while minimizing information loss and increasing interpretability (Jollife & Cadima, 2016). Where many variables correlate with one another, they will all load highly on the same principal component. Each principal component sums up a certain percentage of the total variation in the dataset (Hayden, 2018). Principal components successively maximize variance and can be found from the eigenvalues/eigenvectors of a covariance matrix (Jollife & Cadima, 2016). The first principal component explains the most substantial variance in the data (i.e. the eigenvector with the highest eigenvalue), while subsequent components explain lesser variance (i.e., lower eigenvalues). This essentially transforms a set of x correlated variables over y samples to a set of p uncorrelated principal components over the same samples (Hayden, 2018).

Regarding the XRF data, the element counts at the beginning and end of each core section were either uncharacteristically high or low, which can be attributed to mixing/squishing of material during core splitting and errors associated with the XRF scanner. To overcome this challenge and obtain more accurate/continuous curves, we deleted such entries at the top and bottom of each core section, as well as any entry throughout the core which had a validity of 0 in the XRF scan.

Standardization of the data was required to allow comparison between different resolution and units. Since grain-size had a different resolution (1 cm) than the XRF data (1 mm), we first resampled the XRF data to the cm scale by filtering every 10^{th} row of data from the XRF database. In cases where the 10^{th} mm was not valid, we used the closest values either below or above within ± 0.5 cm. In the case of invalid data spanning greater than 0.5 cm, we took the average of the two closest values. A separate database was created using the mm-resolution XRF data to examine in more depth short-duration signals, especially in the most recent ~2900 years, when sedimentation rate was fast, thus providing a very high-resolution record. The cm-resolution data can be useful to reduce noise and produce smoother curves to reveal more general trends (see Appendix B).

Next, grain-size and XRF data were standardized for comparison using the following equation:

$$\frac{x_i - mean(x)}{sd(x)} \qquad \text{(Eq. 1)}$$

*Where **Xi** is the value, **mean(x)** is the mean of x values and **sd(x)** is the standard deviation of the data*.

By default, the function PCA() in FactoMineR standardizes data automatically in this fashion, thus removing the influence of extreme values on PCA (Kassambara, 2017; Schreiber et al., 2014).

Results and analysis are presented in stratigraphic zones. The decision of where these zones should begin and end is not straightforward. Numerous methods exist to do so, and there is no consensus about how to deal with such highly dimensional datasets in a statistical manner (Schroeter et al., 2020). Many studies analyze multi-proxy data qualitatively, based solely on visually identifying changes within the proxy data and matching these to other proxy records (*e.g.*, McCloskey & Liu, 2012; Naquin et al., 2014: Peros et al., 2017). While statistical analyses are not necessarily required, they can be useful in determining where visually identified zones should start and end (K. D. Bennett, 1996).

Zones and sub-zones were identified using a combination of visual changes in XRF and grain-size curves, the results of PCA, and stratigraphically-constrained cluster analysis with an incremental sum of squares (CONISS) method of the chclust function from the package "rioja" v.0.9-26, where "d" is a dissimilarity structure produced by the EUCLIDEAN distance function (Juggins, 2020). The number of zones was determined by comparing results to broken stick models (K. D. Bennett, 1996), both for the whole core, and for sub-zones within each of the five major zones.

CHAPTER 4:

Multi-Proxy ~8500 Year Paleoenvironmental Reconstruction of Baie des Baradères, Haiti

Key words: Paleoclimate, Caribbean, Haiti, sediment core, XRF core scanning, Grain-Size Analysis, LOI, PCA, island ecosystems, anthropogenic activity, hurricanes, ITCZ

4.1. Introduction

Paleoenvironmental sediment core-based research has implications for understanding environmental and anthropogenic variables including prevailing oceanographic conditions, climatic anomalies, human-ecosystem interactions, and natural events. However, to understand the long-timescale variations that occurred to the environment and climate throughout the Holocene, high-resolution millennial-scale records with high spatial resolution, which record both climate and human disturbances and subsequent responses are necessary. This project identifies quantifiable environmental changes in the sediment record relating to climatological shifts and human activities both in the historic and prehistoric eras in a region that is both understudied and highly sensitive to the effects of storms, sea level change, tectonics, and anthropogenic impacts.

Anthropogenic disturbances to ecosystems can last a long time, and have significant influences on their functions, networks, and processes (Binford et al., 1987). For example, the cycles of macronutrients such as phosphorous and nitrogen have been fundamentally altered by human activities such as livestock and land management (Goyette et al., 2018). Primary human occupation of the Circum-Caribbean represents one of the most remarkable but least understood patterns of settlement dispersion is history (Napolitano et al., 2019), with the timing and direction of these movements still debated by the paleoenvironmental and archaeological communities. This can often make it a challenging and complex task to distinguish between climate and human signals in the paleorecord, which can in turn make it challenging to relate modern climate change responses to specific long- and short-term environmental and human trends. Further evidence is required to validate when and how early people moved through and altered the Caribbean environment, and therefore better interpret new and existing paleoenvironmental records. This study provides an excellent opportunity to examine the complex dynamics between human impacts, changing hydrological and climatological conditions, and island ecosystem vulnerability.

Human impact on Caribbean karst landscapes can be characterized by a cyclical impact-process-consequence model involving human activity, landscape transformations/responses, and resulting obstacles for human habitation (Day, 2010). This can be illustrated by reference to the karst hydrologic system, in which "forest clearance, agriculture, groundwater abstraction and modification of surface drainage courses has resulted in increased runoff, decreased infiltration, increased surface sediment transport, and decreased spring discharge" (Day, 2010), which has exposed ecosystems and communities in karst environments to risks through increased flood susceptibility, aridity of springs and accelerated soil erosion.

Haiti is highly vulnerable to numerous environmental threats including sea level rise, droughts, floods, hurricanes, earthquakes, and landslides. Furthermore, the southern peninsula of the country lies directly along the boundary of two tectonic plates, as well as upon several active faults and folds, resulting in frequent and high-magnitude seismic movement and earthquakes (Hashimoto et al., 2011). The country is also situated in a geographical location that has an important relationship with the Intertropical Convergence Zone (ITCZ), potentially making it sensitive to droughts and changes in hydrological regimes (Schneider et al., 2014). Additionally, most Atlantic Tropical Cyclones (TCs) form from easterly waves propagating westward toward the tropical North Atlantic and Caribbean Sea along the northern edge of the ITCZ (primarily between 10° and 20°N), meaning that the country falls within the North Atlantic "hurricane belt", and is frequently impacted by TCs of varying intensity (Goldenberg et al., 2001). Changes in shorter timescale atmospheric dynamics such as the NAO (Trouet et al., 2009), the AMO (Gray et al., 2004), and the ENSO (Li et al., 2013) have also played a major role on hydrological regimes including hurricanes and periods of drought. Using paleoenvironmental data to assess pre-observational climatological variation is imperative to understanding how these climate factors will change (and are already changing) with modern global warming. Despite this, high-resolution paleoenvironmental records spanning millennial timescales are rare, especially on the island of Hispaniola, where there are few paleolimnological sites, and only one paleotempestological (hurricane) study site (Leblanc et al., 2017).

This project analyzes a ~9-meter-long marine sediment core, "HATC1", that has a basal radiocarbon age of ~8500 cal BP, using grain-size analysis, X-Ray Fluorescence (XRF) core scanning data, and Loss on Ignition (LOI) as proxies for environmental variations relating to climate changes and human activities. The core was collected from a coastal karst basin (CKB) (also referred to as a blue hole) in Baradères Bay, approximately one km from the Baradères river delta on Haiti's southwestern peninsula.

4.1.1. Caribbean Paleoclimate in the Holocene

Sea level rise has been one of the most prevalent natural drivers of environmental change since the last deglaciation and throughout the Holocene. In general, relative sea level (RSL) rise in North America was greatest between about 10,000 and 8000 cal BP when the Laurentide ice sheet was melting rapidly (Khan et al., 2017; Milne & Peros, 2013). Late Pleistocene and early Holocene RSL change in the Caribbean was dominated by eustatic sea level rise (Khan et al., 2017). By

~8000-6000 cal BP, the eustatic component slowed and much of the subsequent RSL rise was driven by the continual collapse of the peripheral bulge, which lead to regional land subsidence and continued sea level rise, albeit at a much slower rate compared to the early Holocene (Milne & Peros, 2013).

Another prominent forcing mechanism of Caribbean millennial-timescale climate change in the Caribbean is the varying parameters of Milankovitch cycles relating to earth's orbit around the sun, which cause changes to the seasonal cycle of solar irradiance and shifts in the occurrence of maximum average insolation throughout the year, (Lorenz et al., 2006). Between ~8000-6000 cal BP boreal summer occurred near perihelion. Gradual, long-term increases in solar insolation in the early to middle Holocene likely resulted in warmer SSTs in the Caribbean Sea and a northerly mean boreal summer position of the ITCZ, which resulted in increased precipitation (Haug et al., 2001; Schneider et al., 2014). Humid conditions at this time have been verified from several proxies including micropaleontological indicators from a sinkhole in the Bahamas (van Hengstum et al., 2018) and oxygen isotopes from Lake Miragoâne, Haiti (Hodell et al., 1991). An exception to this condition is the 8.2 kyr event, which was a dry anomaly recorded in numerous proxies, including a sediment core from a sinkhole in Cuba, which was characterized by abrupt peaks in Cl and Br between ~8120 and ~8275 cal BP (Peros et al., 2017).

There has been an overall drying pattern in the northern Caribbean over the last ~5000 years, associated with a southerly migration of the ITCZ (Fensterer et al., 2013; Haug et al., 2001; Higuera-Gundy et al., 1999; Hodell et al., 1991), with lake levels remaining relatively high, though declining gradually though the middle Holocene, with an abrupt acceleration at ~3.2-3.4 kyr BP (Hodell et al., 1991; Kennedy et al., 2006). There is lack of uniformity among paleoclimate records after ~3000 cal BP in the Circum-Caribbean largely due to greater inter and intra-regional variability, as well as human disturbances. However, most records agree that between ~3400 and ~2500 cal BP there was an abrupt shift to drier conditions with a trend toward higher evaporation rates and lower lake levels (van Hengstum et al., 2018), and after ~3400 cal BP, moist-forest taxa diminished, and lake levels remained low until the present, with only brief returns to moister conditions (ie. ~1200-900 cal BP) (Curtis & Hodell, 1993; Higuera-Gundy et al., 1999; Hodell et al., 1991; Kennedy et al., 2006). Additionally, the North Atlantic Basin has shown dramatic multidecadal/centennial variations in hurricane activity in the Holocene, generally with enhanced hurricane activity during warmer periods. For example, from 2500 to 1000 cal BP the North Atlantic Basin experienced a period of intense hurricane activity related to a more northern ITCZ position compared to the present, but not as far north as its position in the middle Holocene (van Hengstum et al., 2016).

Early in the common era (100-500 CE) the climate was characterized by a warm interval (known as the Roman Warm Period), with a corresponding positive anomaly in SST (Schmitt et al., 2020). Subsequently, the following time interval of 500-900 CE was characterized by global cooling, known as the Dark Ages Cold Period, with fewer positive SST anomalies globally and regionally. The Medieval Warm Period (900-1400 CE) is the most recent past warm climate interval, with SST anomalies surpassing present-day temperatures (Schmitt et al., 2020). The Little Ice Age from ~1400-1850 CE, is the most recent cold interval that correlates with significant negative global and regional SST anomalies with surface ocean temperatures distinctly below present conditions (Black et al., 2007; Kilbourne et al., 2008; Schmitt et al., 2020). In recent decades and centuries there has been an increase in global and relative SST, but with the increase in Atlantic SST being greater than in the tropics (Black et al., 2007; Ramsay & Sobel, 2011).

It is predicted that in the Caribbean, the effects of modern global warming will lead to increasing air and water temperatures, accompanied by rising sea levels and more variable weather patterns, including decreasing total annual precipitations with increasing frequency of extreme events such as droughts and hurricanes (Day, 2010; Nurse & Sem, 2001; Pelling & Uitto, 2001). The most significant and immediate consequences will likely occur to coastal locations, where socioeconomic activities, infrastructure, and population are concentrated, and will relate to the rising sea level, changing hydrological cycles, rainfall regimes, soil moisture budgets, prevailing wind speeds/directions, and patterns of wave action (Nurse & Sem, 2001).

4.1.2. Human Settlement and Impacts

During the Holocene, the insular Caribbean experienced more mammalian extinction than any other global region. While this appears to be partly due to habitat loss induced by sea level rise (Cooke et al., 2017; Dávalos & Turvey, 2012), most postglacial species losses of island faunas are associated with the regional arrival of prehistoric settlers (Cooke et al., 2017). Archeologists recognize four waves of settlement in this region: Lithic (~7000-4000 cal BP), Archaic (~5000-2000 cal BP), Ceramic (~2500 cal BP in some area, somewhat later in others), and historic (since 1492 CE, i.e. ~500 cal BP) (Cooke et al., 2017), although early sites were usually near coasts and were often abandoned and recolonized, suggesting non-linear population growth (Rick et al., 2013). The environmental footprint and subsequent impact on terrestrial and coastal landscapes increased with each successive migration wave, with early settlers leaving a limited signal on the environment, and more recent human activities causing long-term or even permanent alterations.

Archaeological sites signify human settlements on Hispaniola as early as the Lithic period (Vignier II, ~6100 cal BP; Moore 1991), although none appear to be on southern peninsula of Haiti, whose large deposits of Eocene limestone apparently did not yield the type of flint desired by the first settlers (Moore, 1991). Sites from Archaic peoples are identified on Hispaniola as early as ~5.2 cal kyr BP, mostly on shorelines suggesting seasonal occupation, but with increasing evidence of land management and fire use to convert natural environments into agricultural landscapes (Keegan, 1994). Archaic people introduced crops such as avocado, wild fig, primrose, and wild beans to Hispaniola and other Caribbean islands (Cooke et al., 2017; Fitzpatrick, 2015).

Settlements identified by archeologists as belonging to the "Ceramic culture" demonstrated that such groups established sedentary villages further inland, usually within 3 km of the shore and often along rivers, and systematically practiced horticulture and agriculture (Moore, 1991; Rick et al., 2013). They regularly travelled between bays and neighbouring islands for trade, including making daily trips between the western coast of Hispaniola and Puerto Rico, the southern and western tips of southwestern Haiti's peninsula and Jamaica's eastern coast, and between Haiti and eastern Cuba via the Windward Passage (Rouse & Moore, 1984). The Ceramic-era peoples introduced dogs, guinea pigs, and other mammals to several Caribbean islands along with a wide variety of crops including beans, tobacco, chilis, peanuts, and guava (Cooke et al., 2017). This wave of settlement has been linked to drastic landscape changes, unprecedented in scale, with long lasting effects on terrestrial and coastal marine ecosystems (Rick et al., 2013).

During the "historic" era, Caribbean island ecosystems underwent significant landscape transformations in the centuries following the arrival of Europeans, with poor land use and minimal land management practices leading to degraded or destroyed soils, vegetation, and hydrological systems (Lewis & Coffey, 1985). The prevalence of deforestation in Haiti is almost entirely due to the production, distribution, and consumption of firewood and charcoal (Stevenson, 1989), as well as the burning of household solid waste (McGillis et al., 2015). The burning and creation of charcoal is often near river beds (McGillis et al., 2015), with fires resulting in increased sediment discharge (Warrick & Rubin, 2007). Today, land degradation due to deforestation and consequent soil erosion are serious problems in the drainage systems of Hispaniola, which create problems for agricultural production, and food insecurity (Brenner & Binford, 1988). Soil infertility is one of the most substantial factors contributing to chronic poverty and malnutrition in Haiti (Bargout & Raizada, 2013).

4.1.3. Site Description

Haiti shares the island of Hispaniola with the Dominican Republic and occupies an area of about 28,000 km^2. Haiti occupies the western third of the island, with the Dominican Republic to its east, and Cuba approximately 80 km to its west, across the Windward Passage. The climate is Tropical savanna, and the landscape is mountainous, with mountain ranges separated by fertile but overpopulated lowlands, which are susceptible to flooding (Hadden & Minson, 2010). Hispaniola's major plant communities are tropical lowland dry forests, highland mesic and pine forests, and coastal mangrove swamps (Holdridge, 1945). Haiti's southern peninsula lacks modern vegetational surveys but is generally dominated by tropical dry forests on coastal lowlands and mesic plant and pine forests on mountainous slopes (Judd, 1987). Northeast trade winds drive the wet season from April to November, and because the country lies within the North Atlantic Basin's so called "hurricane belt", it is subject to tropical storms from June to October (Knowles et al., 1999).

The study site is in Baie des Baradères, approximately one km from the Baradères River Delta, which was created through sediment discharge accumulating from the Baradères River. Baradères Bay covers ~7 km^2 and has a maximum water depth of 29 meters. The bay is presently surrounded by mangroves and is protected by a chain of islets that stretch between the towns of Petit-Trou-de-Nippes and Grand-Boucan. The main basin is hydrologically connected to a smaller secondary basin west of the coring site through a very shallow channel, typically 1-5m depth. The core was collected from a blue hole with vertical depth of approximately 11.5 m, at coordinates 18.514571° N, 73.628903° W (Figure 4.1). Site selection was based on proximity to the delta, and the relatively low energy of the basin, making the sediment likely to preserve both terrestrial land-use changes and high energy events such as flooding, hurricanes, and earthquakes.

The Baradères River is about 45 km long and eventually disappears into depressed limestone (Knowles et al., 1999). The river crosses the town of Baradères, whose population was 47,060 in 2015 (IHSI 2015). The local economy is extremely dependent on its river, as locals, as well as tourists, use it for transportation and trade (Bertrand, 2017). After intense storms or heavy rains, the river rises rapidly- with swift currents and floating debris often damaging or even destroying waterways (Knowles et al., 1999). Flooding is one of the main risks faced by the Baradères community. In an effort to mitigate the risks of floods, projects are ongoing to divert the river by digging a new river-bed and constructing bank reinforcements (Haiti-Politic, 2020; IciHaiti, 2021a, 2021b).

Human impacts on the terrestrial and marine karstic ecosystems in this region have been long-lasting and severe, particularly from exploitation of natural resources (primarily through agricultural and deforestation practices), contamination of water supplies, urbanization and quarrying (Day, 2010). In addition to human influences, a system of interrelated natural processes control the biogeochemical cycles (hydrometrical, seismological, geochemical) in the rivers of southwestern Haiti, and contribute to variations in chemical transport and fluvial discharge (McGillis et al., 2015)

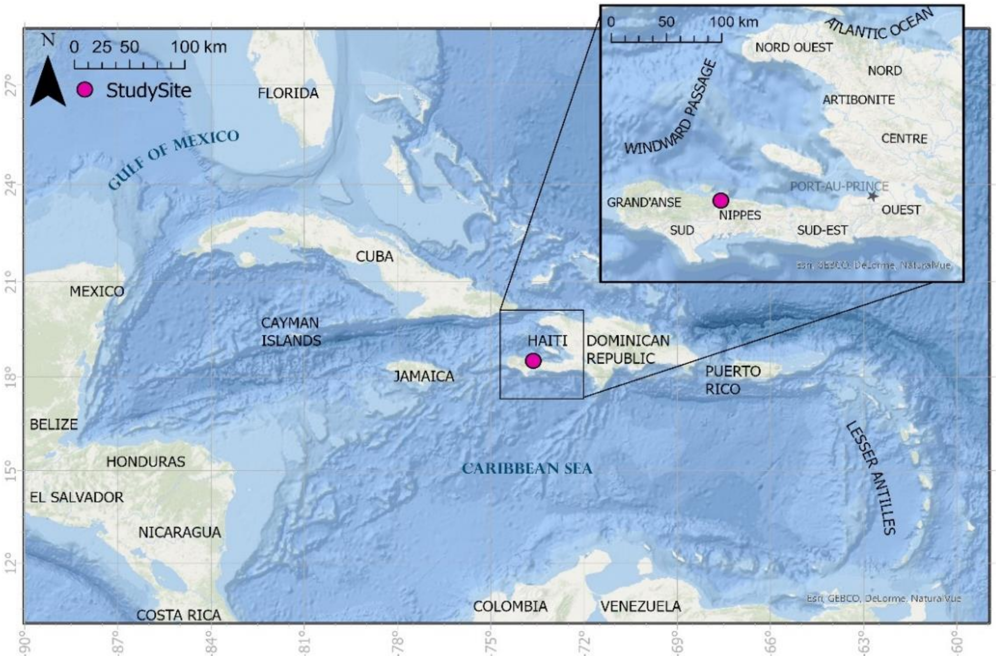

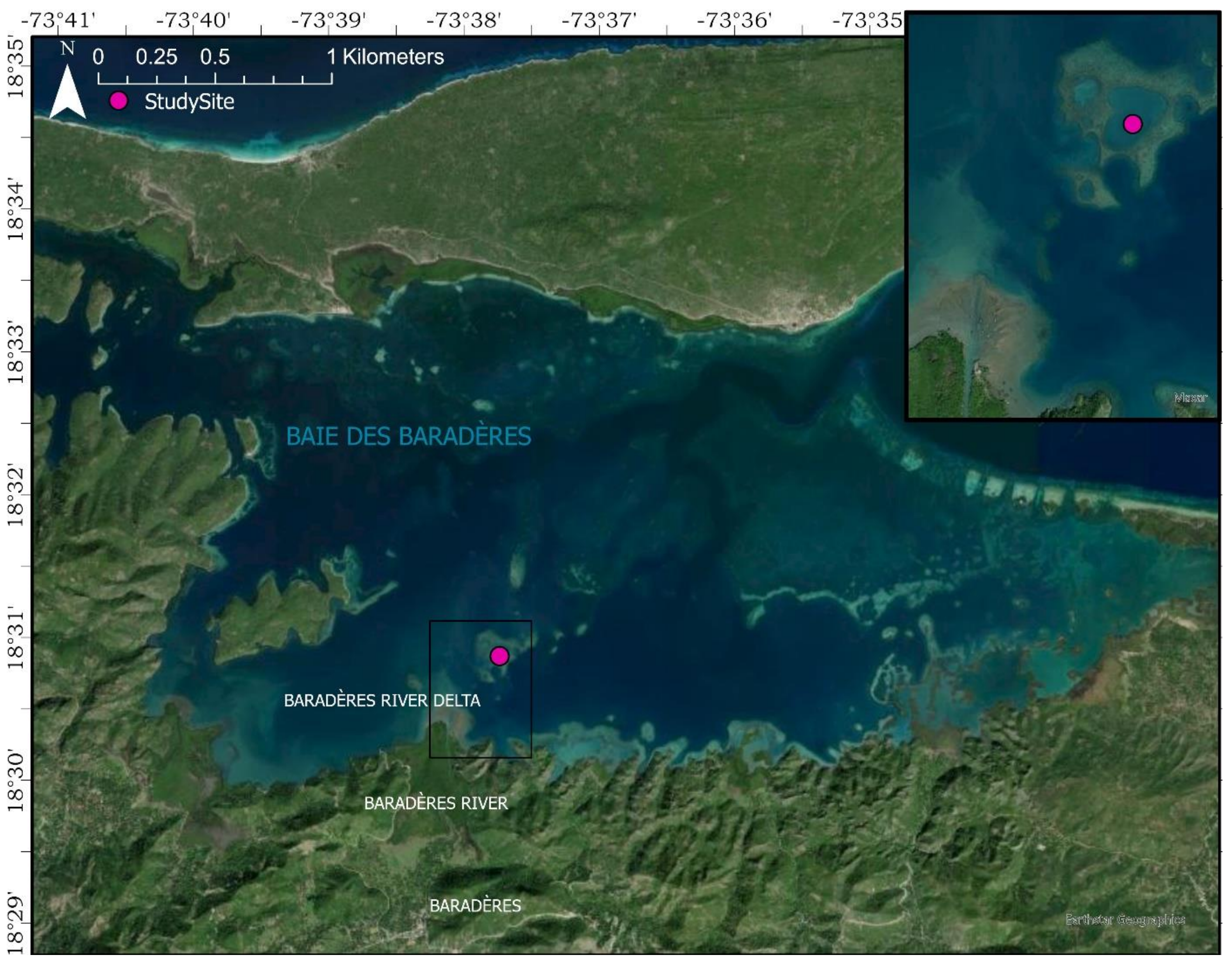

Figure 4.1: Regional map of coring site within the Caribbean (above) with an inset of Haiti, and within Baie des Baradères (below) with an inset of the CKB. Maps created using ArcGIS.

4.2. Methods

4.2.1. Field Methods

Sediment cores HATCI (D1 and D2) were collected during a scientific cruise in May 2016 lead by Dr. Jeffrey Donnelly (WHOI). Once in Baradères bay, coring was performed with a Rossfelder vibracorer from a 20-foot pontoon boat. Core HATC1 D1 is 145 cm long and was collected in a 3-inch poly tube as a control directly beside core HATC1 D2, which is a continuous 896 cm core and was collected in a 3-inch aluminum tube. A CHIRP sonar transect was performed across the widest section of the bay to study the bathymetry and sub-bottom stratigraphy. Several other cores were collected at different areas of the bay which are being studied by our co-authors and their graduate students, and which will eventually be combined with this study to provide a more elaborate regional environmental reconstruction.

4.2.2. Multi-proxy Analysis: Grain Size, XRF data, LOI

Sedimentary properties including grain size and grain shape are important for identifying changes in depositional environments. Grain-size analysis is widely used as an indicator of past environmental changes, particularly as they relate to energy transport conditions (Donnelly & Woodruff, 2007; Liu, 2004). Moreover, when high energy events occur, such as hurricanes and flooding, sediment is transported into coastal basins with much higher energy than under "normal" sedimentation. Thus, the composition of sediment changes during such flooding events.

Grain-size analysis was performed manually by sampling the core at 1 cm intervals and collecting approximately 2 grams of wet sediment. Samples were weighed and dried overnight in an oven at 110 degrees Celsius, subsequently re-weighed with the dry sediment to calculate water loss, and sieved through a 63 µm sieve so that only sand remained. The material that did not pass through the sieve was collected and dried again overnight or until fully dry. The crucibles were then reweighed, along with the remaining dried sand, removing any rocks or shells greater than half a centimeter in diameter. The weight of these rocks and shells was also measured to use as an additional proxy. The weight of the sand was then subtracted from the original material and crucible to calculate the % sand in each subsample, which was used as a proxy for changes in terrestrial sediment influx. We also used the inverse value, % fines (particles smaller than 63 µm) as a proxy for smaller silt and clay. Finally, six samples of sand from intermittent depths throughout the core were examined under a binocular microscope to better characterize the nature of this material.

Loss-on-ignition (LOI) was performed at 3 cm intervals throughout the core, in a similar manner to grain-size analysis but with the aim to quantify organic matter, carbonate, and silicate content as a function of dry sediment weight. This involved drying in an oven at 105°C, followed by combustion in a high-temperature furnace at 550°C, and then 950°C, followed by weighing the residue to estimate mass lost at each step. Organic matter can act as a signal for hurricane-induced flooding in different ways at different sites and throughout cores, but in our core, we hypothesize that increased periods of organic matter input might indicate increased river discharge from flooded plains bringing increased OM through the river system into the basin.

The final proxy used is X-Ray Fluorescence (XRF) core scanning, which, in recent decades has become a geochemical techniques commonly used in the analysis of marine sediments (De Boer et al., 2014). Our research partners at the WHOI produced 1-mm resolution XRF data using an ITRAX™ XRF system. This geochemical data provides data on the elemental composition of sediment throughout time, which can then be interpreted as landscape transformations resulting from climatological, environmental, or anthropogenic forcings (Rothwell & Croudace, 2015a). For example, several researchers (McCloskey & Liu, 2013; Naquin et al., 2014) interpreted decreases in terrestrially-derived elements (Ti, Fe, and Zn) as indicators of TC overwash in the Atlantic Basin and used this to support LOI and grain size data previously generated for their cores. Ca can be used as a salinity indicator as it is strongly marine driven and could indicate occurrence of carbonate precipitation in the sediment column (Schreiber et al., 2014), while variations in K and Ti have been correlated to higher terrestrial discharge into basins through either higher precipitation/runoff or through high coastal erosion due to storm surges and currents (Rothwell & Croudace, 2015b). A detrital origin of Ca may be inferred by correlation with Fe or Ti to see if Ca mirrors terrigenous supply, rather than productivity changes. Similarly, ratios of Ti/Ca and Fe/Ca have been used in marine environments as indicators of terrestrial input at a lagoon in western Cuba (Gregory et al., 2015), and K/Ti has been shown to represent variations in silicate input and reveal changes in sediment provenance, largely controlled by sea-level changes (Diekmann et al., 2008). Additionally, Mn/Fe is used as an assessment of redox conditions, with Mn/Fe peaks occurring during suboxic diagenesis when Mn is mobilized (Demina et al., 2019; Fritz et al., 2018).

Finally, Rb/Sr has been widely used to demonstrate changes in weathering regimes (Yang et al., 2020), which can relate to significant erosion. Rb is an alkali metal with a similar ionic radius to that of K, while Sr is an alkaline earth element with an ionic radius only slightly larger than that of Ca, thus substituting for Ca isotopes in minerals such as calcite, dolomite, and aragonite (Bentley, 2006). In the Caribbean, Sr is primarily released from rocks via bedrock weathering, or in some cases is cycled through soil, vegetation, animals, and atmospheric deposition, and is transported to oceans primarily through river sediment runoff (Bataille et al., 2012; Bentley, 2006). Since these elements have considerable geochemical differences, Rb/Sr in sediment can vary by many orders of magnitude, with older rocks having orders of magnitude higher Rb/Sr ratios than recently-formed rocks (Bentley, 2006).

4.2.3. Chronology

The chronology for this study is based on four terrestrial macrofossils (plant/wood) (Table 1) which were radiocarbon dated at the National Ocean Sciences Accelerator Mass Spectrometry (NOSAMS) facility at Woods Hole Oceanographic Institution (WHOI) and calibrated using the Intcal20 calibration curve (Reimer et al., 2020). The age-depth model was established using Bacon v2.5.6 (Blaauw et al., 2021; Blaauw & Christen, 2011).

4.2.4. Numerical and Statistical Analysis

All statistical data analysis was completed in R v.4.0.4 (R Core Team, 2021). Principal component analysis (PCA) was performed on the geochemical and grain-size data using the "FactoMineR" package v.2.0 (Lê et al., 2008) and visualized using the "factoextra" package v.3.6.3 (Kassambara & Mundt, 2020). XRF data was rescaled from mm to cm-resolution to match grain-size data, and both grain-size and XRF data were standardized to have mean 0 and standard deviation 1. By default, the function PCA() in FactoMineR standardizes data automatically in this fashion, thus removing the influence of extreme values on PCA (Kassambara, 2017; Schreiber et al., 2014). Grain size and geochemical data were qualitatively explored using excel and C2. Stratigraphic diagrams were used as visual aids to remove data from either end of each core section, as the sediment near the section cuts were disturbed and the data therefore deemed erroneous.

To present and interpret geochemical XRF data in a cohesive and organised manner, results are often presented in stratigraphic zones. The decision of where these zones of related data should begin and end is not a simple one, as numerous methods exist to do so, and there is no consensus about how to deal with such highly dimensional datasets in a statistical manner (Schroeter et al., 2020). Many studies analyze multi-proxy data qualitatively, based solely on visually identifying changes within the proxy data and matching these to other proxy records (*e.g.*, McCloskey & Liu, 2012; Naquin et al., 2014: Peros et al., 2017). While statistical analyses are not necessarily required, they can be useful in determining where visually identified zones should start and end (K. D. Bennett, 1996). In the case of core HATC1, when investigating the entire reconstruction, prior to ~2900 cal BP the curves of several elements and element ratios appear almost flat. However, upon dividing the core into smaller sections and re-scaling, more defined trends emerge, such as the variance of element ratios such as Ti/Ca and Fe/Ca (See appendix A). For this reason, all statistical analyses were performed once on the entire core, and again on different sub-sections of the core.

Zones and sub-zones were identified using a combination of visual changes in XRF and grain-size curves, the results of PCA, and stratigraphically-constrained cluster analysis with an incremental sum of squares (CONISS) method of the chclust function from the package "rioja" v.0.9-26, where "d" is a dissimilarity structure produced by the EUCLIDEAN dist function (Juggins, 2020). The number of zones was determined by comparing results to broken stick models (K. D. Bennett, 1996), both for the whole core, and for sub-zones within each of the five major zones.

4.3. Results

4.3.1. Age-Depth Model

Core HATC1-D2 is 8.96 meters long with a basal radiocarbon date of 7920 ±65 14C years BP. At this site, changes in sedimentation rate throughout time likely reflect major hydrological changes such as sea level rise, the formation of the delta, hurricane-related flooding-induced river discharge, and river flow changes from human impacts on the karst landscape. Throughout the lab procedures and sampling of the entire core length, only four terrestrial macrofossils were found. This in itself is an interesting finding given the site's depth and proximity to the Baradères delta, river, and mangrove shoreline. Of the four terrestrial macrofossils located in the core (Table 1), two were located within the bottom cm of the core and had calibrated ages between 8411-8543 and 8599-8986 cal BP, respectively, with a probability of 95.4%. Another terrestrial macrofossil from 744.5cm downcore yielded a calibrated age range of 2494-2723 cal BP, with the same probability, and the final macrofossil from 214.5cm downcore yielded two possible ranges of 348-456 cal BP (76.2%) or 313-341 cal BP (19.2%).

Depth from surface (cm)	I.d.	Type	FModern	Age + error (BP)	Calibration curve	Calibrated age range (cal BP)	Median calibrated age (cal BP)
214.5	HATC1_D2_2:7_90-91cm	Plant/Wood	0.95980	330 ±15	Intcal20	348-456, 313-341	382
744.5	HATC1_D2_6:7_40-41cm	Plant/Wood	0.74150	2400 ±75	Intcal20	2494-2723	2476
895.5	HATC1_D2_7:7_48-49cm	Plant/Wood	N/A	7690 ±30	Intcal20	8411-8543	8471
895.5	HATC1_D2_7:7_48-49cm	Plant/Wood	0.37310	7920 ±65	Intcal20	8599-8986	8768

Table 1: Summary of the four terrestrial macrofossils radiocarbon dated for this study at the National Ocean Sciences Accelerator Mass Spectrometry (NOSAMS) facility at Woods Hole Oceanographic Institution (WHOI).

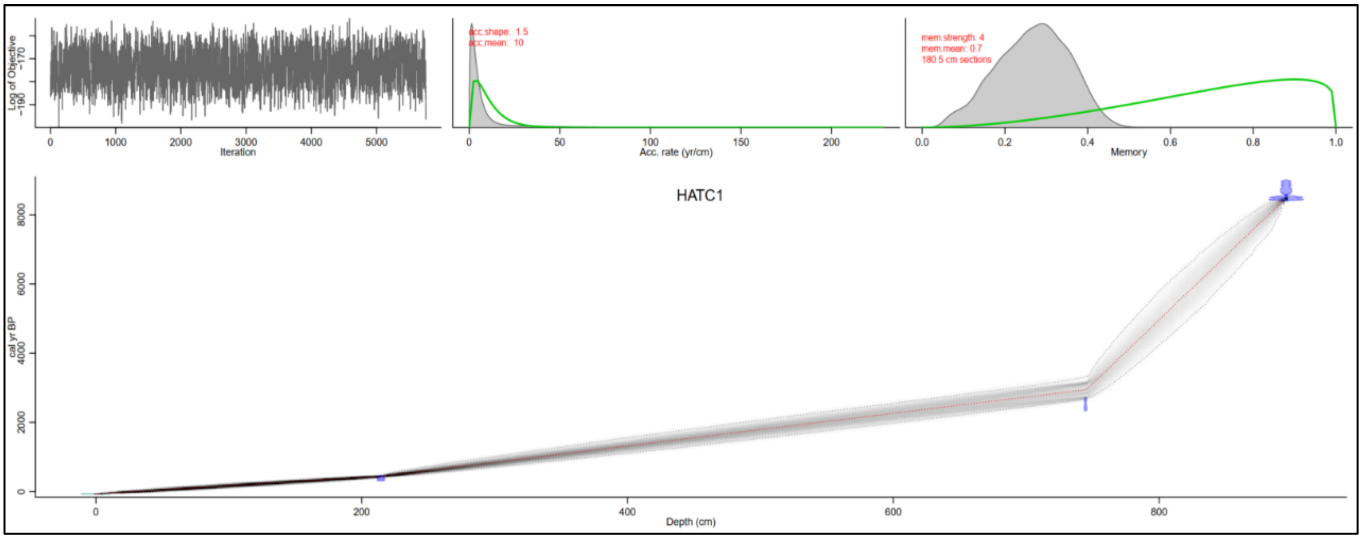

Figure 4.2: Age-depth model for Baradères Bay, Haiti- created using four terrestrial C14 dates from Table 1.

The age depth model (Figure 4.2) is limited by its minimal quantity of radiocarbon dates, but nonetheless effective for a preliminary chronology, showing slow sedimentation in the early-middle Holocene, and a sharp inflection reflecting a shift to a much faster sedimentation rate in the late Holocene-present. It is possible that the exact location of this inflection will change in the future when additional data from marine macrofossils are added to the model in future studies of core HATC1. In fact, given the low resolution of the age-depth model and the multitude of environmental, climatological, and socioeconomic factors influencing the region, it is quite possible that more than one change in sedimentation rate occurred throughout the entire chronology.

4.3.2. Core Description

Sediment core HATC1-D2 (Figure 4.3) is characterized by extreme variations in wetness and presence of shells. Layers of shell fragments are present between layers of scarce, but often complete, bivalve shells. Fragments of finger corals *(Porites divaricata)* (Figure 4.4) are present between ~857 and ~765 cm, which is equivalent to ~7075 to ~3600 cal BP, according to the present age-depth model (see appendix E for ages at each cm downcore from BACON age-depth model). The six samples of microscopically examined sand exhibit a clear change in the coarse sediment content from the base of the core (higher coarse fraction) to the top of the core (less coarse fraction), with shelly components such as bivalve and gastropod fragments being the main contributors to the larger particles. Foraminiferal diversity is generally high (>50 taxa could be easily detected per sample), suggesting relatively high salinity throughout the core (Scott et al., 2001), but most foraminifers are quite small, making them challenging to identify (van Hengstrum, 2021, personal communication). Miliolid foraminifers generally are higher at the base of the core and decrease towards the core top, while *Ammonia* and *Elphidium* taxa appear to increase towards the core top. However, the samples contained no agglutinated foraminifera such as *Miliammina*, *Tiphotrphca*, and *Trochammina*, which have been used as indicators of brackish water (Scott et al., 2001), so there is no clear evidence of low salinity (<10 ppt) in any of the samples examined thus far, indicating that the site was in some capacity connected to the ocean at all times.

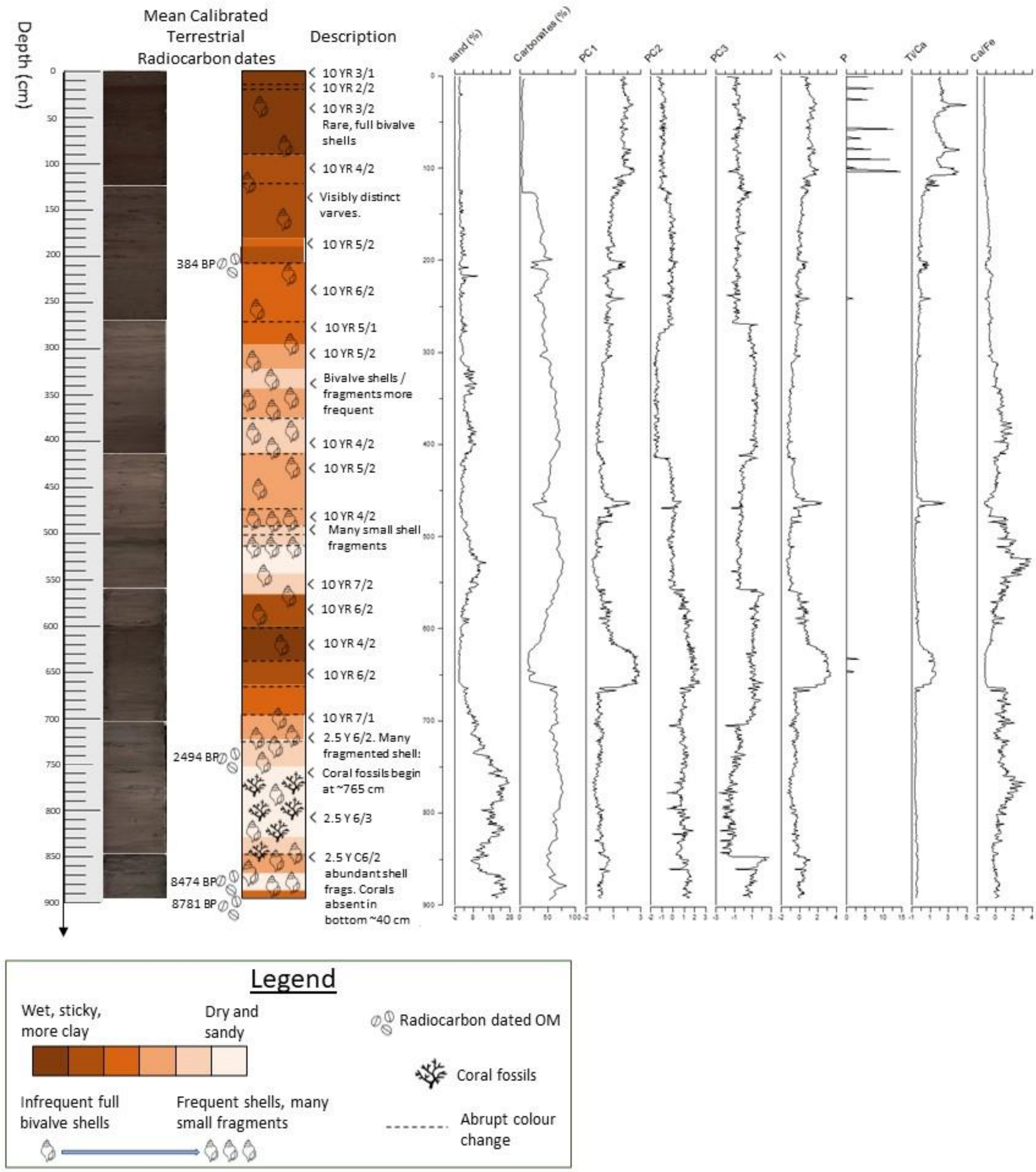

Figure 4.3: Core log of HATC1 D2. Core sections where the core tube was cut for transportation are visible in the image on the left. The colour description is based on the Munsell Soil Colour Chart classification. Select LOI and XRF series are presented, as well as the first three components of the geochemical and grain size PCA.

Figure 4.4: Finger corals *(Porites divaricata)* present between ~765 cm and ~857 cm, which is equivalent to ~3600 to ~7075 cal BP, according to our present age-depth model.

4.3.3. PCA and zonation

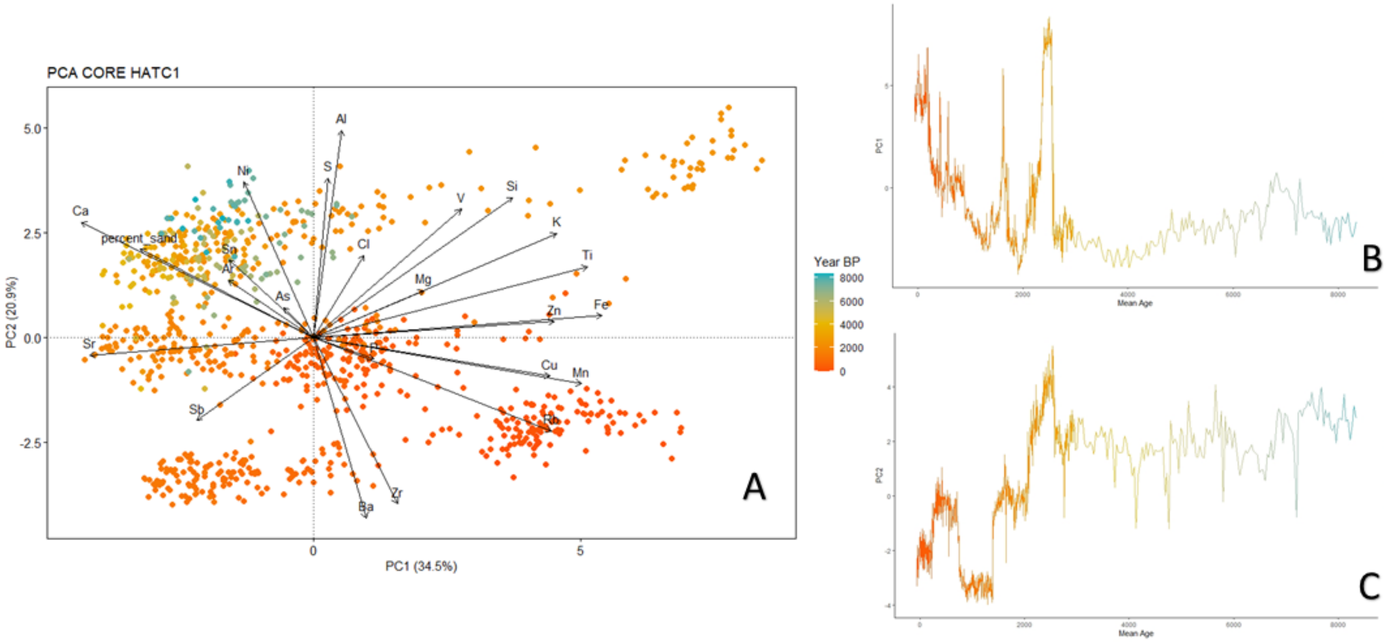

Figure 4.5: Principal Component Analysis for the entire core at the cm scale (A) Biplot, (B) scores of the first component through time, (C) scores of the second component through time.

The first component of PCA accounts for 34.5% of the variance while the second component accounts for 20.9%. The third and fourth components account for 10.5% and 8.2% respectively, and the following components become less important. The first two components collectively account for over half of the database variance and are therefore useful to compare (Figure 4.5). The resulting biplot reveals chronologically-constrained clusters, and the correlation between certain elements. For instance, Ni, Sn, and % sand contribute towards the variance in the oldest part of the core, while Ca and % sand are strongly corelated, and load toward a yellow cluster, representing a time around 4 kyr BP. The first component is largely influenced by elements of terrestrial origin such as Fe, Ti, Mn, K, Zn, Rb, and Cu, while the variance of the second component is contributed to by elements including Al, Ba, Zr, S, Ni, Ca, Rb, and K (See appendix B for related figures). The first component is almost identical to the curves of Ti and Fe, and the first through fourth components validate the importance of major changes in the core within the last ~2900 year.

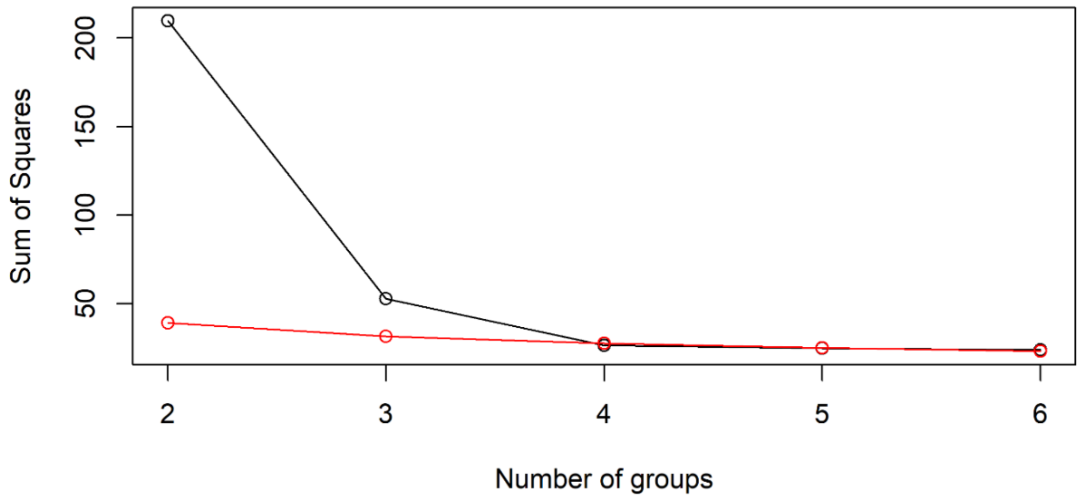

Figure 4.6: Sum of squares of the proxy data (black) compared to that from a broken stick model (red) for core HATC1.

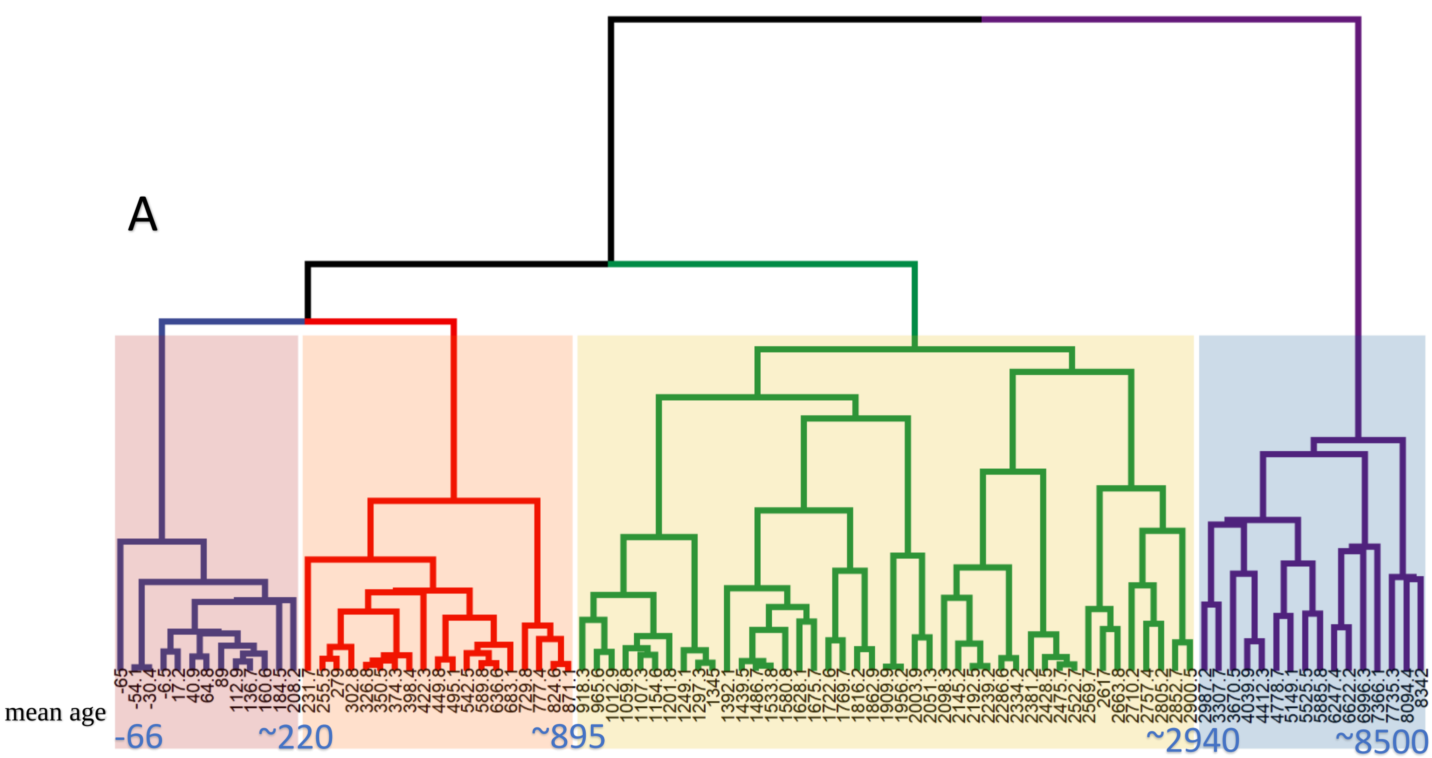

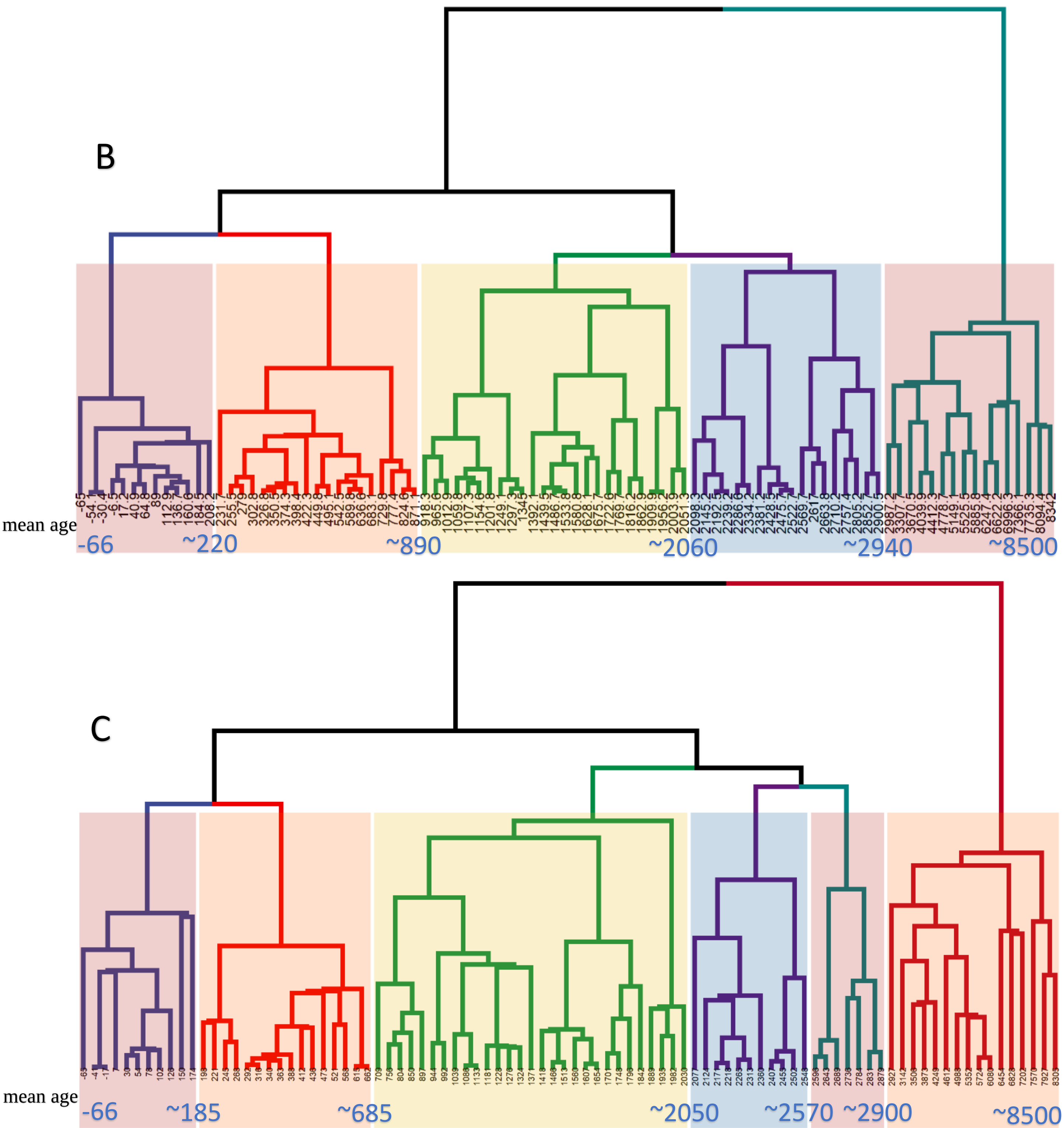

Figure 4.7: Dendograms visually depicting stratigraphically-constrained cluster analysis of core HATC1 with 4 (A), 5 (B), and 6 (C) zones.

The broken stick model provides a recommendation for the number of significant zones, although the number of zones rapidly increases in correlation with the increase in sample size (K. D. Bennett, 1996). The results of the broken stick model compared to the sum of squares of the proxy data for the entire length of core HATC1 (Figure 4.6) imply that there are at least four statistically significant downcore zones, based on the intersection between the two models. However, this number could be larger, as according to the model, 5 or 6 zones would also be significant. The usefulness of this statistical procedure is that in all variations of the cluster analysis, the models agreed that there should be a zone beginning around 2900 cal BP and continuing until the bottom of the core (Figure 4.7 A, B, and C).

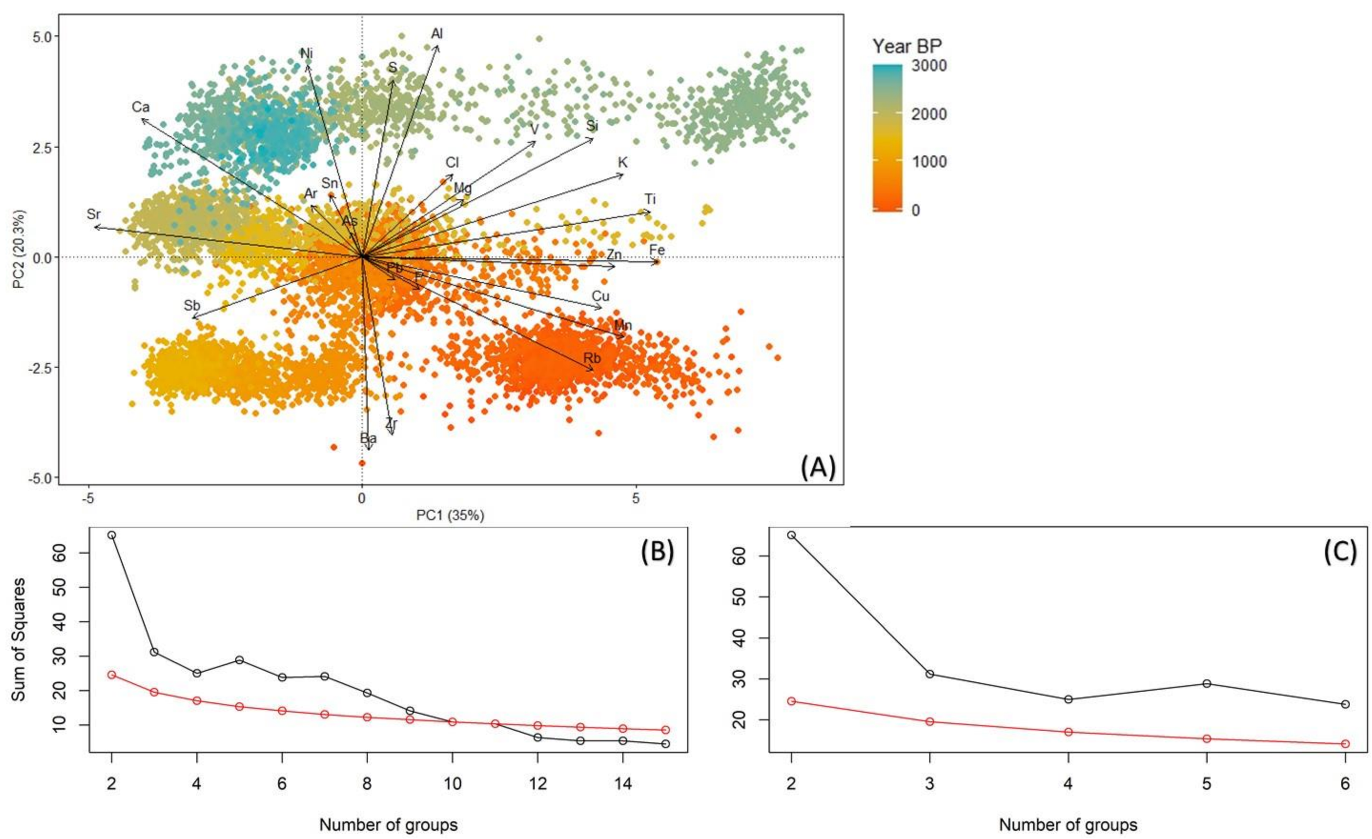

Figure 4.8: (A) PCA of XRF data at the mm-scale from -66 to 3000 cal BP. (B) Sum of squares of all proxy data from -66 to 2900 cal BP (black) compared to that from a broken stick model (red) with 15 groups. (C) Sum of squares from all proxy data from -66 to 2900 cal BP (black) with 6 groups.

Because of the major change in the core at around 2900 cal BP identified by the full core PCA and constrained cluster analysis, another PCA was conducted on the XRF data from this more recent sediment. Figure 4.8 presents the biplot of the first two components of this PCA at the mm-scale. In this case, the first component accounted for 35% of the variance, the second component accounted for 20.3% of the variance, and the third and fourth components accounted for 10.3% and 5.8% respectively. The main contributors to PC1 are Fe, Ti, Sr, Mn, Zn, K, Cu, Rb, and Ca. Ca loads toward the oldest date, while the cluster relating to zone 5 (i.e., the youngest data) is highly loaded with Cu, Mn, and Rb. Comparing this to the broken stick model with 15 groups (Figure 4.8B), we can see that there are up to 10 significant clusters, based on where the two models intersect. However, for the purposes of limiting the number of sections of subdivision for the analysis section, we have chosen to divide the results into 4 zones prior to 2900 cal BP, based on the proximity of the sum of squares to the broken stick model with 4 groups (Figure 4.8 C). Therefore, the results are divided into 5 zones, one between the bottom of the core and ~2900 cal BP, and 4 Zones after ~2900 cal BP. The zonation we chose was therefore based on the results of stratigraphically-constrained cluster analysis model of five zones (Figure 4.8 B). The results are thus presented in the following zones (Figure 4.9): Zone I, ~8500 to ~2910 cal BP (~896 to 736 cm), Zone II: ~2910 to ~2060 cal BP (~736 to ~557 cm), Zone III: ~2060 to ~890 cal BP(~557 to ~309 cm), Zone IV: ~890 to ~220 cal BP (~309 to ~120 cm), and Zone V: ~220 to -66 cal BP (~120 to 0 cm).

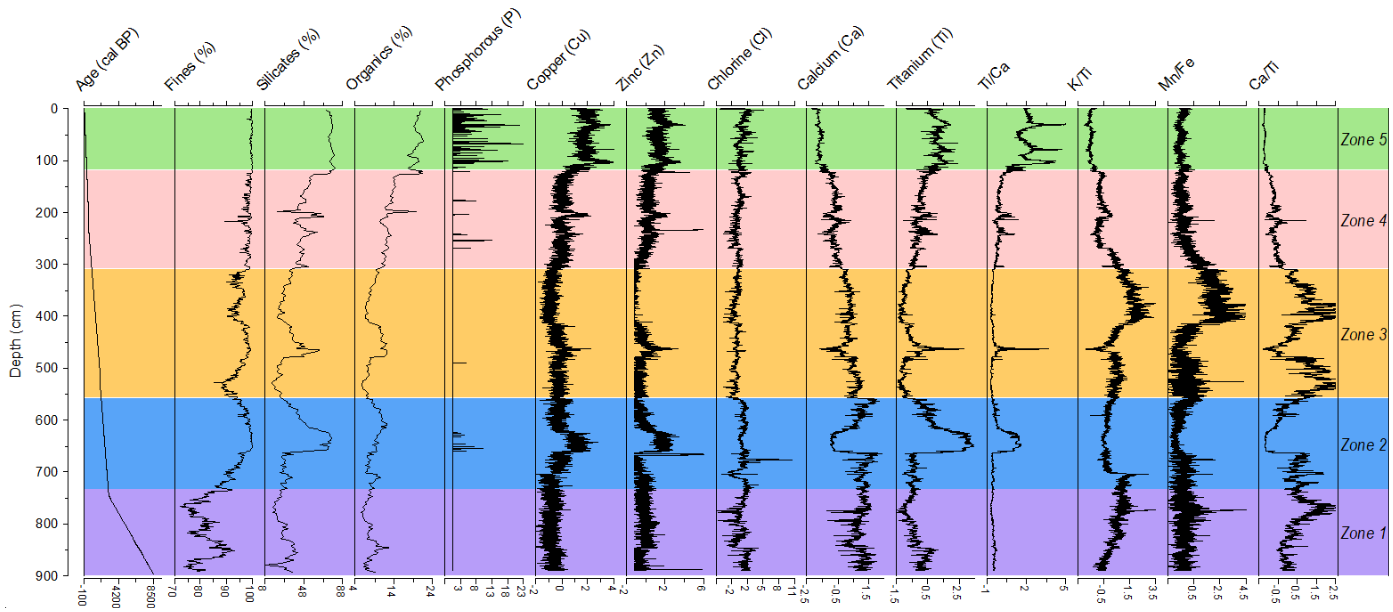

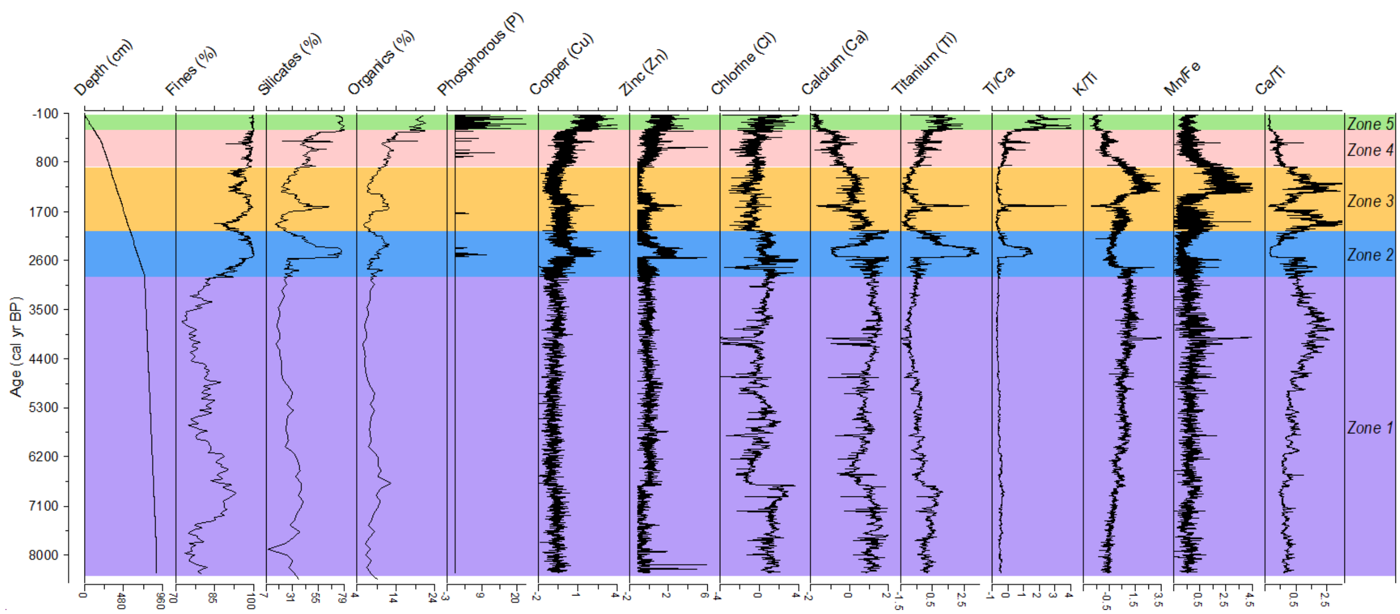

Figure 4.9 Stratigraphic diagrams of proxies from core HATC1 on the y-axis of depth (above) and age (below), divided into five zones. Data is standardized to mean 0 and standard deviation 1, excluding percentages, and unit of XRF data is counts per second (CPS).

4.3.4. Zone I: ~8500 to ~2910cal BP (~896 to ~736 cm)

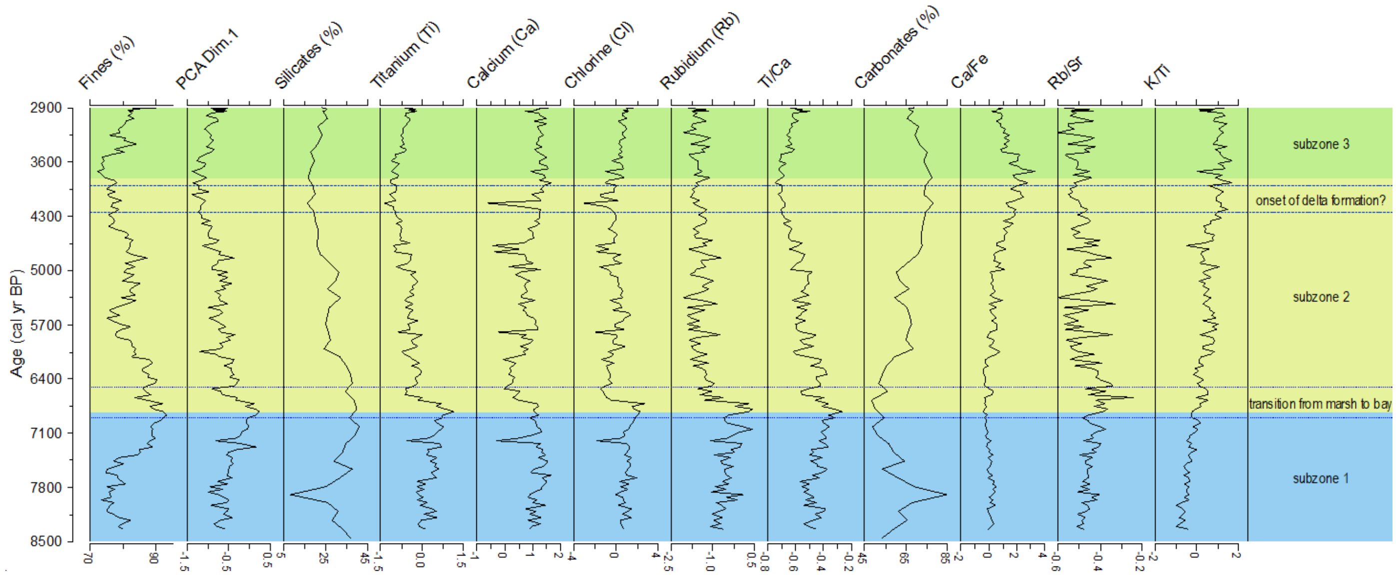

Figure 4.10: Stratigraphic diagram of Zone I with three subzones. Data is standardized to mean 0 and standard deviation 1, excluding percentages, and unit of XRF data is counts per second (CPS). Coral fossils are present within subzone II.

Zone I (Figure 4.10) is characterized by high proportions of sand (between 10 and 30%), versus the remaining zones, which do not exceed 10% sand, and are instead mainly composed of silt and clay. The bottom ~40 cm of the core contains a large number of shells and broken shell fragments, but no corals. When sampling, it was impossible to cut through the sediment without slicing through shells. There is also a large quantity of Zn in the bottom few centimeters of the core. Corals first appear at ~857 cm and continue to ~765 cm (which is equivalent to ~7075 to ~3600 cal BP), during which time water conditions were appropriate for their growth.

During this early part of the core, the curves of sand, fines, and several elements and element ratios including Ti, Ca, Cl, Rb, Al, Cu, Ca/Fe and Ti/Ca follow an undulating pattern that is less pronounced in some elements than others, but clearly defined in the first dimension of the PCA (Figure 4.10). The trends of terrestrial and marine-derived elements, such as Ti and Ca, respectively, follow very similar trends in the earliest part of the core, until after the "thermal maximum"- the maximum of Holocene average temperature identified by other researchers in the area, when the trends seem to become inverse, although still with similar short-duration peaks within the longer timescale pattern.

To elaborate, from the bottom of the core to ~5900 cal BP, the curves of Ti, Ca, and Cl are high, but after this period, Ca begins to trend very gently upward, while Cl and Ti trend very gently downward until ~4200 cal BP. At ~4200 cal BP there is a sharp reduction of Ca and Cl, with an influx of carbonates, followed by a peak at 3900 cal BP and subsequent decline in Ca/Fe. This is the beginning of a continuous increase in % fines, which leads to a permanent shift in the core. One possible explanation for this is the creation and expansion of the delta, which would change the main source of sediment in the basin from that which is produced in the ocean to sediment derived from land. This is also consistent with the age-depth model (Figure 4.2) that shows a rapid increased in sedimentation after this time, due to an influx of finer sediment from the Baradères River. Finally, in the most recent part of zone I (subzone 3, Figure 4.10), Ti and Cl begin to trend upward while Ca returns to the same relatively stable level as the earliest stages in subzone 1 (Figure 4.10). Starting at ~3600 cal BP, there is an increase in % fines, silicates, Ti, and Ti/Ca, which accelerate abruptly at ~3200 cal BP.

Two samples of sand were collected and examined in this section, the first at 769-770 cm downcore, and the second at 857-858 cm downcore, which encloses almost exactly the timespan of the coral reef on either side. The sand is quite similar before and after the corals begin, and is composed of biogenic materials such as foraminifera fragments, including full ostracods, bivalve shells, calcareous coralline algae, echinoid spines, and gastropods (see Appendix C).

4.3.5. Zone II: ~2910 to ~2060 cal BP (~736 to ~557 cm)

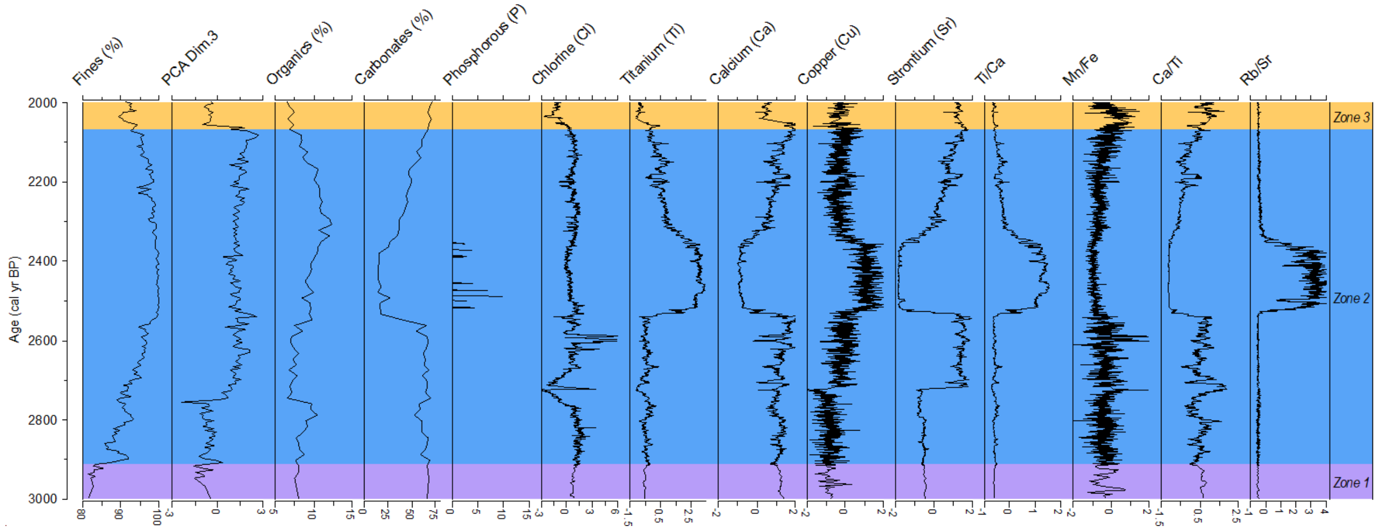

Figure 4.11: Stratigraphic diagram of Zone II. Data is standardized to mean 0 and standard deviation 1, excluding percentages, and unit of XRF data is counts per second (CPS).

The beginning of zone II (Figure 4.11) is associated with an increase in Pb, Mg, % fines, and a more variable signal in all proxies, which is at least in part due to a transformation to a new depositional environment with a much faster sedimentation rate and a very different climate signal. Within zone II, we see the extension of the transition zone likely associated with the continued development and expansions of the delta. As the delta expands, more sand is deposited at the river's mouth and accumulates, increasingly blocking the river's mouth and preventing larger sand particles from being deposited into the karst hole. Rather, we see a pronounced increase in % fines starting at ~3600 and reaching a maximum at ~2500 cal BP, as silt increasingly enters the basin. Moreover, starting at ~3300 this increase in fines becomes relatively constant, reaching a maximum at the same moment when Ti, Fe, and Ti/Ca, and Rb/Sr begin to peak. This zone contains an important event between ~2500 and ~2350 cal BP which is characterized by a peak in % fines, organics, and terrestrially-derived elements such as Ti and Fe, with the sudden onset of P.

Two samples of sand were collected and examined under the microscope in this section, one at 661-662 cm depth (~2560 cal BP), and the other at 664-665 cm depth (~2575 cal BP), i.e., one directly on either side of the colour change associated with the change in sedimentation rate. The sand deposited earlier is composed mainly of biogenic materials, and although particles are small, colourful corals, bivalves, foraminifera, and OM are identifiable. After the colour change, however, the sediment becomes muddier, and there are almost no distinguishable foraminifera. Rather, we see more quartz, which is consistent with high silicates from the LOI and a peak in fine sediment. As well, this corresponds to a period in the core with almost no shells fragments recorded or collected, and high Ti values.

4.3.5. Zone III: ~2060 to ~890 cal BP (~557 to ~309 cm)

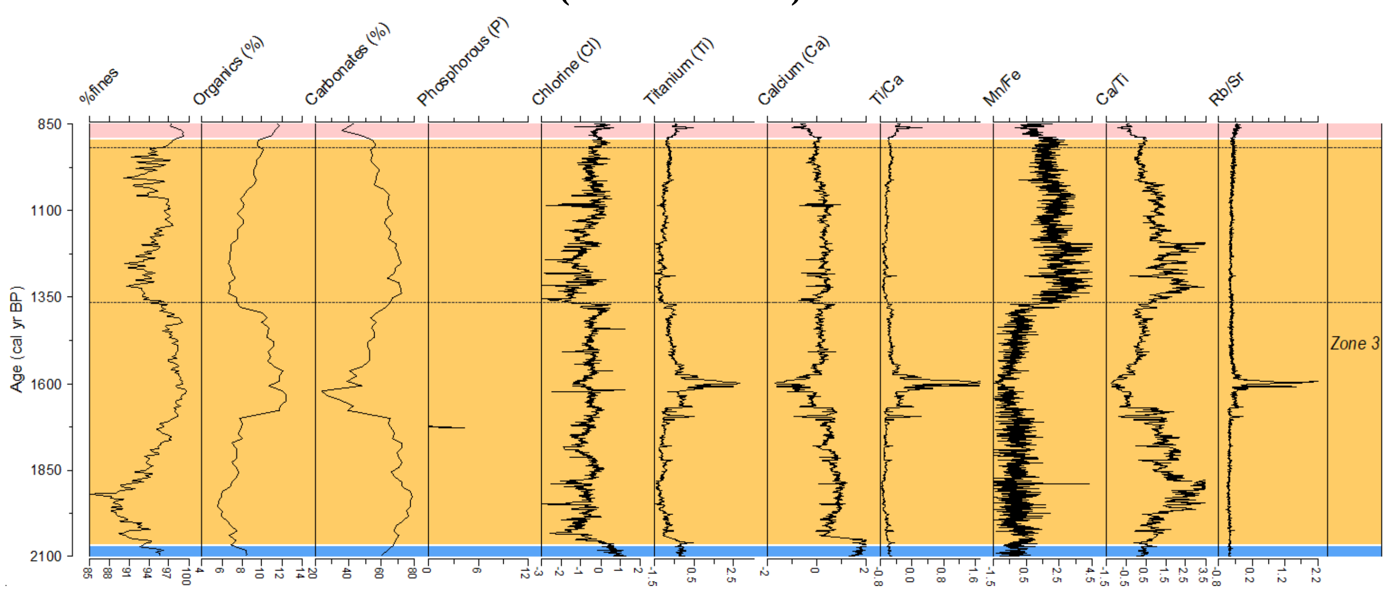

Figure 4.12: Stratigraphic diagram of Zone III. Data is standardized to mean 0 and standard deviation 1, excluding percentages, and unit of XRF data is counts per second (CPS).

In zone III (Figure 4.12) there is one abrupt peak in Rb/Sr at ~1600 cal BP, in conjunction with a peak in Ti and Ti/Ca and an inverse peak in Ca and carbonates. The proxy signal of this peak is similar, though quite shorter in duration to the large peak in zone II. Mn/Fe and Ca/Ti have two maxima in this zone, first a sharp peak at ~1900 cal BP, followed by a larger peak at ~1360 cal

BP. Mn/Fe, Ca/Ti, K/Ti and Cl show a major shift at ~1360 cal BP followed by a period of peaks in % sand. The curves of % carbonates and Ca are almost exactly opposite to those of Ti and Ti/Ca. There is a very short signal of P immediately before the large peak at ~1600 cal BP.

Two sand samples were examined in this zone, the first 358-359 cm into the core and the second 509-510 cm into the core, which correspond to ~ 1100 and ~1830 cal BP, respectively. Although both samples are primarily biogenic sand composed of relatively similar components including bits of organic material including plant matter, possible wood, echinoid spines, calcareous coralline algae, and carbonate foraminifera shells, the older sample had fewer large bivalve fragments, and overall contained less sand.

4.3.6. Zone IV: ~890 to ~220 cal BP (~309 cm to 120 cm)

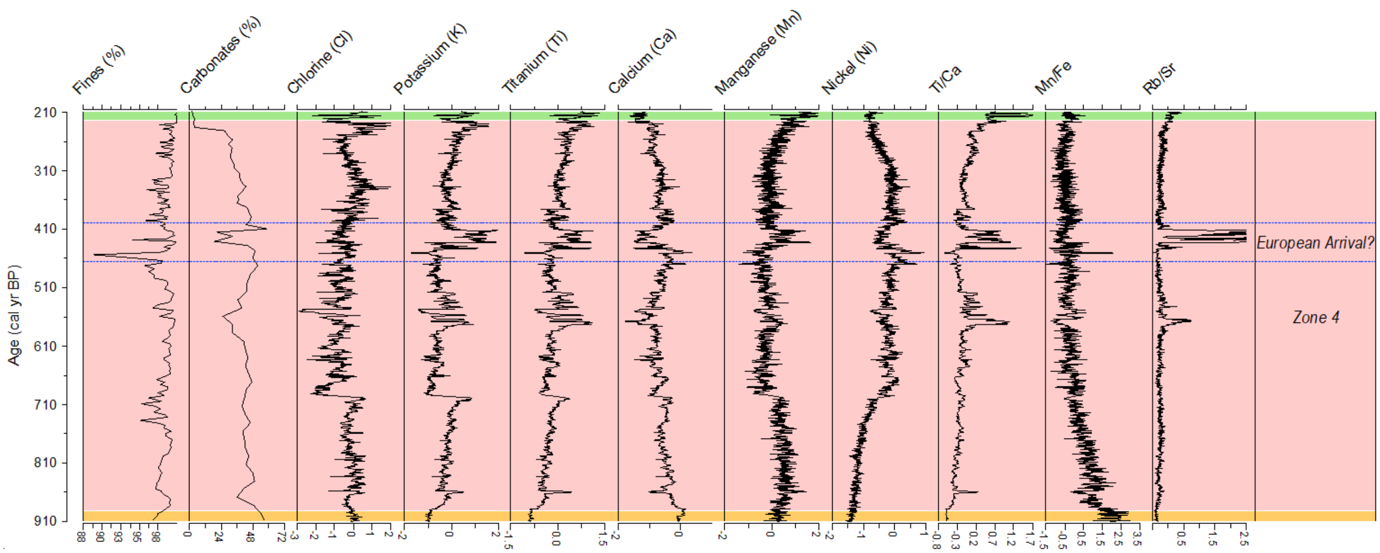

Figure 4.13: Stratigraphic diagram of Zone IV. Data is standardized to mean 0 and standard deviation 1, excluding percentages, and unit of XRF data is counts per second (CPS).

It was during this zone, ~500 years ago, that Europeans colonized Hispaniola, erasing the sustainable farming practices of the indigenous *Taino* people, and transforming the landscape into plantation-style sugar-cane farming (Bargout & Raizada, 2013). This could be reflected by the large peak in Rb/Sr and Ti/Ca (Figure 4.13), which have been used as an indicator of weathering and increased erosion (Fritz et al., 2018) potentially related to human activities. However, this signal could be another potential indicator of a storm-related flooding event, especially given the correlation to a sharp influx of sand and organics. In this zone there is a general increase in Ti and decrease in Ca. Already near the end of zone IV at ~260 cal BP we begin to see the influence of human activities which results in increased organics, silicates, elements of terrestrial origin such as P, K, Ti, and Fe, with more frequent peaks in Ti/Ca and Rb/Sr. It is also possible that peaks in % sand and Cl, variability of Ti and K, and general increases in Mn and Ti/Ca between ~500 and 200 cal BP (1450 to 1750 CE) correspond to the LIA. Additionally, sand collected from 205-206 cm depth (~400 cal BP) contained a large amount of organic matter including small pieces of wood and plant matter, and very infrequent carbonate fragments compared to other samples (Appendix C).

4.3.7. Zone V: ~220 to -66 cal BP (~120 to 0 cm)

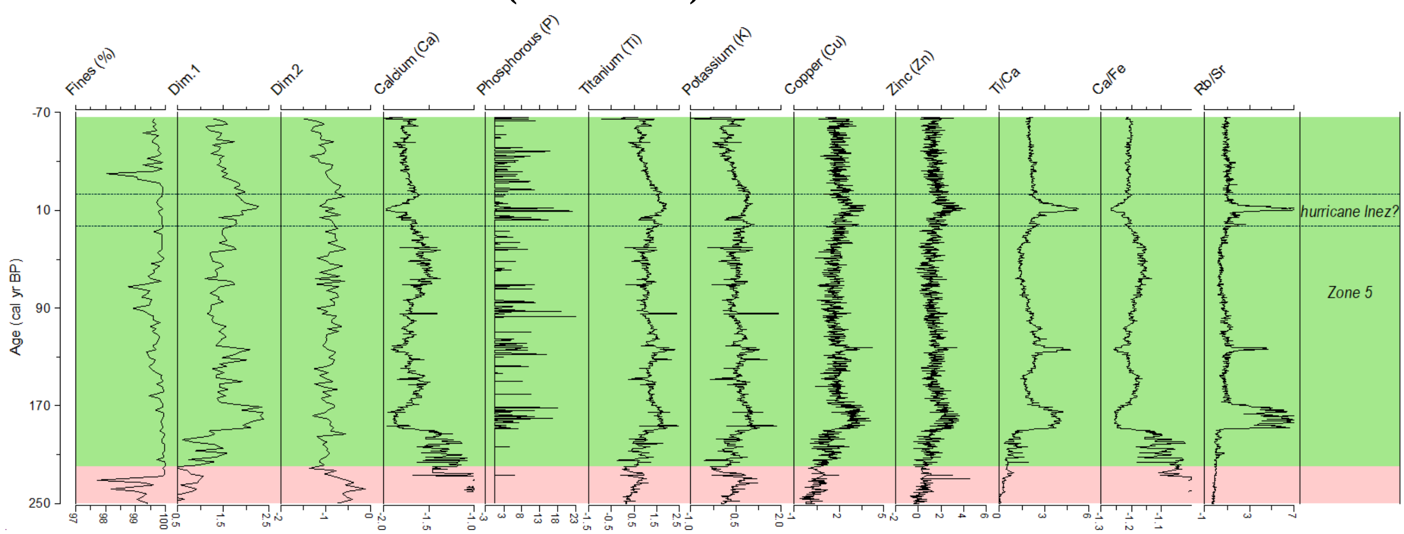

Figure 4.14: Stratigraphic diagram of Zone V. Data is standardized to mean 0 and standard deviation 1, excluding percentages, and unit of XRF data is counts per second (CPS).

Zone V is the most easily identifiable zone, as it contains a unique signal which is strongly terrestrially driven (reflected in high values of Ti/Ca), with unprecedented increases in organics, silicates, and macronutrients such as P. This most recent section of the core (Figure 4.14) is characterized by exceptionally high input of fine-grained sediment (>99%). Cu, Ti, and P are higher than they have been at any point in the past, with the exception of large but short-duration peaks at ~2500 cal BP and ~1600 cal BP. In this zone, the sand is composed mainly of microscopic coral fragments and calcareous foraminifera shells, with small pieces of organic matter and some larger bivalve shells present, but infrequent (Appendix C).

Early in this zone at ~200 cal BP there is a large peak, followed by a shorter peak at ~120 cal BP, of Ti/Ca and Rb/Sr, which are very similar (though at different scales), to the large peaks of the same element ratios in zone II. This, along with increased P, Ti, and Cu provide evidence that the peak we see at ~2500 cal BP could be related to human disturbances, as there is abundant evidence that such activities have led to widescale erosion and changes in hydrological cycles in Haiti in the Historic era. At ~0 cal BP (1950) Si, Ti, F, and K all start a gentle decrease. This is also represented by PCA dimension 1.

4.4. Discussion

4.4.1. General Comments

Our age-depth model is, in very general terms, consistent with other regional sedimentation curves. Based on the calibrated ages of three sediment records from Hispaniola compiled by Caffrey and Horn (2015), similar sedimentation rates exist in the last ca. 2,300 calibrated years in all three sites. Lake Miragoâne, the oldest of the records, has the lowest sedimentation rate overall, and the lowest sedimentation rate before 2,300 cal BP. Laguna Saladilla had the highest overall sedimentation rate, with some distinct changes. Specifically, the sedimentation rate was low between ca. 7,800 cal BP and 3,600 cal BP, but at 3,600 cal BP the lake entered a phase of very rapid sediment accumulation, which slowed at 2,300 cal BP.

Generally, the grain size and geochemical evidence of core HATC1 agree with overall Circum-Caribbean Holocene climate reconstructions in the sense that there is precipitation change over time with a warmer and wetter early to middle-Holocene ~7000-4000 cal BP, followed by a gradual drying trend reflecting a more southward migration of the ITCZ, including a drier period from ~3600-2300 cal BP, and brief returns to humid conditions, such as 2300-900 cal BP. After 2500 cal BP, the series of abrupt influxes of Ti and Ti/Ca are associated with an influx of finer, terrestrially-derived sediment into the bay due to enhanced discharge from the Baradères River, possibly due to short-duration shifts to wetter climate conditions, hurricane-induced precipitation, and/or prehistoric-era human settlement. There is also potential evidence of a drier MWP, and much more variable and extreme conditions following European colonisation.

Moreover, small mountainous river systems deliver significant amounts of terrestrially-derived organic and inorganic carbon into oceanic basins, with anthropogenic activities accelerating river flow, carbon burial, and chemical weathering (McGillis et al., 2015). Increased levels of precipitation can also increase the runoff of terrigenous elements towards coastal basins (Gregory et al., 2015). In this core, the ratios of Rb/Sr, Ti/Ca, and Fe/Ca appear to be potential proxies for TC strikes, specifically after ~2500 cal BP, due to the overall "steady" nature of their curves, where abrupt peaks are prominent at ~2500 cal BP, ~1600 cal BP, ~420 cal BP, ~183 cal BP, ~124 cal BP, and ~9 cal BP. Storm signals vary from site to site, but in this case the hurricane signal might be terrestrially-derived sediment washed into the bay from precipitation, flooding, and erosion related to individual storm events. This pattern can be seen both at the full-core scale, and in more detail in the most recent centuries, although the size of peaks is not consistent, which could be due to certain wider peaks essentially reflecting several different flooding events in a short time period, or an event that passed exactly through the coring site as opposed to one that passed somewhat further from the Baradères Bay. It is also possible that the size of some peaks might be altered due to the low resolution of the age-depth model.

Throughout the entire core, Ca/Ti increases when % sand is greater than % fines because sand settles more quickly than silt and clay, resulting in decreased turbidity in the basin and therefore more sun penetration, dissolved oxygen, and biogenic activity. Cu might be a proxy for fires as during fire events metals become more mobilized due to increase in soil surface exposure leading to increased concentrations in soil and water systems (Abraham et al., 2017). Cu also binds with OM, which is evident in the similarities between their curves. Finally, sea level in the Caribbean directly and indirectly affects components of the sediment core. Corals require clear and clean water (*e.g.*, low pollution), sunlight (meaning shallow waters of one to two meters penetrable by sunbeams), and high levels of salinity (low river drainage into the ocean) (Braithwaite, 2016). Thus, the presence of corals concentrated toward to base of the core is consistent with a particularly low sea level at this time (Toscano & Macintyre, 2003).

4.4.2. Zone I: ~8500 to ~2910 cal BP (~896 to ~736 cm)

In zone I, the curves of sand, fines, and several elements and element ratios including Ti, Ca, Cl, Rb, Al, Cu, Ca/Fe and Ti/Ca follow a pattern that is likely forced primarily by atmospheric phenomena such as solar insolation variability and migration of the ITCZ (Haug et al., 2001). A core from Lake Miragoâne (~60 km from our site) demonstrates a relationship between solar insolation at 10° N and oxygen isotopes throughout the Holocene, with a peak at around 6500 cal BP, during the so called "Holocene Thermal Maximum" (Hodell et al., 1991). Relatively high levels of Ti/Ca, Ti/Fe, Ti, Ca, Cl, and Rb in the early part of this zone reflect the wetter period of the early Holocene, when sea level was low and thus the water in the basin shallow, with the abrupt shift at ~6900 cal BP potentially marking the shift between a salt marsh and basin with a freshwater lake or lagoon. This is somewhat consistent with regional data from Peros et al., (2017) who note a similar shift from marsh to basin in coastal Cuba at ~7500 cal BP, with the difference in age likely related to our simplistic age-depth model. Additionally, it is at around this time that corals begin to be present in the sediment, which is consistent with increasing sea level rise and salinity, as *Porites divaricata* are typically found in shallow and protected mangrove or lagoon habitats (Lord et al., 2021).

Corals disappear at ~3600 cal BP along with an increase in Cl and Ti, which coincides with reduced hurricane activity in Belize (Adomat & Gischler, 2017), and a major increase in charcoal and sedimentation rate in the Dominican Republic (Caffrey, 2011). Element ratios such as K/Ti may be a proxy for sea level rise (Diekmann et al., 2008), and within this zone undergo an increase in the early Holocene (subzone 1, Figure 4.10), followed by a more stable but still gradual increase in the middle Holocene (subzone 2, Figure 4.10), and reaching a plateau starting between ~4100 and 3600 cal BP which continues until the end of zone I (green subzone of Figure 4.10). Thus, the deposition of corals in the basin from the Baradères River mouth in zone I appear roughly consistent with hydrological regime that was established as a consequence of decelerating middle Holocene sea level rise.

With respect to a lower early Holocene sea level, Moore (1991) suggests that there may have been two separate land bridges stretching out to the island of La Gonave in the bay of Porte-au-Prince, with a large freshwater lake or lagoon (Moore, 1991). Similarly, this could have been the case in the Baradères Bay, with Baradères possibly attached by land to ile de la Gonave with a coastal lagoon within the karst, rather than today's coastal basin (Figure 4.15). The lack of corals in the bottom ~40 cm of the core provides evidence that the depth of water in the blue hole was shallower and fresher, which was due to the significantly lower-than-present sea level. Furthermore, the presence of Zn adds further evidence as Zn has low abundance in marine environments and in coastal sediments is either a signal of anthropogenic sources, or extremely high terrigenous supply (Rothwell & Croudace, 2015b).

Figure 4.15: Close-up image of Baradères Bay in which submerged coastlines and underwater karstic figures are visible including a possible channel and coastal lagoon.

This coastal marsh/lagoon environment would have been an ideal habitat for local marine animals and reptiles as well as migrating species. Very early settlers in Haiti could have been drawn here from the mainland by following migrating sea mammals, which would have to move through narrow channels to get between open sea and the lagoon or lake, where they would be most easily captured by early populations (Moore, 1991). Archaic-era shell mounds are found in the North Atlantic Basin as early as 9000-5800 cal BP at sites including Florida, Haiti, and Guatemala (Binford et al., 1987). It is now understood that many coastal sites pre-dating the middle Holocene sea level stabilization were either destroyed or submerged during marine transgression, and changes in hydrological riverine systems. Future archaeological work should focus on identifying such sites, potentially in this region.

Additionally, the higher values in the curve of Ca/Ti between ~4900 and 2900 cal BP coincides with a mesic climate with high lake levels from lake Miragoâne (Hodell et al., 1991). This timeframe correlates with low Ti but potentially high aeolian dust, as Ca/Ti has been correlated to dust content in mountain river ecosystems (Munroe et al., 2021). The delta likely formed around ~4000 cal BP, due to wetter conditions which Kennedy et al., (2006) similarly attribute with the formation of a bog in the Dominican Republic and Peros et al. (2015) associate to the formation of a lagoon in Cuba. Kennedy et al., (2006) also report low pollen and organic content influx reflecting periodic drying of the bog surface between ~3700 and 1200 cal BP, which is similar to our results, although our core has brief periods of increased organics during this time.

In the most recent part of zone I, starting at ~3600 cal BP, there is an increase in the elements of the first component of PCA which appears to be a continuation of the long timescale trends of this zone mainly forced by Milankovitch precessions and sea level rise, however, at ~3200 cal BP and we see the ratios of fine sediment, organics, and silicates increase abruptly. This is consistent with other paleoclimate records in the region which attribute this change to a sudden drought (van Hengstum et al., 2018). Furthermore, pollen assemblages from Laguna Saladilla, Dominican Republic indicate saline mangrove conditions from 8030 to 3500 cal BP, followed by progression toward brackish conditions beginning at ~3500 cal BP (Caffrey, 2011).

4.4.3. Zone II: ~2910 to ~2060 cal BP (~736 to ~557 cm)

We associate the drastic change in sedimentation rate at ~2900 cal BP with sea level rise in conjunction with mangrove growth the continued expansion of the delta, possible human activities increasing the rate of erosion and sediment deposition, and potential flooding related to hurricane activity, or some combination of these factors. Many sites in the Lesser Antilles were abandoned and later re-occupied for various reasons. For example, Haug et al. (2003) found that "in the anoxic Cariaco basin of the southern Caribbean, titanium content reflects variations in riverine input and the hydrological cycle… suggesting that a century-scale decline in rainfall put a general strain on resources in the region, which was then exacerbated by abrupt drought events, and contributed to the social stresses that led to the Maya demise" (Haug et al., 2003).

Binford et al., 1987 studied the oldest known Maya settlements, which dated to the Ceramic period (Figure 4.16) and demonstrated a good example of the potential settlement-impact-response dynamic caused by early human settlements in the Caribbean. As phosphorous loading increased in response to human population growth in Guatemala, aquatic productivity as measured by accumulation rate and concentration of aquatic microfossils decreased. High sedimentation rates of silt appear to have supressed lacustrine productivity, although where the deposited sediment in Guatemala was inorganic, at our site the deposited sediment is highly organic. In this case, the high organic deposition could have been a result of the introduction of livestock and farming, in conjunction with arid or windy conditions, resulting in organic material entering and mixing in the water system. Otherwise, our system reacts in the same way as the one depicted in Guatemala, with a surge in sedimentation rate, an increase in fine sediment and silicates, an abrupt phosphorous influx, and a decrease in lacustrine productivity (Ca/Ti, Mn/Fe). It is common that low values of Mn/Fe correlate with increased fluxes of OM during anoxic conditions in the bottom of a basin while lake mixing occurs in the upper part of a basin (Naeher et al., 2013).

Further evidence of human presence in zone II comes from 1) the apparent irreversibility of the shift in depositional environment following the transition between zone I and zone II, and 2) the similarity between the patterns in zone II and zone V. Zone V is driven by anthropogenic activities in the post-European colonization of Haiti, and involves high silt deposition, few large shell fragments, high P, Cu, and Zn loadings, and high silicates/organics with low carbonates. This trend is very similar to what occurred in zone II, with these two zones having the highest overall percentage of silicates of any point in the core.

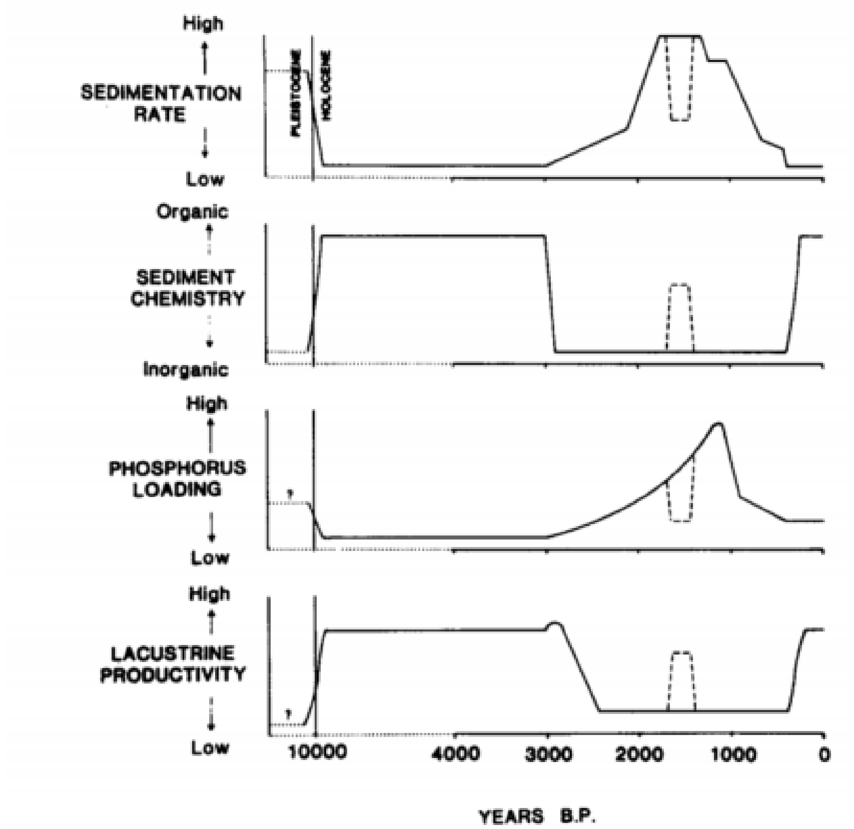

Figure 4.16: Modified from Binford et al. (1987). Summary of the impact of Maya settlement on the Peten lakes, Guatemala. Bulk sediment rates and Phosphorous loading accelerated as Maya population densities increased. High export rates of silt and inorganics during the Maya episode appear to have suppressed lacustrine productivity.

Another theory relating to the very large peak at ~2500 cal BP is that a high energy flooding event forced a large volume of fine sediment into the basin in a short amount of time. This type of event is best explained by a hurricane which passed exactly though the study site. The increase in organics would then be explained by the flooding of coastal planes and erosion into the river. Because many proxies such as Cu, Pb, % fines, and % water were already increasing prior to the abrupt peak and sudden onset of P at ~2500 cal BP, this indicates that there was a separate mechanism such as human or climate related fire/erosion altering the depositional environment before the flooding event took place. A reasonable explanation is that a climate shift resulted in an environment that was temporarily attractive for short-term settlers, and during this time, a very large hurricane passed by, resulting in coastal agricultural lands being inundated or saturated, as was the case after Hurricane Sandy in 2012 (Figure 4.17A) and an earthquake in 2010 (Figure 4.17B) caused flooding in Baradères. Kennedy et al., (2006) noted remobilized old charcoal, along with peaks in pollen (Poaceae, *Cyathea*, and *Lophhosoria*) at ~2900 cal BP which they suggest may indicate a tropical storm event, and McCloskey & Liu (2012) reported an active hurricane interval between 1450 and 2600 cal BP in Belize, which provides further evidence of potential storm activity during this time in Hispaniola.

In Laguna Saladilla, Dominican Republic, at ~2500 cal BP mangroves declined and charcoal and nonarboreal taxa, particularly *Amaranthaceae* and *Poaceae*, became more abundant, indicating a drier climate and a shift to freshwater conditions in the lake (Caffrey, 2011). There is further evidence of a dry period from ~3.3 to 2.5 kyr in the Caribbean from an abrupt cessation of speleothem growth in Cuba, most likely related to a decrease in regional precipitation (Fensterer et al., 2013), and shallow coastal lagoon drying indicators (*e.g.*, gypsum deposition) in Cuba (Gregory et al., 2015). Additionally, Caffrey & Horn (2015) noted peaks in charcoal at Laguna

Saladilla at 2590 and 2420 cal BP, but generally depressed charcoal values in Lake Miragoâne from 3110 to 1680 cal BP, which was attributed with the return of less fire-adapted pollen and an indication of drier conditions. Finally, the decrease in % sand is consistent with the appearance of mangrove pollen in Cenote Jennifer, Cuba (Agosta G'Meiner, 2016), which started at ~2400 cal BP and over time trap sandy sediments and stabilize shorelines.

Figure 4.17: A) Flood affected land around Baradères. Red indicates vegetation, blue indicates water, light blue indicates sediment filled water, and off-white indicates bare soil. The settlement appears to have saturated soil around it (UNITAR 2012). B) Arial view of Baradères, a commune in the Nippes Department of Haiti after the 2010 earthquake and subsequent flooding killed 12 people and damaged over 3000 homes. Photo by Jose Manuel Jimnez /IFRC (IFRC 2014).

4.4.5. Zone III: ~2060 to ~890 cal BP (~557 to ~309 cm)

Zone III appears to be either partially, or entirely, a zone of increased hurricane activity. There is one abrupt peak in Rb/Sr at ~1600 cal BP, in conjunction with a peak in Ti and Ti/Ca and an inverse peak in Ca and carbonates. This is potentially a hurricane but given that there is no drastic peak in sand, and the short presence of P this could also be a deforestation event, or even a potential wave of human settlement. Sites at both Miragoâne and Saladilla on Hispaniola show increases in charcoal in the last ~1700 cal BP, with the Miragoâne site showing a spike, followed by a decrease in charcoal at 1475 cal BP, which was attributed to human-set fires and the arrival of agriculturalists in the region, although it predates the earliest evidence of maize (Caffrey & Horn, 2015). This peak is very similar to, though quite shorter in duration to the large peak in zone II. It would be unsurprising that the signal left of the environment by the Taino people who inhabited Hispaniola before the arrival of Europeans would not be very large as they practiced a sustainable farming practice known as Conuco- cultivating on large mounds of soil embedded with plant matter such as branches and leaves which provided organic enrichment, improved water drainage and aeration, and reduced erosion (Bargout & Raizada, 2013). The peaks in Mn/Fe at ~1900 and ~1360 cal BP mark periods of oxic conditions at the bottom of the basin, which also correspond to intervals of sharp peaks in sand influx. The shift in Mn/Fe along with Ca/Ti, Cl, and % organics at ~1360 could potentially represent the beginning of the MWP.

From 2500 to 1000 BP the North Atlantic experienced an interval of intense hurricane activity related to a more northern ITCZ position relative to present, but not as far north as the middle Holocene (van Hengstum et al., 2016). This timeframe is slightly contested, with some researchers finding an active hurricane period from ~2600 to 1800 cal BP (Peros et al., 2015). Regardless, this was the beginning of Caribbean aridity relative to the middle Holocene, with the abrupt shift of

ITCZ favouring cyclogeneses in the central MDR and reducing vertical wind shear. At 1000 BP, intense hurricane activity decreased in the western North Atlantic, in conjunction with a southern displacement of the ITCZ leading to decreased cyclogenesis in the MDR (van Hengstum et al., 2016).

4.4.6. Zone IV: ~890 to ~220 cal BP (~309 to ~120 cm)

Anthropogenic activities such as agriculture, horticulture, deforestation, and urban development result in increases in nutrient and sediment loadings in lakes, wetlands, estuaries, and coastal waters (Fink et al., 2018; Russell et al., 2008). For example, human activities have fundamentally altered the global phosphorus (P) cycle (Goyette et al., 2018; Russell et al., 2008). Fertilizer application to crops, human sewage, animal waste, and trade of feed and food result in high P inputs to watersheds, which increases P transfer to surface waters (E. M. Bennett et al., 2001). At our site, P increases at an unprecedented volume in the top ~1.25 cm, along with Ti, Cu, Fe, silicates, and organics. Large P accumulations can occur is relatively short timeframes (decades). This often leads to eutrophication (Fink et al., 2018), which has become a major economic and public health concern both globally, and at the local level in coastal communities (Goyette et al., 2018).

Eutrophication is a potential explanation as to why this sediment core contains fewer shells at the top of the core, and in sections with low % sand (and therefore inversely high % fines). The larger quantity of suspended fine particles, which do not sink as quickly and therefore linger longer within the basin, result in increased turbidity of the water column and decreased sun penetration and dissolved oxygen, limiting the growth of organisms and clogging the feeding apparatus of aquatic herbivores. Higher concentrations of silt therefore limit productivity, and at the same time, accumulation of sand at the mouth of the basin and in the delta prevent larger terrestrial matter such as twigs or seeds from breaching the delta and entering the CKB.

4.4.7. Zone V: ~220 to -66 cal BP (~120 to 0 cm)

In the last few centuries, erosion and sedimentation has increased in the Baradères river, blocking the mouth (opening), reducing waterflow into the bay, and making the water shallow and difficult to commute through for locals who use the bay to transport to work (UNDP 2013). This has occurred due to deforestation and land use changes which have caused an increase in erosion, and due to persistent flooding, resulting in a feedback loop. Evidence of Haiti's deforestation has previously been recorded in sediment cores such as Brenner & Binford (1998), who showed evidence of three deforestation episodes following European colonization. Also, Higuera-Gundy et al. (1999) found pollen signals for European deforestation in a 7.6-meter core in Haiti. The large increase in Ti/Ca closest to the present is thus best explained by deforestation, and increased runoff and detrital input caused by human activity. We interpret this pattern as increased precipitation variability and aridity, with increased erosion and storm-related flooding events in the most recent ~220 years, which generally agrees with other sedimentary records from the Circum-Caribbean (Leblanc et al., 2017)

At this point in our study the accuracy of ages is relatively low, but we can attempt to corelate the more recent peak in many proxies including sand, Ti/Ca, and Rb/Sr at ~9 cal BP, which is equivalent to ~1941 CE to a known Hurricane strike, keeping in mind that the model could be off by several decades. Two likely events that could account for this peak could be Hurricane Inez, and Hurricane Flora, which occurred in 1966 and 1963, respectively. Hurricane Flora was a major (category 4) hurricane from September 26th to October 12th, 1963, which passed quite close to the study site, with the closest recorded coordinate of 19.1 N, 74.2 W and a wind speed of about 104 kt at this location. Overall, Hurricane Flora had maximum sustained wind speeds of 126 kt and maximum recorded storm surges of over 12 feet. The more likely hurricane to account for this peak is Hurricane Inez, which struck southwestern Haiti in late September 1966, passing directly though the Baradères bay, and was considered the worst hurricane since the 1920's. As many as 1000 people were killed, and 60,000 people were left homeless, with damages totalling $20.35 million in Haiti ("Inez Again Threatens Florida and Gulf Coast," 1966; "Inez Hurt Haiti," 1966).

Additionally, it is likely that this zone contains a signal at ~65 cm downcore of the 1860 earthquake which had an aftershock epicenter in Baradères. This appears to be represented by a very sharp spike in Ti, Si, K, Ca, and Fe, although it is not apparent in most of the element ratios examined. The sudden and sharp onset of so many elements could have been caused by a seismic event which would cause this sudden input of terrestrial and marine elements. If we are to accept that this peak is a signal of earthquakes, and specifically the sharp peak in K and Ti, then it is possible to infer other potential earthquakes which present similar signals in the core. For example, there is a similar peak in K and Ti at ~190 cal BP and another such signal at ~445 cal BP, both of which appear just prior to important peaks in Rb/Sr. More work is required to understand the specific geochemical signal that earthquakes leave at this site which is highly affected by seismic activity.

Finally, the slight relative decrease of the elements of PCA dimension 1 starting at ~0 cal BP (1950 CE) likely represents lost soil minerals not being replenished by synthetic fertilizers due to poverty-related low fertilizer application rates in Haiti (Bargout & Raizada, 2013). The predominant fertilizer 12-12-20 (nitrogen-phosphorous-potassium) appears to limit plant production and cause a soil nutrient imbalance (Bargout & Raizada, 2013). Unsustainable farming practices contribute to this problem.

4.5. Conclusion

Sediment core HATC1 provides and excellent opportunity to reconstruct the poorly understood climate patterns in the Caribbean during the Holocene but will require several more detailed research studies to effectively interpret the data. After ~2900 cal BP, the sediment rate has been very high, yielding a paleorecord of very high temporal resolution (approximately 4 years per cm). Due to this very high-resolution data, this record has the potential to track changes in very short-term climate variability, and thus makes a unique contribution to the literature.

There are three main conclusions from this initial study. Firstly, it is very clear that post-European settlement has resulted in dramatic changes in almost every proxy in this region, specifically in the most recent ~220 years due to lag effects and extremely high deforestation rates, which result in increased erosion and riverine input. The second conclusion is that there is a drastic increase in sedimentation rate beginning around 2900 years ago, and an equally important event at ~2500 cal BP, which likely relate to both climatic shifts, and/or pre-historic era human disturbances to the landscape. Following this important change in depositional environment, the resolution of climate reconstruction is very high, making this a very important study in terms of providing evidence from small islands for the contested "Anthropocene" epoch. With that said, it seems likely that this core contains, at least in part, a hurricane signal, specifically with the ratios of Ti/Ca and Rb/Sr. This is especially important as other researchers have suggested that between

4800 to 3600, 2500 to 1000, 550 to 450, and potentially in recent decades the North Atlantic Basin experienced intervals of heightened hurricane activity (Donnelly & Woodruff, 2007).

Lastly, we can conclude that the signal prior to ~2900 cal BP was strongly affected by Holocene sea level rise and forced predominantly by Milankovitch cycles, solar radiation changes, and the migration of the ITCZ. The very bottom ~40 cm of the core was deposited in a time before sea level rise was appropriate for coral growth, meaning that the site was very shallow, and likely a marsh or coastal lagoon, connected to the ocean via a narrow channel. The future addition of proxies such as pollen, charcoal, and stable isotope analysis would be highly beneficial to the interpretation of climate versus human signals in this study. Ultimately, knowledge of the relationships between paleoclimate variability, human populations, and the ecosystems of Hispaniola will require an increase in the number of studies and study sites to allow discrimination between systematic climate fluctuations across all sites and anthropogenic, site-specific forcings.

CHAPTER 5:

Summary of Contributions

5.1. Conclusions

Numerous studies identify Haiti as a global biodiversity hotspot containing one of the highest concentrations of endemic species on earth (Mittermeier et al., 2000; Smucker et al., 2007). Southwestern Haiti's coral reefs and mangrove deltas rank the highest in the Caribbean in biodiversity vulnerability (Smucker et al., 2007). The driving forces of this vulnerability relate to Haiti's rapid and uncontrolled urbanization and population growth, coupled with acute poverty, environmental hazards such as hurricanes, floods and landslides, and lack of environmental education (Smucker et al., 2007). This study presents an ideal opportunity to further our understanding of the diverse relationships between ecosystem dynamics and socio-political changes and provides important evidence of how islands with long histories of human settlement can be valuable in the assessment of mechanisms of ecosystem degradation and recovery. Such islands require continuous, high resolution reconstructions of climatic and anthropogenic changes to the environment to improve both our understanding of the driving mechanisms that affect Caribbean ecosystems, and our ability to predict and attenuate costly damages to island ecosystems and populations (Nogué et al., 2017). Moreover, there exists a spatiotemporal gap in paleoclimatological and paleotempestological studies on Circum-Caribbean islands (Oliva et al., 2018), which, for the reasons stated above, are integral in resolving.

The goal of this thesis was to answer three fundamental questions:

1) Does the site record sedimentary and/or geochemical evidence of climate variability and/or human activity during the Holocene and if so, what is the nature of this variability?
2) What long- and short-term climate factors best account for this variability?
3) How does this compare to other paleoclimatological work in the region?

The answer to the first question is undoubtedly, yes - this sediment core is a prime example of an ideal specimen for paleoenvironmental reconstruction. Although the core is ~9 meters long and contains ~8500 years of data, the most recent ~2900 years are much higher in resolution, with a much faster sedimentation rate, accumulating over 7 meters of sediment during this time, whereas in the previous ~5600 years, only a couple meters of sediment accumulated. The change in sedimentation was likely due to a co-incidence between multiple factors, likely including a strong flooding event (probably a hurricane), in conjunction with a shift toward dryer climate conditions, and the possible presence of pre-historic-era human settlement resulting in land-use changes and increased erosion influencing the river drainage system. Prior to this change in sedimentation, sea level was much higher than at present, and the basin was likely above sea level. This would imply that the CKB was not the same deep, low energy basin, ideal for undisturbed sedimentation, that it is today, which would explain the very slow sedimentation rate and presence of large quantities of shell fragments within the bottom ~40 cm of the core, as well as the presence of corals between ~7075 and ~3600 cal BP in conjunction with decelerating mid-Holocene sea level rise.

Regarding our second research question, this multiproxy analysis appears to document environmental variability related to both long- and short-term climatic and anthropogenic changes in the Holocene. After ~2900 cal BP the depositional environment appears to document hydrological regimes and human activities affecting sediment transport into the Baradères Bay. Prior to ~2900 cal BP, the curves of sand, fines, and several element ratios including Ca/Fe and

Ti/Ca follow precessional patterns, likely forced primarily by atmospheric phenomena such as solar insolation variability and migration of the ITCZ. The exact nature of this long- and short-term variability will need to be explored in more detail using a more developed age-depth model, possibly with a statistical analysis of the relationship between precessional forcing and XRF data.

In answer to the third question, our results complement other regional paleoclimate studies relatively well. In particular, data collected from a bog in the Dominican Republic (Kennedy et al., 2006) reported wetter conditions at ~4000 cal BP which they attributed with the formation of the bog. Peros et al. (2015) similarly noted the initial formation of a lagoon in Cuba at around ~4000 cal BP. Our data suggests a similar wet and windy period at ~4000 cal BP reflected in high values of sand, and likely resulting in the initial formation of the Baradères river delta. Kennedy et al. (2006) also report low pollen influx and OM suggesting regional periodic drying between ~3700 and 1200 cal BP which is consistent with the overall drying we see from ~3700 cal BP onward.

Additionally, Hodell et al. (1991) found evidence of an increasingly mesic environment at Lake Miragoâne from 8200 to 2500 cal BP, during which time Higuera-Gundy et al. (1999) found an increase in charcoal and pollen of fire-resistant fauna, which was interpreted as a reflection of this wet environment, and which is in general agreement with our data. More generally, high values of Ti and Ti/Ca are associated with finer sediments in the core and indicate relatively humid conditions at ~6500 cal BP, followed by a gradual drying trend, which is consistent with data from elsewhere in the Caribbean that reflects a more southward migration of the ITCZ. Moreover, van Hengstrum et al. (2016) suggested that from 2500 to 1000 cal BP the North Atlantic experienced an interval of intense hurricane activity related to a more northern ITCZ position that favoured cyclogeneses in the central MDR and reduced vertical wind shear. Our data similarly has several short-duration peaks in organics and sand between ~2500 and ~900 cal BP which could very likely be attributed to hurricane strikes, but which require further evidence from additional proxies to verify.

5.2. Limitations and Recommendations for Future Work

A major limitation in the analysis of this core, which could also be seen as a benefit to the study, was simply the volume of information that it provided. When identifying patterns in the core, it became essential to split the graphs and figures into smaller sections (zones) to be able to distinguish different patterns. Specifically, the scale of XRF and grain-size data is so drastically different before and after ~664 cm depth that when looking at the entire core, no pattern emerges in many of the elements prior to this change in sedimentation.

Of course, statistics like PCA and cluster analysis can help us solve the mystery and start putting pieces of the puzzle together, but these methods are limited by the knowledge of the researcher and the constraints they ultimately apply to the data. While the fields of paleoclimatology and paleolimnology have been developed and perfected since the early 1900's, the use of long timescale, high-resolution XRF data is relatively new, and the practical approaches have been largely qualitative in nature. Further research is required to develop the best practices for statistical analysis of such specimens, and this core has the potential to be a prime example for such a study.

Another major limitation of this study is the lack of radiocarbon dating samples that I was basing my assumptions upon. Given a sediment core of this length, with the distinct variations in sedimentation rates, four terrestrial dates (with two found within the same cm of the core) provide a decidedly low resolution and therefore account for a rather high uncertainty in the age-depth model- especially after the large peak and abrupt sediment rate change at ~664 cm. We very recently obtained 15 additional marine C-14 dates from various mollusc and coral species, however for reasons relating to the Covid-19 pandemic, setbacks relating to unsuccessful Pb-210 dating, and time constraints that come with working with several international research partners, we did not have the time to address these new dates within the timeframe of this thesis.

That being said, preliminary assessment of the additional dates (corrected for Marine Reservoir Effect using Marine20 calibration) reveal that the new data correlates well with existing terrestrial C-14 dates, and that the age-depth model is likely skewed in such a way that some of the existing peaks become much narrower than they appear in our current model. For example, we dated two mollusks, one on either end of the large peak in Ti/Ca and Rb/Sr starting at ~664 cm (Table 2), whose median calibrated ages were only ~20 years apart, despite having half a meter of sediment separating them. This leads us to suspect that the theory relating to hurricane-related patterns in ratios like Rb/Sr is likely correct, and this theory will be explored in more detail prior to the publication of the article in Chapter 4, hopefully with 5-10 additional marine dates to solidify our hypothesis and further reduce uncertainty in the age-depth model.

Another limitation of this approach is that coastal basins, while providing a relatively low-energy depositional environment, are complex paleoenvironmental archives because their geomorphic histories can be affected by climate, human activities, and also sea-level change (Gregory et al., 2015). The overall results of this study indicate that Baie des Baradères has been affected by a multitude of components including sea level rise, tectonic activity, anthropogenic forcings, and atmospheric phenomena such as hurricanes and droughts, because of its coastal setting and its karst topography, both of which increase its sensitivity to sea level rise and human impacts. Given this complex relationship between natural and anthropogenic climate change and the sensitive tropical coastal ecosystem, it can be expected that such Caribbean islands will continue to undergo profound changes over the upcoming decades and centuries.

Depth from Surface (cm)	I.d.	Type	FModern	Age + error (BP)	Calibration curve	Median Calibrated age (cal BP)
12.5	HATC1_D1_1:1_12-13cm	Mollusc	1.0629	>Modern	Marine20	N/A
81.5	HATC1_D1_1:1_81-82cm	Mollusc	1.1362	>Modern	Marine20	N/A
214.5	HATC1_D2_2:7_90-91cm	Plant/Wood	0.95980	330 ±15	Intcal20	382
214.5	HATC1_D2_2:7_90-91cm	Mollusc	0.9217	655 ±15	Marine20	325
294.5	HATC1_D2_3:7_25-26cm	Mollusc	0.9140	720 ±15	Marine20	378
343.5	HATC1_D2_3:7_73-74cm	Mollusc	0.8778	1050 ±15	Marine20	658
424.5	HATC1_D2_4:7_10-11cm	Mollusc	0.8502	1300 ±20	Marine20	893
504.5	HATC1_D2_4:7_95-96cm	Mollusc	0.8296	1500 ±15	Marine20	1112
616.5	HATC1_D2_5:7_57-58cm	Mollusc	0.7555	2250 ±15	Marine20	1938
667.5	HATC1_D2_5:7_108-109cm	Mollusc	0.7543	2270 ±15	Marine20	1957
743.5	HATC1_D2_6:7_39-40cm	Mollusc	0.6946	2930 ±20	Marine20	2778
744.5	HATC1_D2_6:7_40-41cm	Plant/Wood	0.74150	2400 ±75	Intcal20	2476
764.5	HATC1_D2_6:7_60-61cm	Coral	0.6631	3300 ±20	Marine20	3222
794.5	HATC1_D2_6:7_90-91cm	Mollusc	0.6682	3240 ±25	Marine20	3146
824.5	HATC1_D2_6:7_120-121cm	Coral	0.6062	4020 ±20	Marine20	4134
855.5	HATC1_D2_7:7_8-9cm	Mollusc	0.5402	4950 ±25	Marine20	5321
894.5	HATC1_D2_7:7_47-48cm	Mollusc	0.4309	6760 ±25	Marine20	7278
895.5	HATC1_D2_7:7_48-49cm	Plant/Wood	NA	7690 ±30	Intcal20	8471
895.5	HATC1_D2_7:7_48-49cm	Plant/Wood	0.37310	7920 ±65	Intcal20	8768

Table 2: Summary of terrestrial and marine macrofossils radiocarbon dated at the National Ocean Sciences Accelerator Mass Spectrometry (NOSAMS) facility at Woods Hole Oceanographic Institution (WHOI) for sediment core HATC1. Only those highlighted in green were applied to this study due to time constraints related to the Covid-19 pandemic. All data, plus 5-6 additional dates will be applied to this study before it is submitted for peer-review.

Future work should include the addition of proxies from this sediment core including pollen, charcoal, and stable isotope analysis. Charcoal and pollen identification will be especially helpful in the interpretation of climatic versus anthropogenic shifts in the environment, while isotope analysis will provide insight into the variations of hydrological cycles, and their relationship to the position of the ITCZ. Ultimately, a complete comprehension of the relationships between climate variability, human activity, and the ecosystems of the Caribbean will require an increase in the number of studies and study sites to allow discrimination between systematic climate fluctuations across all sites and anthropogenic, site-specific forcings. The collaboration with our research partners as this project grows will be greatly beneficial in this sharing of knowledge and improvement of our interpretations. Finally, I would suggest that a potential next step in this project should be another field trip to Hispaniola and surrounding islands to collect additional sediment cores and other potential proxies (speleothems, tree cores) which can be valuable in this interpretation, and which would also now cover several additional years of data, including Hurricane Matthew (2016), Hurricane Elsa (2021) and an Mw 7.2 earthquake on August 14, 2021.

References

Abraham, J., Dowling, K., & Florentine, S. (2017). The Unquantified Risk of Post-Fire Metal Concentration in Soil: a Review. *Water, Air, and Soil Pollution*, *228*(5), 1–33. https://doi.org/10.1007/s11270-017-3338-0

Adomat, F., & Gischler, E. (2017). Assessing the suitability of Holocene environments along the central Belize coast, Central America, for the reconstruction of hurricane records. *International Journal of Earth Sciences*, *106*(1), 283–309. https://doi.org/10.1007/s00531-016-1319-y

Agosta G'Meiner, A. (2016). *Holocene environmental change inferred from fossil pollen and microcharcoal*. McGill University.

Bakun, W. H., Flores, C. H., & ten Brink, U. S. (2012). Significant Earthquakes on the Enriquillo Fault System, Hispaniola, 1500-2010: Implications for Seismic Hazard. *Bulletin of the Seismological Society of America*, *102*(1), 18–30. https://doi.org/10.1785/0120110077

Bargout, R. N., & Raizada, M. N. (2013). Soil nutrient management in Haiti, pre-Columbus to the present day: Lessons for future agricultural interventions. *Agriculture and Food Security*, *2*(1), 1–20. https://doi.org/10.1186/2048-7010-2-11

Bataille, C. P., Laffoon, J., & Bowen, G. J. (2012). Mapping multiple source effects on the strontium isotopic signatures of ecosystems from the circum-Caribbean region. *Ecosphere*, *3*(12), art118. https://doi.org/10.1890/es12-00155.1

Bennett, E. M., Carpenter, S. R., & Caraco, N. F. (2001). Human impact on erodable phosphorus and eutrophication: A global perspective. *BioScience*, *51*(3), 227–234. https://doi.org/10.1641/0006-3568(2001)051[0227:HIOEPA]2.0.CO;2

Bennett, K. D. (1996). Determination of the number of zones in a biostratigraphical sequence. *New Phytologist*, *132*(1), 155–170. https://doi.org/10.1111/j.1469-8137.1996.tb04521.x

Bentley, R. A. (2006). Strontium isotopes from the earth to the archaeological skeleton: A review. In *Journal of Archaeological Method and Theory* (Vol. 13, Issue 3, pp. 135–187). Springer. https://doi.org/10.1007/s10816-006-9009-x

Berman, M. J., & Pearsall, D. M. (2000). Plants, People, and Culture in the Prehistorc Central Bahamas: A View From the Three Dogs Site, an Early Lucayan Settlement on San Salvador Island, Bahamas. *Latin American Antiquety, Cambridge University Press*, *11*(3), 219–239.

Bertrand, K. (2017). *Baraderes: Mystical Venice of Haiti*. Haitian Observer. http://www.haitiobserver.com/blog/baraderes-mystical-venice-of-haiti.html

Binford, M. W., Brenner, M., Whitmore, T. J., Higuera-Gundy, A., Deevey, E. S., & Leyden, B. (1987). Ecosystems, paleoecology and human disturbance in subtropical and tropical america. *Quaternary Science Reviews*, *6*(2), 115–128. https://doi.org/10.1016/0277-3791(87)90029-1

Blaauw, M., & Christen, J. A. (2011). Flexible paleoclimate age-depth models using an autoregressive gamma process. *Bayesian Analysis*, *6*(3), 457–474. https://doi.org/10.1214/11-BA618

Blaauw, M., Christen, J. A., Aquino, M. A., Esquivel, J., Theiler, J., Gough, B., & Karney, C. (2021). *Package ' rbacon ': Age-Depth Modelling using Bayesian Statistics: Vol. Version2.5*.

Black, D. E., Abahazi, M. A., Thunell, R. C., Kaplan, A., Tappa, E. J., & Peterson, L. C. (2007). An 8-century tropical Atlantic SST record from the Cariaco Basin: Baseline variability, twentieth-century warming, and Atlantic hurricane frequency. *Paleoceanography*, *22*(4), PA4204. https://doi.org/10.1029/2007PA001427

Boldt, K. V., Lane, P., Woodruff, J. D., & Donnelly, J. P. (2010). Calibrating a sedimentary record of overwash from Southeastern New England using modeled historic hurricane surges. *Marine Geology*, *275*(1–4), 127–139. https://doi.org/10.1016/j.margeo.2010.05.002

Braithwaite, C. J. R. (2016). Coral-reef records of Quaternary changes in climate and sea-level. *Earth-Science Reviews*, *156*, 137–154. https://doi.org/10.1016/j.earscirev.2016.03.002

Brandon, C. M., Woodruff, J. D., Donnelly, J. P., & Sullivan, R. M. (2014). How unique was hurricane sandy? sedimentary reconstructions of extreme flooding from New York Harbor. *Scientific Reports*, *4*. https://doi.org/10.1038/srep07366

Brenner, M., & Binford, M. W. (1988). A sedimentary record of human disturbance from Lake Miragoane, Haiti. *Journal of Paleolimnology*, *1*(2), 85–97. https://doi.org/10.1007/BF00196066

Brown, S. (1996). Tropical forests and the global carbon cycle: estimating state and change in biomass density. In *Forest Ecosystems, Forest Management and the Global Carbon Cycle* (pp. 135–144). Springer Berlin Heidelberg. https://doi.org/10.1007/978-3-642-61111-7_13

Burney, D. A., Burney, L. P., & MacPhee, R. D. E. (1994). Holocene charcoal stratigraphy from Laguna Tortuguero, Puerto Rico, and the timing of human arrival on the Island. *Journal of Archaeological Science*, *21*(2), 273–281. https://doi.org/10.1006/jasc.1994.1027

Caffrey, M. A. (2011). *Holocene Climate and Environmental History of Laguna Saladilla, Dominican Republic*. University of Tennessee, Knoxville.

Caffrey, M. A., & Horn, S. P. (2015). Long-Term Fire Trends in Hispaniola and Puerto Rico from Sedimentary Charcoal: A Comparison of Three Records. *Professional Geographer*, *67*(2), 229–241. https://doi.org/10.1080/00330124.2014.922017

Camargo, S. J., Ting, M., & Kushnir, Y. (2013). Influence of local and remote SST on North Atlantic tropical cyclone potential intensity. *Climate Dynamics*, *40*(5–6), 1515–1529. https://doi.org/10.1007/s00382-012-1536-4

Castilla-Beltrán, A., Hooghiemstra, H., Hoogland, M. L. P., Donders, T. H., Pagán-Jiménez, J.

R., McMichael, C. N. H., Rolefes, S. M. F., Olijhoek, T., Herrera-Malatesta, E., Hung, J. U., & Hofman, C. L. (2020). Ecological responses to land use change in the face of European colonization of Haytí island. *Quaternary Science Reviews*, *241*. https://doi.org/10.1016/j.quascirev.2020.106407

Chandler, D., & Pugh, J. (2021). Anthropocene islands: There are only islands after the end of the world. *Dialogues in Human Geography*, *1–21*. https://doi.org/10.1177/2043820621997018

Cooke, S. B., Dávalos, L. M., Mychajliw, A. M., Turvey, S. T., & Upham, N. S. (2017). Anthropogenic Extinction Dominates Holocene Declines of West Indian Mammals. *Annual Review of Ecology, Evolution, and Systematics*, *48*(1), 301–327. https://doi.org/10.1146/annurev-ecolsys-110316-022754

Curtis, J. H., & Hodell, D. A. (1993). An Isotopic and Trace Element Study of Ostracods from Lake Miragoane, Haiti: A 10,500 Year Record of Paleosalinity and Paleotemperature Changes in the Caribbean. In P. K. Swart, K. C. Lohmann, J. McKenzie, & S. Savin (Eds.), *American Geophysical Union Geophysical Monograph Series* (pp. 135–152). American Geophysical Union (AGU). https://doi.org/10.1029/gm078p0135

Dávalos, L. M., & Turvey, S. T. (2012). West Indian Mammals The Old, the New, and the Recently Extinct. In *Bones, Clones, and Biomes: THE HISTORY AND GEOGRAPHY OF RECENT NEOTROPICAL MAMMALS* (pp. 157–202). https://lmdavalos.github.io/publication/book_section_west_indian_mammals/

Day, M. (2010). Challenges to sustainability in the Caribbean karst. *Geologia Croatica*, *63*(2), 149–154. https://doi.org/10.4154/gc.2010.12

De Boer, E. J., Tjallingii, R., Vélez, M. I., Rijsdijk, K. F., Vlug, A., Reichart, G. J., Prendergast, A. L., de Louw, P. G. B., Florens, F. B. V., Baider, C., & Hooghiemstra, H. (2014). Climate variability in the SW Indian Ocean from an 8000-yr long multi-proxy record in the Mauritian lowlands shows a middle to late Holocene shift from negative IOD-state to ENSO-state. *Quaternary Science Reviews*, *86*, 175–189. https://doi.org/10.1016/j.quascirev.2013.12.026

DeLong, K. L., Flannery, J. A., Poore, R. Z., Quinn, T. M., Maupin, C. R., Lin, K., & Shen, C. C. (2014). A reconstruction of sea surface temperature variability in the southeastern Gulf of Mexico from 1734 to 2008 C.E. using cross-dated Sr/Ca records from the coral Siderastrea siderea. In *Paleoceanography* (Vol. 29, Issue 5, pp. 403–422). Blackwell Publishing Ltd. https://doi.org/10.1002/2013PA002524

Demina, L. L., Novichkova, K. A., Lisitzin, A. P., & Kozina, N. V. (2019). Geochemical signatures of paleoclimate changes in the sediment cores from the gloria and snorri drifts (Northwest atlantic) over the holocene-mid pleistocene. *Geosciences (Switzerland)*, *9*(10). https://doi.org/10.3390/geosciences9100432

Denommee, K. C., Bentley, S. J., & Droxler, A. W. (2014). Climatic controls on hurricane patterns: A 1200-y near-annual record from Lighthouse Reef, Belize. *Scientific Reports*, *4*, 1–7. https://doi.org/10.1038/srep03876

Diekmann, B., Hofmann, J., Henrich, R., Fütterer, D. K., Röhl, U., & Wei, K. Y. (2008). Detrital sediment supply in the southern Okinawa Trough and its relation to sea-level and Kuroshio dynamics during the late Quaternary. *Marine Geology*, *255*(1–2), 83–95. https://doi.org/10.1016/j.margeo.2008.08.001

Donnelly, J. P., Butler, J., Roll, S., Wengren, M., & Webb, T. (2004). A backbarrier overwash record of intense storms from Brigantine, New Jersey. *Marine Geology*, *210*(1–4), 107–121. https://doi.org/10.1016/j.margeo.2004.05.005

Donnelly, J. P., Hawkes, A. D., Lane, P., Macdonald, D., Shuman, B. N., Toomey, M. R., Van Hengstum, P. J., & Woodruff, J. D. (2015). Climate forcing of unprecedented intense-hurricane activity in the last 2000 years. *Earth's Future*, *3*(2), 49–65. https://doi.org/10.1002/2014EF000274

Donnelly, J. P., Roll, S., Wengren, M., Butler, J., Lederer, R., & Webb, T. (2001). Sedimentary evidence of intense hurricane strikes from New Jersey. *Geology*, *29*(7), 615–618. https://doi.org/10.1130/0091-7613(2001)029<0615:SEOIHS>2.0.CO;2

Donnelly, J. P., & Woodruff, J. D. (2007). Intense hurricane activity over the past 5,000 years controlled by El Niño and the West African monsoon. *Nature*, *447*(7143), 465–468. https://doi.org/10.1038/nature05834

Emanuel, K. (2005). Increasing destructiveness of tropical cyclones over the past 30 years. *Nature*, *436*(7051), 686–688. https://doi.org/10.1038/nature03906

Enfield, D. B., Mestas-Nuñez, A. M., & Trimble, P. J. (2001). The Atlantic multidecadal oscillation and its relation to rainfall and river flows in the continental U.S. *Geophysical Research Letters*, *28*(10), 2077–2080. https://doi.org/10.1029/2000GL012745

Fensterer, C., Scholz, D., Hoffmann, D. L., Spötl, C., Schröder-Ritzrau, A., Horn, C., Pajón, J. M., & Mangini, A. (2013). Millennial-scale climate variability during the last 12.5ka recorded in a Caribbean speleothem. *Earth and Planetary Science Letters*, *361*, 143–151. https://doi.org/10.1016/j.epsl.2012.11.019

Fink, G., Alcamo, J., Flörke, M., & Reder, K. (2018). Phosphorus Loadings to the World's Largest Lakes: Sources and Trends. *Global Biogeochemical Cycles*, *32*(4), 617–634. https://doi.org/10.1002/2017GB005858

Fitzpatrick, P. J. (2006). *Hurricanes: A Reference Handbook*. *2nd ed*(ABC-CLIO). http://library1.nida.ac.th/termpaper6/sd/2554/19755.pdf

Fitzpatrick, S. M. (2013). Seafaring Capabilities in the Pre-Columbian Caribbean. *Journal of Maritime Archaeology*, *8*(1), 101–138. https://doi.org/10.1007/s11457-013-9110-8

Fitzpatrick, S. M. (2015). The Pre-Columbian Caribbean: Colonization, Population Dispersal, and Island Adaptations. In *PaleoAmerica* (Vol. 1, Issue 4, pp. 305–331). Taylor and Francis

Ltd. https://doi.org/10.1179/2055557115Y.0000000010

Flannery, J. A., & Poore, R. Z. (2013). Sr/Ca Proxy Sea-Surface Temperature Reconstructions from Modern and Holocene *Montastraea faveolata* Specimens from the Dry Tortugas National Park, Florida, U.S.A. *Journal of Coastal Research*, *63*(SPL.ISSUE), 20–31. https://doi.org/10.2112/SI63-003.1

Foley, J. A., DeFries, R., Asner, G. P., Barford, C., Bonan, G., Carpenter, S. R., Chapin, F. S., Coe, M. T., Daily, G. C., Gibbs, H. K., Helkowski, J. H., Holloway, T., Howard, E. A., Kucharik, C. J., Monfreda, C., Patz, J. A., Prentice, I. C., Ramankutty, N., & Snyder, P. K. (2005). Global consequences of land use. *Science*, *309*(5734), 570–574. https://doi.org/10.1126/science.1111772

Fritz, M., Unkel, I., Lenz, J., Gajewski, K., Frenzel, P., Paquette, N., Lantuit, H., Körte, L., & Wetterich, S. (2018). Regional environmental change versus local signal preservation in Holocene thermokarst lake sediments: A case study from Herschel Island, Yukon (Canada). *Journal of Paleolimnology*, *60*(1), 77–96. https://doi.org/10.1007/s10933-018-0025-0

Gischler, E. (2011). Blue hole. *Encyclopedia of Earth Sciences Series*, *Part 2*, 164–165. https://doi.org/10.1007/978-90-481-2639-2_190

Gischler, E., Shinn, E. A., Oschmann, W., Fiebig, J., & Buster, N. A. (2008). A 1500-year holocene caribbean climate archive from the Blue Hole, lighthouse reef, belize. *Journal of Coastal Research*, *24*(6), 1495–1505. https://doi.org/10.2112/07-0891.1

Goldenberg, S. B., Landsea, C. W., Mestas-Nuñez, A. M., & Gray, W. M. (2001). The recent increase in Atlantic hurricane activity: Causes and implications. *Science*, *293*(5529), 474–479. https://doi.org/10.1126/science.1060040

Goyette, J. O., Bennett, E. M., & Maranger, R. (2018). Low buffering capacity and slow recovery of anthropogenic phosphorus pollution in watersheds. *Nature Geoscience*, *11*(12), 921–925. https://doi.org/10.1038/s41561-018-0238-x

Gray, S. T., Graumlich, L. J., Betancourt, J. L., & Pederson, G. T. (2004). A tree-ring based reconstruction of the Atlantic Multidecadal Oscillation since 1567 A.D. *Geophysical Research Letters*, *31*(12), n/a-n/a. https://doi.org/10.1029/2004GL019932

Gregory, B. R. B., Peros, M. C., Reinhardt, E. G., & Donnelly, J. P. (2015). Middle-late Holocene Caribbean aridity inferred from foraminifera and elemental data in sediment cores from two Cuban lagoons. *Palaeogeography, Palaeoclimatology, Palaeoecology*, *426*, 229–241. https://doi.org/10.1016/j.palaeo.2015.02.029

Grimm, E. C., Jacobson, G. L., Watts, W. A., Hansen, B. C. S., & Maasch, K. A. (1993). A 50,000-year record of climate oscillations from Florida and its temporal correlation with the Heinrich events. *Science*, *261*(5118), 198–200. https://doi.org/10.1126/science.261.5118.198

Haase-Schramm, A., Böhm, F., Eisenhauer, A., Dullo, W. C., Joachimski, M. M., Hansen, B., &

Reitner, J. (2003). Sr/Ca ratios and oxygen isotopes from sclerosponges: Temperature history of the Caribbean mixed layer and thermocline during the Little Ice Age. *Paleoceanography*, *18*(3), n/a-n/a. https://doi.org/10.1029/2002PA000830

Hadden, R. L., & Minson, S. G. (2010). The Geology of Haiti : An Annotated Bibliography of Haiti ' s Geology , Geography and Earth Science. *Army Geospatial Center, US Army Corps of Engineers*, *July*, 256.

Haiti-Politic. (2020, December 26). Digging of a new bed for the Barradères river. *HaitiLibre*. https://www.haitilibre.com/en/news-32621-haiti-politic-digging-of-a-new-bed-for-the-barraderes-river.html

Hashimoto, M., Fukushima, Y., & Fukahata, Y. (2011). Fan-delta uplift and mountain subsidence during the Haiti 2010 earthquake. *Nature Geoscience*, *4*(4), 255–259. https://doi.org/10.1038/ngeo1115

Haug, G. H., Günther, D., Peterson, L. C., Sigman, D. M., Hughen, K. A., & Aeschlimann, B. (2003). Climate and the collapse of Maya civilization. *Science*, *299*(5613), 1731–1735. https://doi.org/10.1126/science.1080444

Haug, G. H., Hughen, K. A., Sigman, D. M., Peterson, L. C., & Röhl, U. (2001). Southward migration of the intertropical convergence zone through the holocene. *Science*, *293*(5533), 1304–1308. https://doi.org/10.1126/science.1059725

Hayden, L. (2018). *Principal Component Analysis in R*. Datacamp. https://www.datacamp.com/community/tutorials/pca-analysis-r

Hayes, G. P., Briggs, R. W., Sladen, A., Fielding, E. J., Prentice, C., Hudnut, K., Mann, P., Taylor, F. W., Crone, A. J., Gold, R., Ito, T., & Simons, M. (2010). Complex rupture during the 12 January 2010 Haiti earthquake. *Nature Geoscience*, *3*(11), 800–805. https://doi.org/10.1038/ngeo977

Hazard, S. (1873). Santo Domingo, past and present : with a glance at Hayti. In *Library of Congress, Washington, D.C. 20540 USA*. Harper & Brothers, New York. https://lccn.loc.gov/02012417

Heaton, T. J., Köhler, P., Butzin, M., Bard, E., Reimer, R. W., Austin, W. E. N., Bronk Ramsey, C., Grootes, P. M., Hughen, K. A., Kromer, B., Reimer, P. J., Adkins, J., Burke, A., Cook, M. S., Olsen, J., & Skinner, L. C. (2020). Marine20 - The Marine Radiocarbon Age Calibration Curve (0-55,000 cal BP). *Radiocarbon*, *62*(4), 779–820. https://doi.org/10.1017/RDC.2020.68

Hedges, S. B., Cohen, W. B., Timyan, J., & Yang, Z. (2018). Haiti's biodiversity threatened by nearly complete loss of primary forest. *Proceedings of the National Academy of Sciences of the United States of America*, *115*(46), 11850–11855. https://doi.org/10.1073/pnas.1809753115

Herrera, D. A., Ault, T. R., Fasullo, J. T., Coats, S. J., Carrillo, C. M., Cook, B. I., & Williams,

A. P. (2018). Exacerbation of the 2013–2016 Pan-Caribbean Drought by Anthropogenic Warming. *Geophysical Research Letters*, *45*(19), 10,619-10,626. https://doi.org/10.1029/2018GL079408

Higuera-Gundy, A., Brenner, M., Hodell, D. A., Curtis, J. H., Leyden, B. W., & Binford, M. W. (1999). A 10,300 14C yr record of climate and vegetation change from Haiti. *Quaternary Research*, *52*(2), 159–170. https://doi.org/10.1006/qres.1999.2062

Hodell, D. A., Curtis, J. H., Jones, G. A., Higuera-Gundy, A., Brenner, M., Binford, M. W., & Dorsey, K. T. (1991). Reconstruction of Caribbean Climate Change over the past 10,500 years. *Letters to Nature*, *353*, 790–793. https://doi.org/10.1038/255242a0

Holdridge, L. R. (1945). A brief sketch of the flora of Hispaniola. In F. Verdoorn (Ed.), *Plants and Plant Science in Latin America* (pp. 76–78). Chronica Botanica Company.

Houghton, R. A., Skole, D. L., Nobre, C. A., Hackler, J. L., Lawrence, K. T., & Chomentowski, W. H. (2000). Annual fluxes of carbon from deforestation and regrowth in the Brazilian Amazon. *Nature*, *403*(6767), 301–304. https://doi.org/10.1038/35002062

IciHaiti. (2021a, January 13). Launch of work to divert the great Baradères river. *HaitiLibre*. https://www.icihaiti.com/en/news-32764-icihaiti-politic-launch-of-work-to-divert-the-great-baraderes-river.html

IciHaiti. (2021b, February 21). Monitoring of works of the deviation of the great Baradères river. *HaitiLibre*. https://www.icihaiti.com/en/news-33070-icihaiti-politic-monitoring-of-works-of-the-deviation-of-the-great-baraderes-river.html

Inez Again Threatens Florida and Gulf Coast. (1966, October 1). *The Victoria Advocate* . https://news.google.com/newspapers?id=_7ZdAAAAIBAJ&pg=5552,7481&dq=hurricane+inez&hl=en

Inez Hurt Haiti. (1966, December 1). *The Calgary Herald*.

INSTITUT HAÏTIEN DE STATISTIQUE ET D'INFORMATIQUE (IHSI). (2015). *Population Totale, De 18 Ans et Plus: Menages et Estimes en 2015*. Direction Des Statistiques Démographiques Et Sociales (DSDS).

International Federation of Red Cross and Red Crescent Societies (IFRC). (2014). *How Law and Regulation Supports Disaster Risk Reduction: Haiti Case- Study Report*. https://www.google.com/url?sa=i&url=http%3A%2F%2Fwww.ifrc.org%2FGlobal%2FPublications%2FIDRL%2Fcountry%2520studies%2FHAITI%2520DRR%2520Report.pdf&psig=AOvVaw2B2q9Ago3u4nVjq5K2zYFK&ust=1627069176103000&source=images&cd=vfe&ved=0CAwQ3YkBahcKEwiw-IOVt_fxAhUA

IPCC. (2014). Climate Change 2014: Synthesis Report. Contribution of Working Groups I, II and III to the Fifth Assessment Report of the Intergovernmental Panel on Climate Change. In *[Core Writing Team, R.K. Pachauri and L.A. Meyer (eds.)]* (p. 151). IPCC, Geneva, Switzerland. https://www.ipcc.ch/report/ar5/syr/

Jollife, I. T., & Cadima, J. (2016). Principal component analysis: A review and recent developments. *Philosophical Transactions of the Royal Society A: Mathematical, Physical and Engineering Sciences*, *374*(2065). https://doi.org/10.1098/rsta.2015.0202

Juggins, S. (2020). Package ' rioja .' *An R Package for the Analysis of Quaternary Science Data.*, *0.9-26*.

Karnauskas, K. B., Schleussner, C. F., Donnelly, J. P., & Anchukaitis, K. J. (2018). Freshwater stress on small island developing states: population projections and aridity changes at 1.5 and 2 °C. *Regional Environmental Change*, *18*(8), 2273–2282. https://doi.org/10.1007/s10113-018-1331-9

Kassambara, A. (2017). PCA - Principal Component Analysis Essentials. In *Practical Guide To Principal Component Methods in R: PCA, M(CA), FAMD, MFA, HCPC, Factoextra*. STHDA. http://www.sthda.com/english/articles/31-principal-component-methods-in-r-practical-guide/112-pca-principal-component-analysis-essentials/

Kassambara, A., & Mundt, F. (2020). Factoextra: Extract and Visualize the Results of Multivariate Data Analyses (Versión 1.0.5). In *CRAN- R Package*. Comprehensive R Archive Network (CRAN). https://cran.r-project.org/package=factoextra

Keegan, W. F. (1994). West Indian archaeology. 1. Overview and foragers. *Journal of Archaeological Research*, *2*(3), 255–284.

Keigwin, L. D., & Jones, G. A. (1989). Glacial-Holocene stratigraphy, chronoly, and paleoceanographic observations on some North Atlantic sediment drifts. *Deep-Sea Research*, *36*(6), 845–867.

Kennedy, L. M., Horn, S. P., & Orvis, K. H. (2006). A 4000-year record of fire and forest history from Valle de Bao, Cordillera Central, Dominican Republic. *Palaeogeography, Palaeoclimatology, Palaeoecology*, *231*(3–4), 279–290. https://doi.org/10.1016/j.palaeo.2005.08.002

Khan, N. S., Ashe, E., Horton, B. P., Dutton, A., Kopp, R. E., Brocard, G., Engelhart, S. E., Hill, D. F., Peltier, W. R., Vane, C. H., & Scatena, F. N. (2017). Drivers of Holocene sea-level change in the Caribbean. In *Quaternary Science Reviews* (Vol. 155, pp. 13–36). Elsevier Ltd. https://doi.org/10.1016/j.quascirev.2016.08.032

Kilbourne, K. H., Quinn, T. M., Webb, R., Guilderson, T., Nyberg, J., & Winter, A. (2008). Paleoclimate proxy perspective on Caribbean climate since the year 1751: Evidence of cooler temperatures and multidecadal variability. *Paleoceanography*, *23*(3), n/a-n/a. https://doi.org/10.1029/2008PA001598

Klotzbach, P. J. (2006). Trends in global tropical cyclone activity over the past twenty years (1986-2005). *Geophysical Research Letters*, *33*(10), 1984–1987. https://doi.org/10.1029/2006GL025881

Klotzbach, P. J., & Landsea, C. W. (2015). Extremely intense hurricanes: Revisiting Webster et al. (2005) after 10 years. *Journal of Climate*, *28*(19), 7621–7629. https://doi.org/10.1175/JCLI-D-15-0188.1

Knowles, R. B., Buckalew, J. O., Markley, B., & Waite Roesbuck, L. (1999). Water Resources Assessment of Haiti. In *Water Resources Assessment of Haiti* (Issue August). http://www.sam.usace.army.mil/Portals/46/docs/military/engineering/docs/WRA/Ecuador/Ecuador WRA English.pdf

Knutson, T. R., McBride, J. L., Chan, J., Emanuel, K., Holland, G., Landsea, C., Held, I., Kossin, J. P., Srivastava, A. K., & Sugi, M. (2010). Tropical cyclones and climate change. *Nature Geoscience*, *3*(3), 157–163. https://doi.org/10.1038/ngeo779

Koch, A., Brierley, C., Maslin, M. M., & Lewis, S. L. (2019). Earth system impacts of the European arrival and Great Dying in the Americas after 1492. *Quaternary Science Reviews*, *207*, 13–36. https://doi.org/10.1016/j.quascirev.2018.12.004

Kueny, J. A., & Day, M. J. (1998). An Assessment of Protected Karst Landscapes in the Caribbean. *Caribbean Geography*, *9*(2), 87–100.

Landsea, C. W., Harper, B. A., Hoarau, K., & Knaff, J. A. (2006). Can we detect trends in extreme tropical cyclones? In *Science* (Vol. 313, Issue 5786, pp. 452–454). American Association for the Advancement of Science. https://doi.org/10.1126/science.1128448

Lane, C. S., Horn, S. P., Orvis, K. H., & Thomason, J. M. (2011). Oxygen isotope evidence of Little Ice Age aridity on the Caribbean slope of the Cordillera Central, Dominican Republic. *Quaternary Research*, *75*(3), 461–470. https://doi.org/10.1016/j.yqres.2011.01.002

Lane, P., Donnelly, J. P., Woodruff, J. D., & Hawkes, A. D. (2011). A decadally-resolved paleohurricane record archived in the late Holocene sediments of a Florida sinkhole. *Marine Geology*, *287*(1–4), 14–30. https://doi.org/10.1016/j.margeo.2011.07.001

Lê, S., Josse, J., & Husson, F. (2008). FactoMineR: An R package for multivariate analysis. *Journal of Statistical Software*, *25*(1), 1–18. https://doi.org/10.18637/jss.v025.i01

Leblanc, A. R., Kennedy, L. M., & Chad, K. L. (2017). Linking hurricane landfalls , precipitation variability , fires , and vegetation response over the past millennium from analysis of coastal lagoon sediments , southwestern Dominican Republic. *Journal of Paleolimnology*, *58*(2), 135–150. https://doi.org/10.1007/s10933-017-9965-z

Lehmann, A., Getzlaff, K., & Harlaß, J. (2011). Detailed assessment of climate variability in the Baltic Sea area for the period 1958 to 2009. *Climate Research*, *46*(2), 185–196. https://doi.org/10.3354/cr00876

Lehner, F., Coats, S., Stocker, T. F., Pendergrass, A. G., Sanderson, B. M., Raible, C. C., & Smerdon, J. E. (2017). Projected drought risk in 1.5°C and 2°C warmer climates. *Geophysical Research Letters*, *44*(14), 7419–7428. https://doi.org/10.1002/2017GL074117

Lewis, L. A., & Coffey, W. J. (1985). The continuing deforestation of Haiti. *Ambio*, *14*(3), 158–

160. https://doi.org/10.2307/4313133

Li, J., Xie, S. P., Cook, E. R., Morales, M. S., Christie, D. A., Johnson, N. C., Chen, F., D'Arrigo, R., Fowler, A. M., Gou, X., & Fang, K. (2013). El Niño modulations over the past seven centuries. *Nature Climate Change*, *3*(9), 822–826. https://doi.org/10.1038/nclimate1936

Liu, K.-B. (2004). Principles, methods, and examples from Gulf Coast lake sediments. In R. J. Murnane & K.-B. Liu (Eds.), *Hurricanes and Typhoons: Past, Present and Future.* (pp. 13–28). New York: Columbia University Press.

Liu, K.-B., & Fearn, M. L. (2000). Reconstruction of prehistoric landfall frequencies of catastrophic hurricanes in Northwestern Florida from lake sediment records. *Quaternary Research*, *54*(2), 238–245. https://doi.org/10.1006/qres.2000.2166

López, G. I. (2016). Grain size analysis. In Gilbert A.S. (Ed.), *Encyclopedia of Geoarchaeology* (pp. 341–348). Springer Netherlands. https://doi.org/10.1007/978-1-4020-4409-0_18

Lord, K. S., Barcala, A., Aichelman, H. E., Kriefall, N. G., Brown, C., Knasin, L., Secor, R., Tone, C., Tsang, L., & Finnerty, J. R. (2021). Distinct phenotypes associated with mangrove and lagoon habitats in two widespread caribbean corals, porites astreoides and porites divaricata. *Biological Bulletin*, *240*(3), 169–190. https://doi.org/10.1086/714047

Lorenz, S. J., Kim, J., Rimbu, N., & Schneider, R. R. (2006). Orbitally driven insolation forcing on Holocene climate trends : Evidence from alkenone data and climate modeling. *Paleoceanography and Paleoclimatology*, *21*, 1–14. https://doi.org/10.1029/2005PA001152

Lozano-Gracia, N., & Garcia Lozano, M. (2017). Haitian Cities : Actions for Today with an Eye on Tomorrow. In *World Bank, World Development Indicators*.

Mann, M. E., Woodruff, J. D., Donnelly, J. P., & Zhang, Z. (2009). Atlantic hurricanes and climate over the past 1,500 years. *Nature*, *460*(7257), 880–883. https://doi.org/10.1038/nature08219

Mann, M. E., Zhang, Z., Hughes, M. K., Bradley, R. S., Miller, S. K., Rutherford, S., & Ni, F. (2008). Proxy-based reconstructions of hemispheric and global surface temperature variations over the past two millennia. *Proceedings of the National Academy of Sciences of the United States of America*, *105*(36), 13252–13257. https://doi.org/10.1073/pnas.0805721105

Mann, P., Calais, E., Ruegg, J.-C., DeMets, C., Jansma, P. E., & Mattioli, G. S. (2002). Oblique collision in the northeastern Caribbean from GPS measurements and geological observations. *Tectonics*, *21*(6), 7-1-7–26. https://doi.org/10.1029/2001TC001304

Marsh, R., Mills, R. A., Green, D. R. H., Salter, I., & Taylor, S. (2007). Controls on sediment geochemistry in the Crozet region. *Deep-Sea Research Part II: Topical Studies in Oceanography*, *54*(18–20), 2260–2274. https://doi.org/10.1016/j.dsr2.2007.06.004

Marshall, J., Kushnir, Y., Battisti, D., Chang, P., Czaja, A., Dickson, R., Hurrell, J., McCartney, M., Saravanan, R., & Visbeck, M. (2001). North Atlantic climate variability: Phenomena, impacts and mechanisms. *International Journal of Climatology*, *21*(15), 1863–1898. https://doi.org/10.1002/joc.693

Mayorga, E., Aufdenkampe, A. K., Masiello, C. A., Krusche, A. V., Hedges, J. I., Quay, P. D., Richey, J. E., & Brown, T. A. (2005). Young organic matter as a source of carbon dioxide outgassing from Amazonian rivers. *Nature*, *436*(7050), 538–541. https://doi.org/10.1038/nature03880

McCloskey, T. A., & Liu, K. biu. (2013). A 7000 year record of paleohurricane activity from a coastal wetland in Belize. *Holocene*, *23*(2), 278–291. https://doi.org/10.1177/0959683612460782

McGillis, W. R., Hsueh, D. Y., Zheng, Y., Markowitz, M., Gibson, R., Bolduc, G., Fevrin, F. J., Thys, J. E., Noel, W., Paine, J. K., Wang, Z. A., Hoering, K., Hakimdavar, R., & Culligan, P. J. (2015). Carbon transport in rivers of southwest Haiti. *Applied Geochemistry*, *63*, 563–572. https://doi.org/10.1016/j.apgeochem.2015.09.004

McHugh, C. M. G., Braudy, N., Çağatay, M. N., Sorlien, C., Cormier, M. H., Seeber, L., & Henry, P. (2014). Seafloor fault ruptures along the North Anatolia Fault in the Marmara Sea, Turkey: Link with the adjacent basin turbidite record. *Marine Geology*, *353*, 65–83. https://doi.org/10.1016/j.margeo.2014.03.005

McHugh, C. M., Seeber, L., Braudy, N., Cormier, M. H., Davis, M. B., Diebold, J. B., Dieudonne, N., Douilly, R., Gulick, S. P. S., Hornbach, M. J., Johnson, H. E., Mishkin, K. R., Sorlien, C. C., Steckler, M. S., Symithe, S. J., & Templeton, J. (2011). Offshore sedimentary effects of the 12 January 2010 Haiti earthquake. *Geology*, *39*(8), 723–726. https://doi.org/10.1130/G31815.1

Metcalfe, S. E., Leng, M. J., Kirby, J. R., Huddart, D., Vane, C. H., & Gonzalez, S. (2016). Early–Mid Pleistocene environments in the Valsequillo Basin, Central Mexico: a reassessment. *Journal of Quaternary Science*, *31*(4), 325–336. https://doi.org/10.1002/jqs.2851

Milne, G. A., Long, A. J., & Bassett, S. E. (2005). Modelling Holocene relative sea-level observations from the Caribbean and South America. *Quaternary Science Reviews*, *24*(10–11), 1183–1202. https://doi.org/10.1016/j.quascirev.2004.10.005

Milne, G. A., & Peros, M. C. (2013). Data-model comparison of Holocene sea-level change in the circum-Caribbean region. *Global and Planetary Change*, *107*, 119–131. https://doi.org/10.1016/j.gloplacha.2013.04.014

Mittermeier, R. A., Myers, N., Mittermeier, C. G., & Robles Gil, P. (2000). Hotspots: Earth's biologically richest and most endangered terrestrial ecoregions. *Choice Reviews Online*, *38*(02), 38-0922-38–0922. https://doi.org/10.5860/choice.38-0922

Moore, C. (1991). Cabaret: Lithic Workshop Sites in Haiti. In J. Haviser & E. Ayubi (Eds.), *Proceedings of the 13th Congress of the Interna-tional Association for Caribbean Archaeology* (pp. 92–104).

Moreau de Saint-Méry, M. L. E. (1796). *Description topographique et politique de la partie espagnole de l'isle Saint-Domingue*. https://books.google.ca/books?hl=en&lr=&id=ZpxaAAAAcAAJ&oi=fnd&pg=PA1&dq=Moreau+de+Saint+Mery,+L.+E.+(1796).+Description+Topographique+et+politique+de+la+partie+espangnole+de+l'isle+Saint-Domingue+1,+Moreau+de+Saint+Mery,+Philadelphia,+307+p&ots=aL8FbHY9t

Moreau de Saint-Méry, M. L. E. (1798). *Description topographique, physique, civile, politique et historique de la partie francause de l'isle Saint-Dominigue*.

Moyer, R. P., Bauer, J. E., & Grottoli, A. G. (2013). Carbon isotope biogeochemistry of tropical small mountainous river, estuarine, and coastal systems of Puerto Rico. *Biogeochemistry*, *112*(1–3), 589–612. https://doi.org/10.1007/s10533-012-9751-y

Muller, J., Collins, J. M., Gibson, S., & Paxton, L. (2017). Recent Advances in the Emerging Field of Paleotempestology. In J. M. Collins & K. Walsh (Eds.), *Hurricanes and Climate Change* (Vol. 3, pp. 1–33). Springer International Publishing. https://doi.org/10.1007/978-3-319-47594-3_1

Munroe, J. S., McElroy, R., O'Keefe, S., Peters, A., & Wasson, L. (2021). Holocene records of eolian dust deposition from high-elevation lakes in the Uinta Mountains, Utah, USA. *Journal of Quaternary Science*, *36*(1), 66–75. https://doi.org/10.1002/jqs.3250

Naeher, S., Gilli, A., North, R. P., Hamann, Y., & Schubert, C. J. (2013). Tracing bottom water oxygenation with sedimentary Mn/Fe ratios in Lake Zurich, Switzerland. *Chemical Geology*, *352*, 125–133. https://doi.org/10.1016/j.chemgeo.2013.06.006

Napolitano, M. F., DiNapoli, R. J., Stone, J. H., Levin, M. J., Jew, N. P., Lane, B. G., O'Connor, J. T., & Fitzpatrick, S. M. (2019). Reevaluating human colonization of the Caribbean using chronometric hygiene and Bayesian modeling. *Science Advances*, *5*(12). https://doi.org/10.1126/sciadv.aar7806

Naquin, J. D., Liu, K. B., McCloskey, T. A., & Bianchette, T. A. (2014). Storm deposition induced by hurricanes in a rapidly subsiding coastal zone. *Journal of Coastal Research*, *70*(70), 308–313. https://doi.org/10.2112/SI70-052.1

NOAA. (2009). *Historical hurricane data*. National Oceanic and Atmospheric Administration, US Department of Commerce. https://coast.noaa.gov/hurricanes/#map=4/32/-80

Nogué, S., De Nascimento, L., Froyd, C. A., Wilmshurst, J. M., De Boer, E. J., Coffey, E. E. D., Whittaker, R. J., Fernández-Palacios, J. M., & Willis, K. J. (2017). Island biodiversity conservation needs palaeoecology. *Nature Ecology and Evolution*, *1*(7). https://doi.org/10.1038/s41559-017-0181

Nurse, L., & Sem, G. (2001). Small Island states. In P. for the I. P. on C. Change (Ed.), *Climate*

Change 2001: Impacts, Adaptation and Vulnerability (pp. 843–876). Cambridge University Press.

Oliva, F. (2017). *Multi-Scale , Multi-Proxy Investigation of Late Holocene Tropical Cyclone Activity in the Western North Atlantic Basin*. University of Ottawa, Ottawa, Ontario.

Oliva, F., Peros, M. C., & Viau, A. (2017). A review of the spatial distribution of and analytical techniques used in paleotempestological studies in the western North Atlantic Basin. *Progress in Physical Geography*, *41*(2), 171–190. https://doi.org/10.1177/0309133316683899

Oliva, F., Viau, A. E., Peros, M. C., & Bouchard, M. (2018). Paleotempestology database for the western North Atlantic basin. *Holocene*, *28*(10), 1664–1671. https://doi.org/10.1177/0959683618782598

Paciorek, C. J., Risbey, J. S., Ventura, V., & Rosen, R. D. (2002). Multiple indices of Northern Hemisphere cyclone activity, winters 1949-99. *Journal of Climate*, *15*(13), 1573–1590. https://doi.org/10.1175/1520-0442(2002)015<1573:MIONHC>2.0.CO;2

Pelling, M., & Uitto, J. I. (2001). Small island developing states: Natural disaster vulnerability and global change. *Environmental Hazards*, *3*(2), 49–62. https://doi.org/10.1016/S1464-2867(01)00018-3

Peros, M. C., Collins, S., Agosta G'Meiner, A., Reinhardt, E., & Pupo, F. M. (2017). Multistage 8.2 kyr event revealed through high-resolution XRF core scanning of Cuban sinkhole sediments. *Geophysical Research Letters*, *44*(14), 7374–7381. https://doi.org/10.1002/2017GL074369

Peros, M. C., Gregory, B., Matos, F., Reinhardt, E., & Desloges, J. (2015). Late-Holocene record of lagoon evolution, climate change, and hurricane activity from southeastern Cuba. *Holocene*, *25*(9), 1483–1497. https://doi.org/10.1177/0959683615585844

Peros, M. C., Reinhardt, E. G., Schwarcz, H. P., & Davis, A. M. (2007). High-resolution paleosalinity reconstruction from Laguna de la Leche, north coastal Cuba, using Sr, O, and C isotopes. *Palaeogeography, Palaeoclimatology, Palaeoecology*, *245*(3–4), 535–550. https://doi.org/10.1016/j.palaeo.2006.09.006

Poore, R. Z., Quinn, T. M., & Verardo, S. (2004). Century-scale movement of the Atlantic Intertropical Convergence Zone linked to solar variability. *Geophysical Research Letters*, *31*(12), n/a-n/a. https://doi.org/10.1029/2004GL019940

Prentice, C. S., Mann, P., Crone, A. J., Gold, R. D., Hudnut, K. W., Briggs, R. W., Koehler, R. D., & Jean, P. (2010). Seismic hazard of the Enriquillog-Plantain Garden fault in Haiti inferred from palaeoseismology. *Nature Geoscience*, *3*(11), 789–793. https://doi.org/10.1038/ngeo991

R Core Team. (2021). *R: A Language and Environment for Statistical Computing.* R Foundation for Statistical Computing, Vienna, Austria. https://www.r-project.org/

Rad, S., Cerdan, O., Rivé, K., & Grandjean, G. (2011). Age of river basins in Guadeloupe impacting chemical weathering rates and land use. *Applied Geochemistry*, *26*(SUPPL.), S123–S126. https://doi.org/10.1016/j.apgeochem.2011.03.046

Rad, S., Louvat, P., Gorge, C., Gaillardet, J., & Allégre, C. J. (2006). River dissolved and solid loads in the Lesser Antilles: New insight into basalt weathering processes. *Journal of Geochemical Exploration*, *88*(1-3 SPEC. ISS.), 308–312. https://doi.org/10.1016/j.gexplo.2005.08.063

Rad, S., Rivé, K., Vittecoq, B., Cerdan, O., & Allègre, C. J. (2013). Chemical weathering and erosion rates in the lesser antilles: An overview in guadeloupe, martinique and dominica. In *Journal of South American Earth Sciences* (Vol. 45, pp. 331–344). Pergamon. https://doi.org/10.1016/j.jsames.2013.03.004

Ramsay, H. A., & Sobel, A. H. (2011). Effects of relative and absolute sea surface temperature on tropical cyclone potential intensity using a single-column model. *Journal of Climate*, *24*(1), 183–193. https://doi.org/10.1175/2010JCLI3690.1

Reimer, P. J., Austin, W. E. N., Bard, E., Bayliss, A., Blackwell, P. G., Bronk Ramsey, C., Butzin, M., Cheng, H., Edwards, R. L., Friedrich, M., Grootes, P. M., Guilderson, T. P., Hajdas, I., Heaton, T. J., Hogg, A. G., Hughen, K. A., Kromer, B., Manning, S. W., Muscheler, R., … Talamo, S. (2020). The IntCal20 Northern Hemisphere Radiocarbon Age Calibration Curve (0-55 cal kBP). *Radiocarbon*, *62*(4), 725–757. https://doi.org/10.1017/RDC.2020.41

Reimer, P. J., Bard, E., Bayliss, A., Beck, J. W., Blackwell, P. G., Ramsey, C. B., Buck, C. E., Cheng, H., Edwards, R. L., Friedrich, M., Grootes, P. M., Guilderson, T. P., Haflidason, H., Hajdas, I., Hatté, C., Heaton, T. J., Hoffmann, D. L., Hogg, A. G., Hughen, K. A., … van der Plicht, J. (2013). IntCal13 and Marine13 Radiocarbon Age Calibration Curves 0–50,000 Years cal BP. *Radiocarbon*, *55*(4), 1869–1887. https://doi.org/10.2458/azu_js_rc.55.16947

Rhein, M., Ritounal, S. R., Aoki, S., Campos, E., Chambers, D., Feely, R. A., Gulev, S., Johnson, G. C., Josey, S. A., Kostianoy, A., Mauritzen, C., Reommich, D., Talley, L. D., & Wang, F. (2013). Observations: Ocean. In H. Freeland, S. Garzoli, & Y. Nojiri (Eds.), *Climate Change 2013: The Physical Science Basis Contribution of Working Group I to the Fifth Assessment Report of the Intergovernmental Panel on Climate Change (IPCC)* (pp. 255–315). Cambridge University Press, Cambridge, United Kingdom and New York, NY, USA.

Rick, T. C., Kirch, P. V., Erlandson, J. M., & Fitzpatrick, S. M. (2013). Archeology, deep history, and the human transformation of island ecosystems. *Anthropocene*, *4*(November 2018), 33–45. https://doi.org/10.1016/j.ancene.2013.08.002

Rosenthal, Y., Kalansky, J., Morley, A., & Linsley, B. (2017). A paleo-perspective on ocean heat content: Lessons from the Holocene and Common Era. In *Quaternary Science Reviews* (Vol. 155, pp. 1–12). Elsevier Ltd. https://doi.org/10.1016/j.quascirev.2016.10.017

Rothwell, R. G., & Croudace, I. w. (2015a). *Micro-XRF Studies of Sediment Cores : Applications* *of a Non-destructive Tool for the Environmental Sciences* (J. P. Smol (Ed.)). Springer. https://web-p-ebscohost-com.proxy.bib.uottawa.ca/ehost/ebookviewer/ebook?sid=b693cd97-f42d-4171-8bef-bb6979487841%40redis&vid=0&format=EB

Rothwell, R. G., & Croudace, I. w. (2015b). *Twenty Years of XRF Core Scanning Marine Sediments: What Do Geochemical Proxies Tell Us?* (pp. 25–102). Springer, Dordrecht. https://doi.org/10.1007/978-94-017-9849-5_2

Rouse, I. (1992). The Tainos: rise and decline of the people who greeted Columbus. In *New Haven, CT: Yale University Press*. Cambridge University Press (CUP). https://doi.org/10.1017/s0003598x00045580

Rouse, I., & Moore, C. (1984). Cultural sequence in southwestern Haiti. *Bulletin de Bureau National d'Ethnologie*, *1*, 25–38.

Russell, M. J., Weller, D. E., Jordan, T. E., Sigwart, K. J., & Sullivan, K. J. (2008). Net anthropogenic phosphorus inputs: Spatial and temporal variability in the Chesapeake Bay region. *Biogeochemistry*, *88*(3), 285–304. https://doi.org/10.1007/s10533-008-9212-9

Scherer, J. (1912). Great earthquakes in the Island of Haiti GeoScienceWorld. *Bulletin of the Seismological Society of America*, *2*, 174–179. https://pubs.geoscienceworld.org/ssa/bssa/article-abstract/2/3/161/100985/Great-earthquakes-in-the-Island-of-Haiti?redirectedFrom=PDF

Schmitt, D., Gischler, E., Birgel, D., Peckmann, J., Anselmetti, F. S., & Vogel, H. (2020). Great Blue Hole (Lighthouse Reef, Belize): A continuous, annually-resolved record of Common Era sea surface temperature, Atlantic Multidecadal Oscillation and cyclone-controlled run-off. *Quaternary Science Reviews*, *247*, 106570. https://doi.org/10.1016/j.quascirev.2020.106570

Schneider, T., Bischoff, T., & Haug, G. H. (2014). Migrations and dynamics of the intertropical convergence zone. In *Nature* (Vol. 513, Issue 7516, pp. 45–53). Nature Publishing Group. https://doi.org/10.1038/nature13636

Schreiber, N., Garcia, E., Kroon, A., Ilsøe, P. C., Kjær, K. H., & Andersen, T. J. (2014). Pattern recognition on X-ray fluorescence records from copenhagen lake sediments using principal component analysis. *Water, Air, and Soil Pollution*, *225*(12). https://doi.org/10.1007/s11270-014-2221-5

Schroeter, N., Toney, J. L., Lauterbach, S., Kalanke, J., Schwarz, A., Schouten, S., & Gleixner, G. (2020). How to Deal With Multi-Proxy Data for Paleoenvironmental Reconstructions: Applications to a Holocene Lake Sediment Record From the Tian Shan, Central Asia. *Frontiers in Earth Science*, *8*, 353. https://doi.org/10.3389/feart.2020.00353

Schwartz, M. L. (1982). *The Encyclopedia of beaches and coastal environments*. Hutchinson Ross Pub. Co. https://catalogue.nla.gov.au/Record/139367

Scott, D. B., Medioli, F. S., & Schafer, C. T. (2001). Monitoring in Coastal Environments Using Foraminifera and Thecamoebian Indicators. In *Monitoring in Coastal Environments Using Foraminifera and Thecamoebian Indicators*. Cambridge University Press. https://doi.org/10.1017/cbo9780511546020

Smucker, G. R., Bannister, M., D'Agnes, H., Gossin, Y., Protnoff, M., Timyan, J., Tobias, S., & Toussaint, R. (2007). Environmental Vulnerability in Haiti. *Chemonics and U.S Forest Service*, 141. http://idbdocs.iadb.org/wsdocs/getdocument.aspx?docnum=39826394

Steadman, D. W., Franz, R., Morgan, G. S., Albury, N. A., Kakuk, B., Broad, K., Franz, S. E., Tinker, K., Pateman, M. P., Lott, T. A., Jarzen, D. M., & Dilcher, D. L. (2007). Exceptionally well preserved late Quaternary plant and vertebrate fossils from a blue hole on Abaco, the Bahamas. In *Proceedings of the National Academy of Sciences of the United States of America* (Vol. 104, Issue 50, pp. 19897–19902). National Academy of Sciences. https://doi.org/10.1073/pnas.0709572104

Stevenson, G. G. (1989). The production, distribution, and consumption of fuelwood in Haiti. *Journal of Developing Areas*, *24*(1), 59–76.

Tarter, A. (2016). *Haiti Is Covered with Trees*. EnviroSociety: The Blog from Environment and Society. https://www.envirosociety.org/2016/05/haiti-is-covered-with-trees/

Tierney, J. E., Abram, N. J., Anchukaitis, K. J., Evans, M. N., Giry, C., Kilbourne, K. H., Saenger, C. P., Wu, H. C., & Zinke, J. (2015). Tropical sea surface temperatures for the past four centuries reconstructed from coral archives. *Paleoceanography*, *30*(3), 226–252. https://doi.org/10.1002/2014PA002717

Tomlinson, P. B. (1986). The botany of mangroves. In *Cambridge University Press, Cambridge*. Elsevier. https://doi.org/10.1016/0304-3770(87)90032-5

Toomey, M. R., Curry, W. B., Donnelly, J. P., & Van Hengstum, P. J. (2013). Reconstructing 7000 years of North Atlantic hurricane variability using deep-sea sediment cores from the western Great Bahama Bank. *Paleoceanography*, *28*(1), 31–41. https://doi.org/10.1002/palo.20012

Toscano, M. A., & Macintyre, I. G. (2003). Corrected western Atlantic sea-level curve for the last 11,000 years based on calibrated 14C dates from Acropora palmata framework and intertidal mangrove peat. *Coral Reefs*, *22*(3), 257–270. https://doi.org/10.1007/s00338-003-0315-4

Trouet, V., Esper, J., Graham, N. E., Baker, A., Scourse, J. D., & Frank, D. C. (2009). Persistent positive north atlantic oscillation mode dominated the medieval climate anomaly. *Science*, *324*(5923), 78–80. https://doi.org/10.1126/science.1166349

Turvey, S. T. (2009). Holocene Extinctions. In *Holocene Extinctions*. Oxford University Press. https://doi.org/10.1093/acprof:oso/9780199535095.001.0001

Ulm, S. (2006). Australian marine reservoir effects: A guide to ΔR values. *Australian*

Archaeology, *63*(63), 57–60. https://doi.org/10.1080/03122417.2006.11681838

United Nations Development Programme (UNDP). (2013). *Increasing resilience of ecosystems and vulnerable communities to CC and anthropic threats through a ridge to reef approach to BD conservation and watershed management*. https://doi.org/10.1016/b978-0-444-86236-5.50086-9

United Nations Institute for Training and Research (UNITAR). (2012). Satellite Assessment over Corail, Baradères, & Les Cayes, Haiti after Hurricane Sandy: Analysis based on SPOT-5 satellite data aquired on 03 November 2012. *UNOSAT: Tropical Cyclone and Flooding*.

van Hengstum, P. J., Donnelly, J. P., Fall, P. L., Toomey, M. R., Albury, N. A., & Kakuk, B. (2016). The intertropical convergence zone modulates intense hurricane strikes on the western North Atlantic margin. *Scientific Reports*, *6*(February), 1–10. https://doi.org/10.1038/srep21728

van Hengstum, P. J., Donnelly, J. P., Toomey, M. R., Albury, N. A., Lane, P., & Kakuk, B. (2014). Heightened hurricane activity on the Little Bahama Bank from 1350 to 1650 AD. *Continental Shelf Research*, *86*(C), 103–115. https://doi.org/10.1016/j.csr.2013.04.032

van Hengstum, P. J., Maale, G., Donnelly, J. P., Albury, N. A., Onac, B. P., Sullivan, R. M., Winkler, T. S., Tamalavage, A. E., & MacDonald, D. (2018). Drought in the northern Bahamas from 3300 to 2500 years ago. *Quaternary Science Reviews*, *186*, 169–185. https://doi.org/10.1016/j.quascirev.2018.02.014

van Hengstum, P. J., Scott, D. B., Gröcke, D. R., & Charette, M. A. (2011). Sea level controls sedimentation and environments in coastal caves and sinkholes. *Marine Geology*, *286*(1–4), 35–50. https://doi.org/10.1016/j.margeo.2011.05.004

van Hengstum, P. J., Winkler, T. S., Tamalavage, A. E., Sullivan, R. M., Little, S. N., MacDonald, D., Donnelly, J. P., & Albury, N. A. (2020). Holocene sedimentation in a blue hole surrounded by carbonate tidal flats in The Bahamas: Autogenic versus allogenic processes. *Marine Geology*, *419*(September 2019). https://doi.org/10.1016/j.margeo.2019.106051

Wallace, E. J., Donnelly, J. P., van Hengstum, P. J., Wiman, C., Sullivan, R. M., Winkler, T. S., E., D. N., Toomey, M., & Albury, N. (2019). Intense Hurricane Activity Over the Past 1500 Years at South Andros Island, The Bahamas. *Paleoceanography and Paleoclimatology*, *34*(11), 1761–1783. https://doi.org/10.1029/2019PA003665

Warrick, J. A., & Rubin, D. M. (2007). Suspended-sediment rating curve response to urbanization and wildfire, Santa Ana River, California. *Journal of Geophysical Research: Earth Surface*, *112*(2), 1–15. https://doi.org/10.1029/2006JF000662

Watts, D. (1987). The West Indies : patterns of development, culture, and environmental change since 1492. In *Cambridge University Press*.

Weinkle, J., Maue, R., & Pielke, R. (2012). Historical global tropical cyclone landfalls. *Journal* *of Climate*, *25*(13), 4729–4735. https://doi.org/10.1175/JCLI-D-11-00719.1

Winter, A., Ishioroshi, H., Watanabe, T., Oba, T., & Christy, J. (2000). Caribbean sea surface temperatures: Two-to-three degrees cooler than present during the Little Ice Age. *Geophysical Research Letters*, *27*(20), 3365–3368. https://doi.org/10.1029/2000GL011426

Yang, H., Huang, Y., Ma, C., Zhang, Z., & Wang, C. (2020). Recognition of Milankovitch cycles in XRF core-scanning records of the Late Cretaceous Nenjiang Formation from the Songliao Basin (northeastern China) and their paleoclimate implications. *Journal of Asian Earth Sciences*, *194*(November 2019), 104183. https://doi.org/10.1016/j.jseaes.2019.104183

Appendix A: Results of XRF scanning, grain size analysis, and LOI

A1: Stratigraphic diagrams of all proxy data from 8500 to -66 cal BP. XRF units are standardized counts per second (CPS).

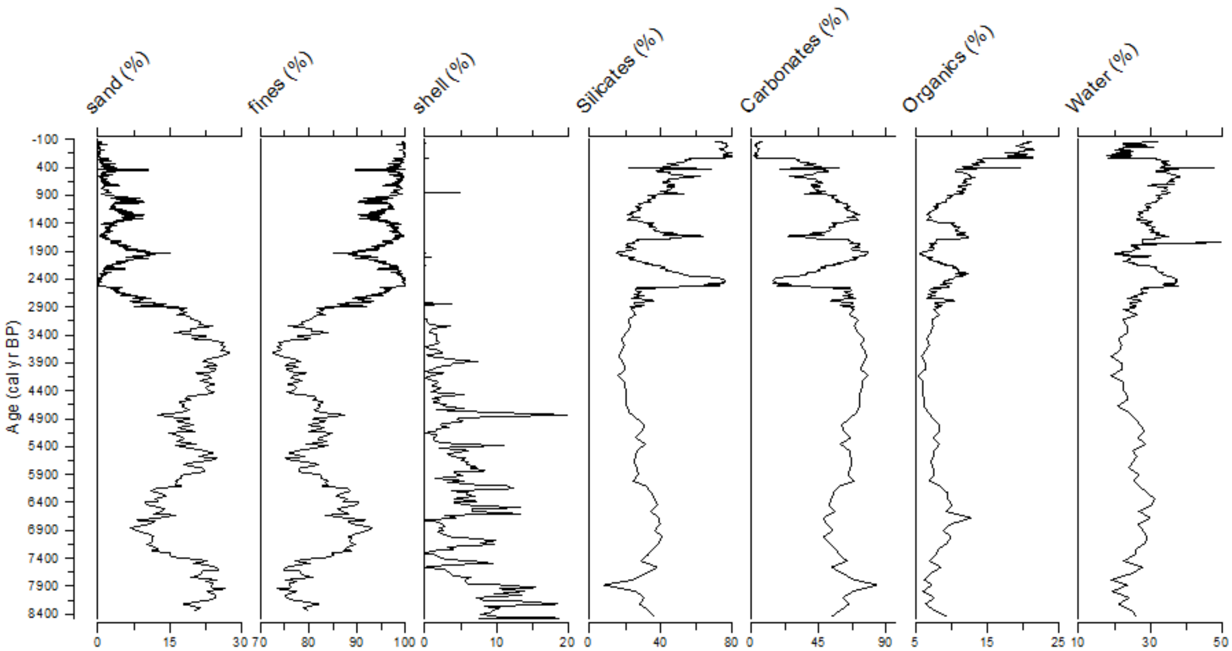

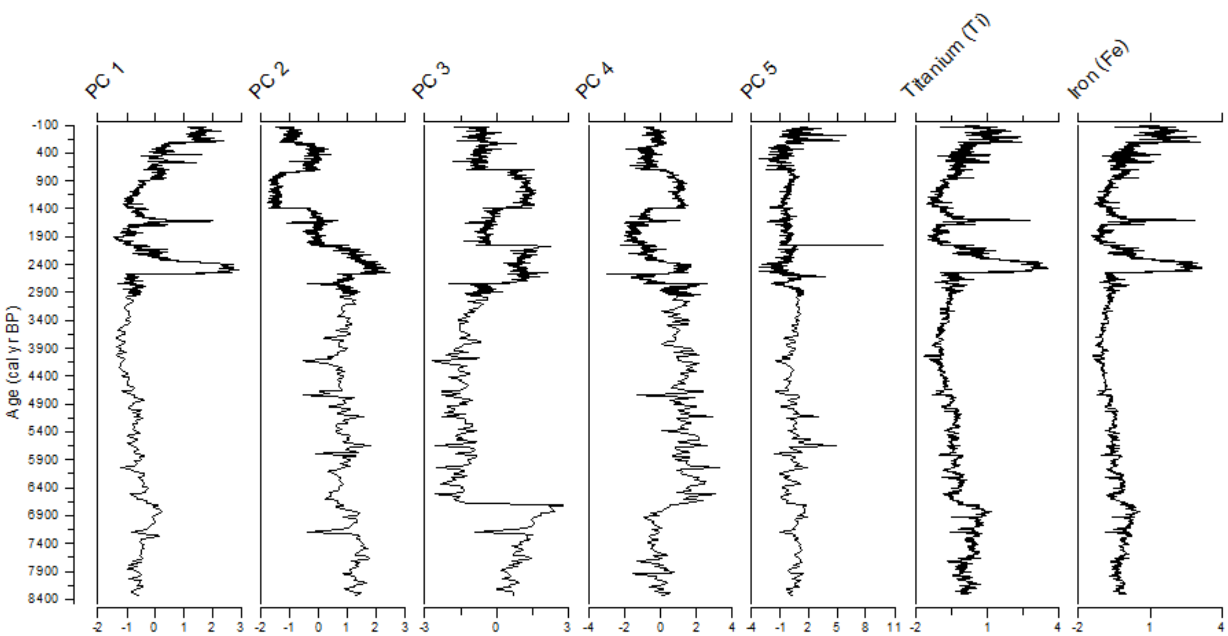

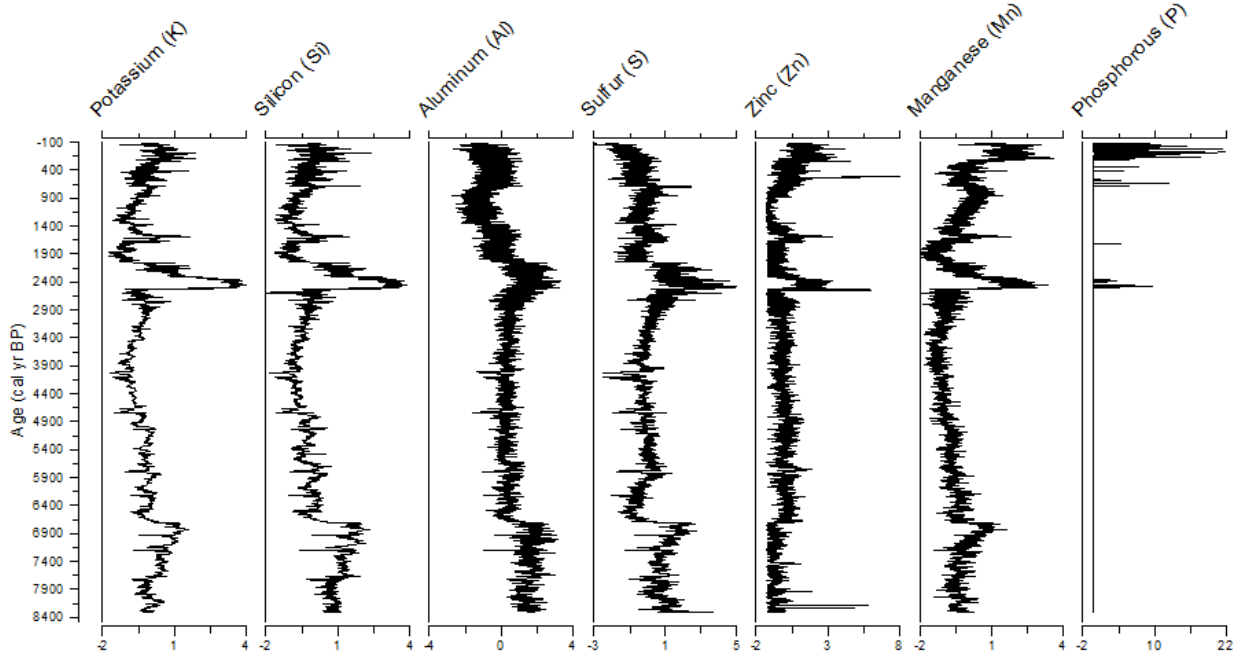
Potassium (K)
Silicon (Si)
Aluminum (Al)
Sulfur (S)
Zinc (Zn)
Manganese (Mn)
Phosphorous (P)
Age (cal yr BP)
-100
400
900
1400
1900
2400
2900
3400
3900
4400
4900
5400
5900
6400
6900
7400
7900
8400
-2 1 4
-2 1 4
-4 0 4
-3 1 5
-2 3 8
-2 1 4
-2 10 22

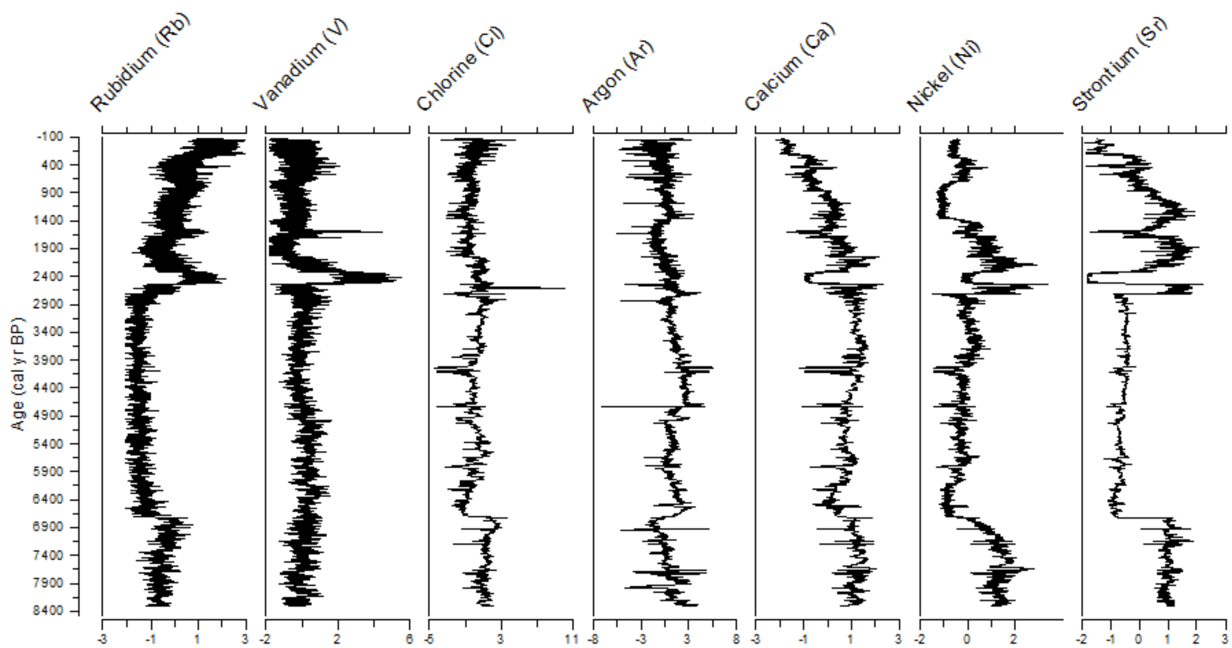
Rubidium (Rb)
Vanadium (V)
Chlorine (Cl)
Argon (Ar)
Calcium (Ca)
Nickel (Ni)
Strontium (Sr)
Age (cal yr BP)
-100
400
900
1400
1900
2400
2900
3400
3900
4400
4900
5400
5900
6400
6900
7400
7900
8400
-3 -1 1 3
-2 2 6
-5 3 11
-8 -3 3 8
-3 -1 1 3
-2 0 2
-2 -1 0 1 2 3

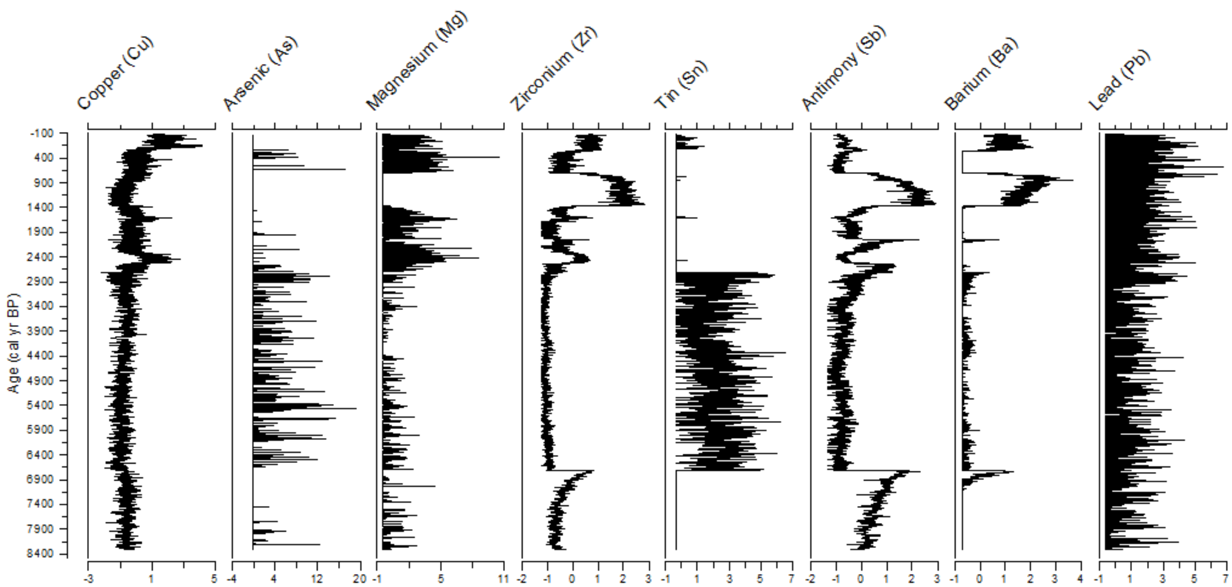
Copper (Cu)
Arsenic (As)
Magnesium (Mg)
Zirconium (Zr)
Tin (Sn)
Antimony (Sb)
Barium (Ba)
Lead (Pb)
Age (cal yr BP)

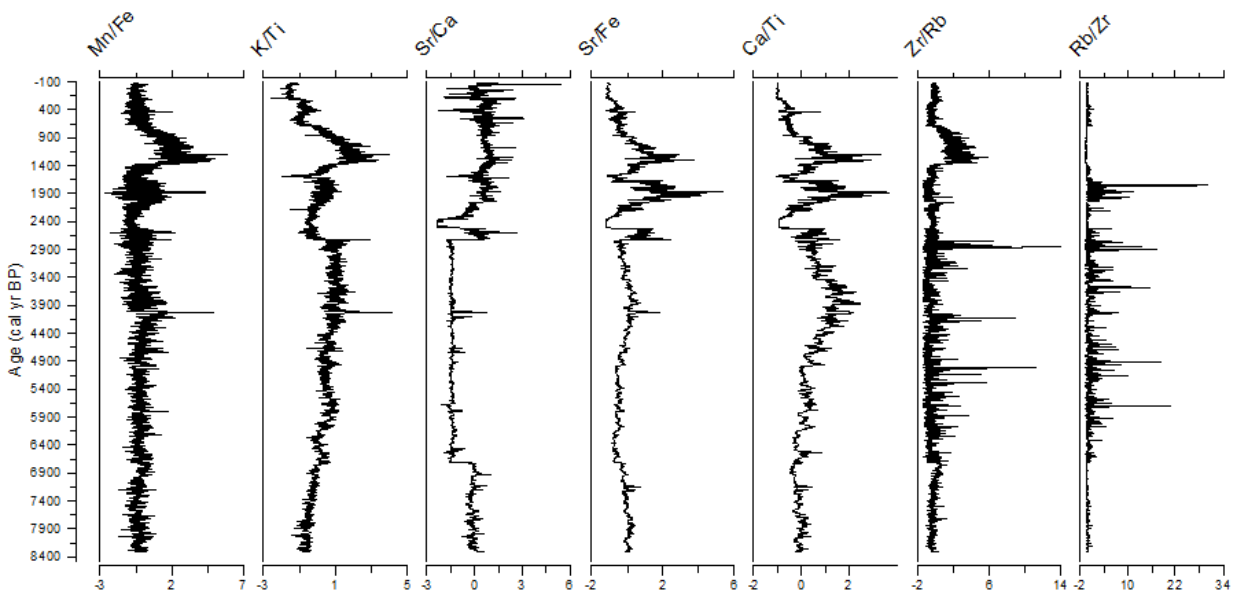
Mn/Fe
K/Ti
Sr/Ca
Sr/Fe
Ca/Ti
Zr/Rb
Rb/Zr
Age (cal yr BP)

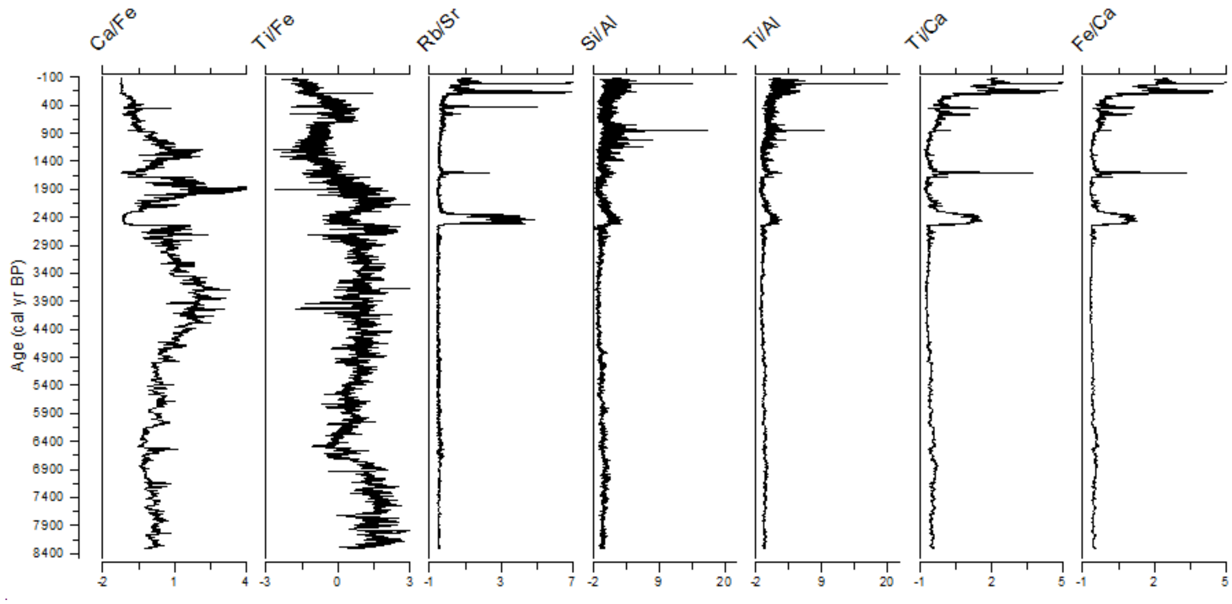

A2: Stratigraphic diagrams of selected proxy data from 8500 to 2900 cal BP. XRF units are standardized counts per second (CPS).

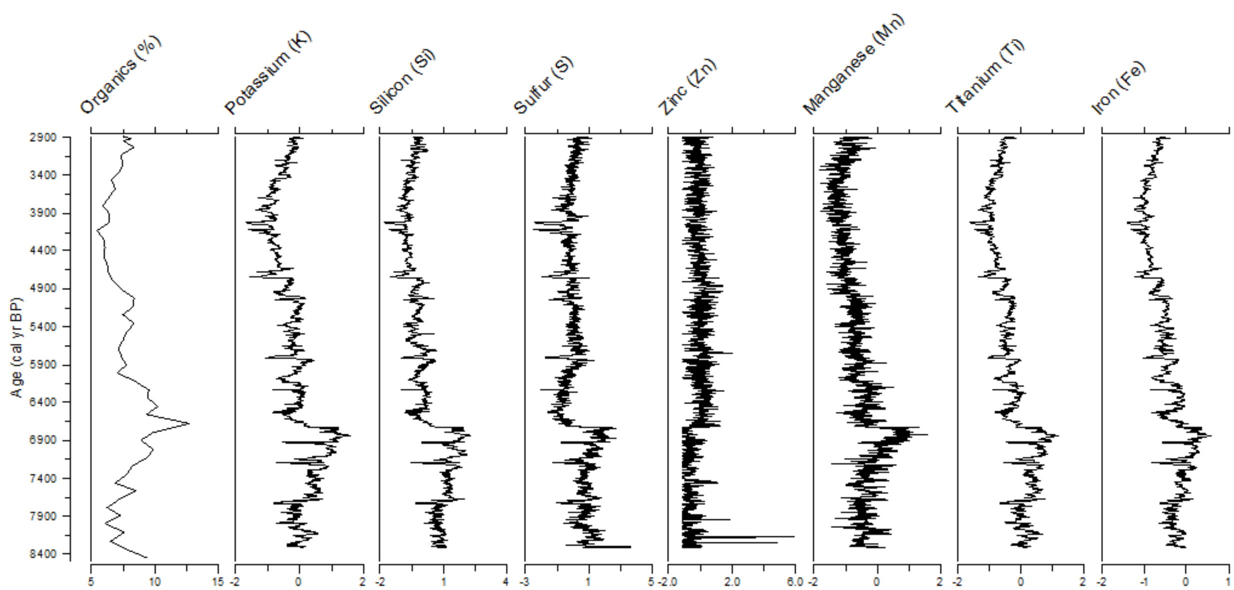

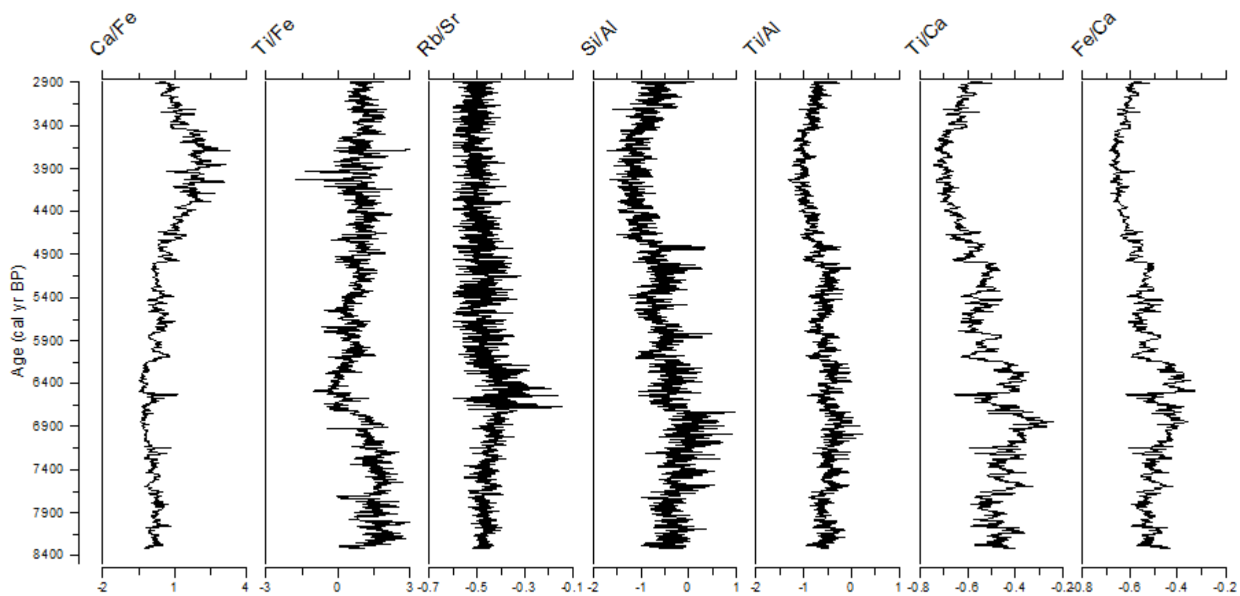

Appendix B: Results of Statistical Analysis

B1: Biplot of PC1 and PC2 of PCA of full core (cm scale).

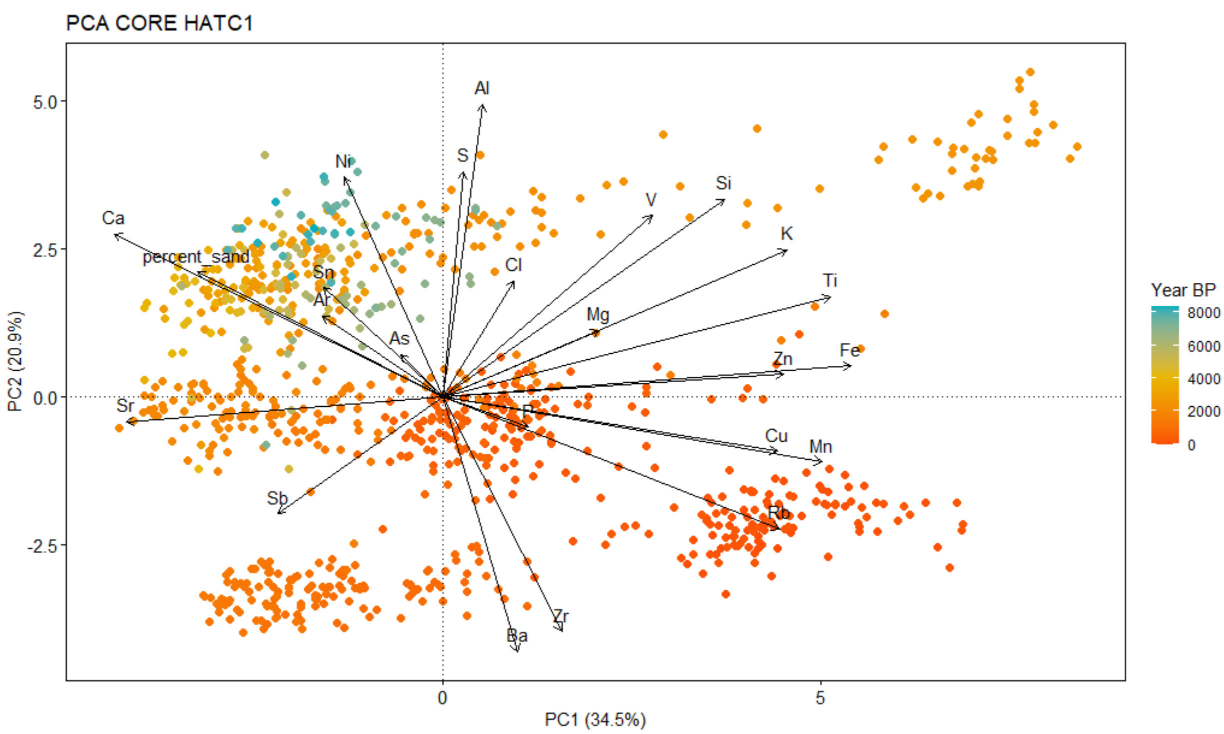

B2: PC1-5 over time from PCA of full core (cm scale).

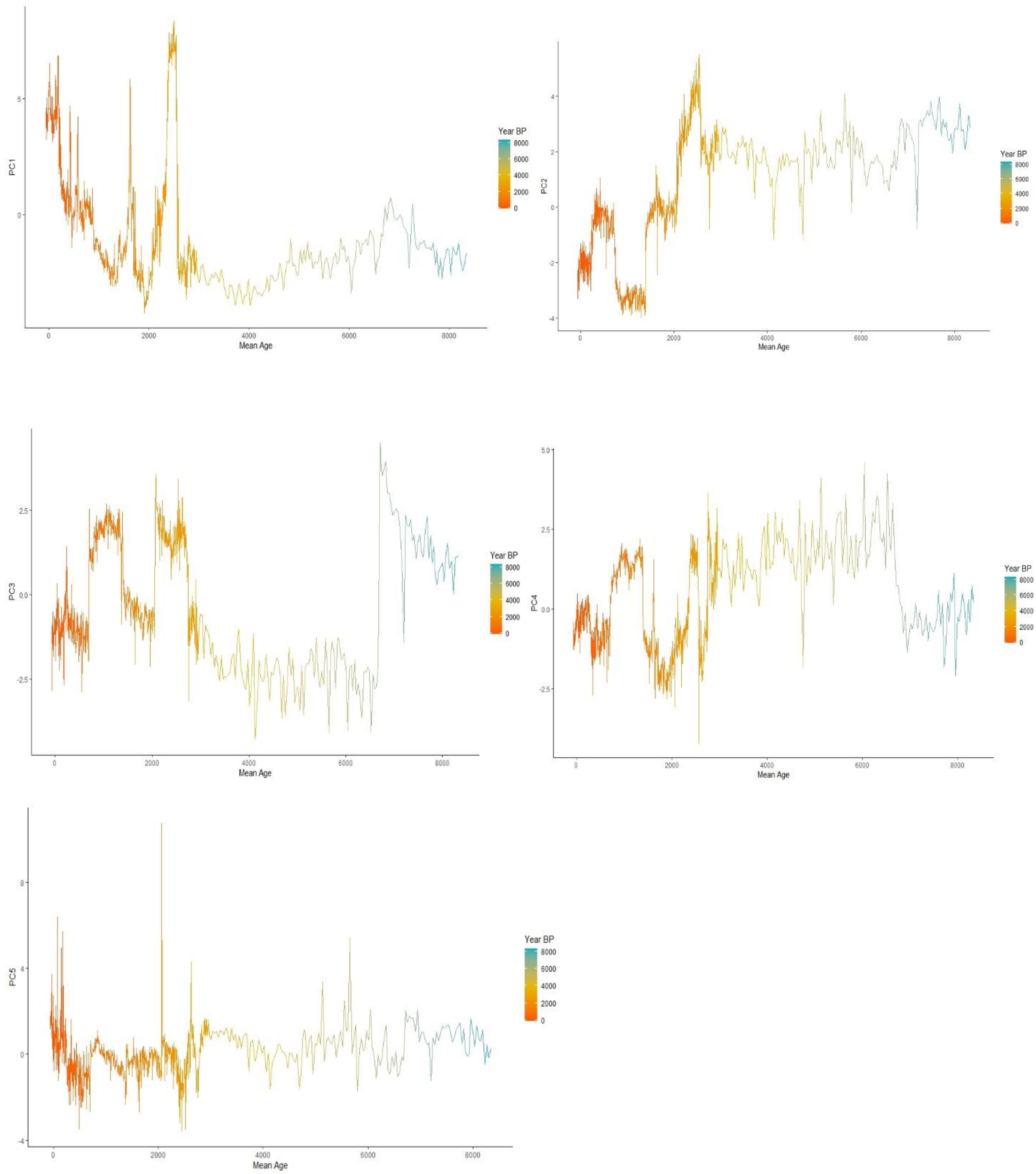

B3: Scree plot for PCA of full core (cm scale). The first 5 principle components explain 79.2% of the variance.

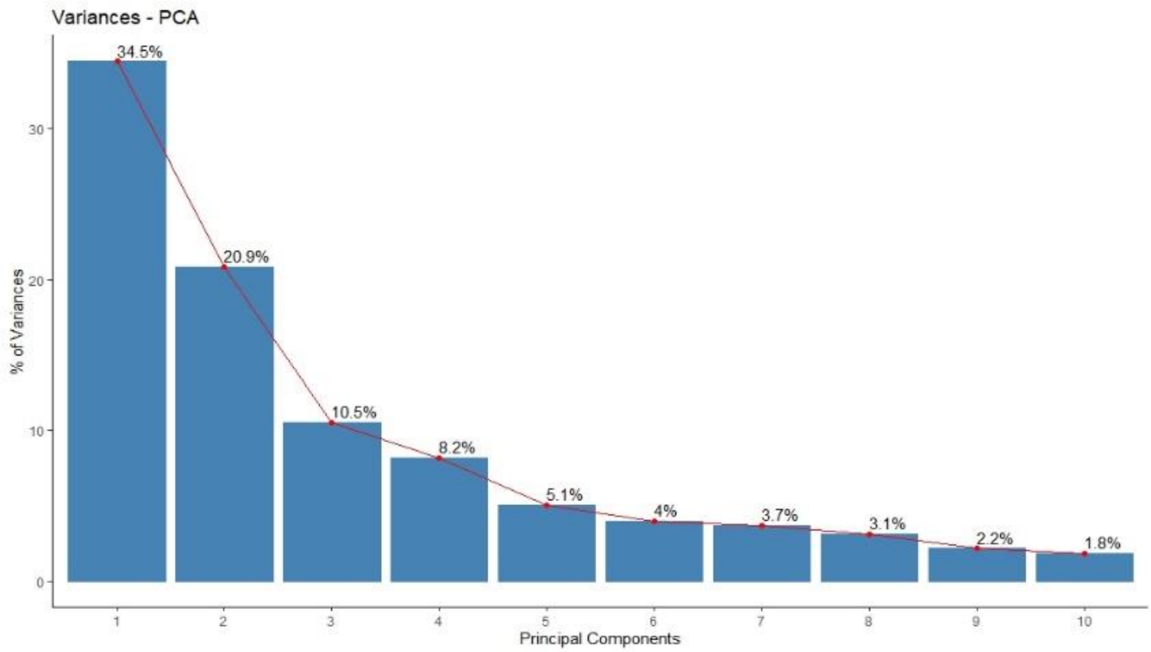

B4: Bar plot of variable contributions to the first five dimensions of PCA of the full core (cm scale).

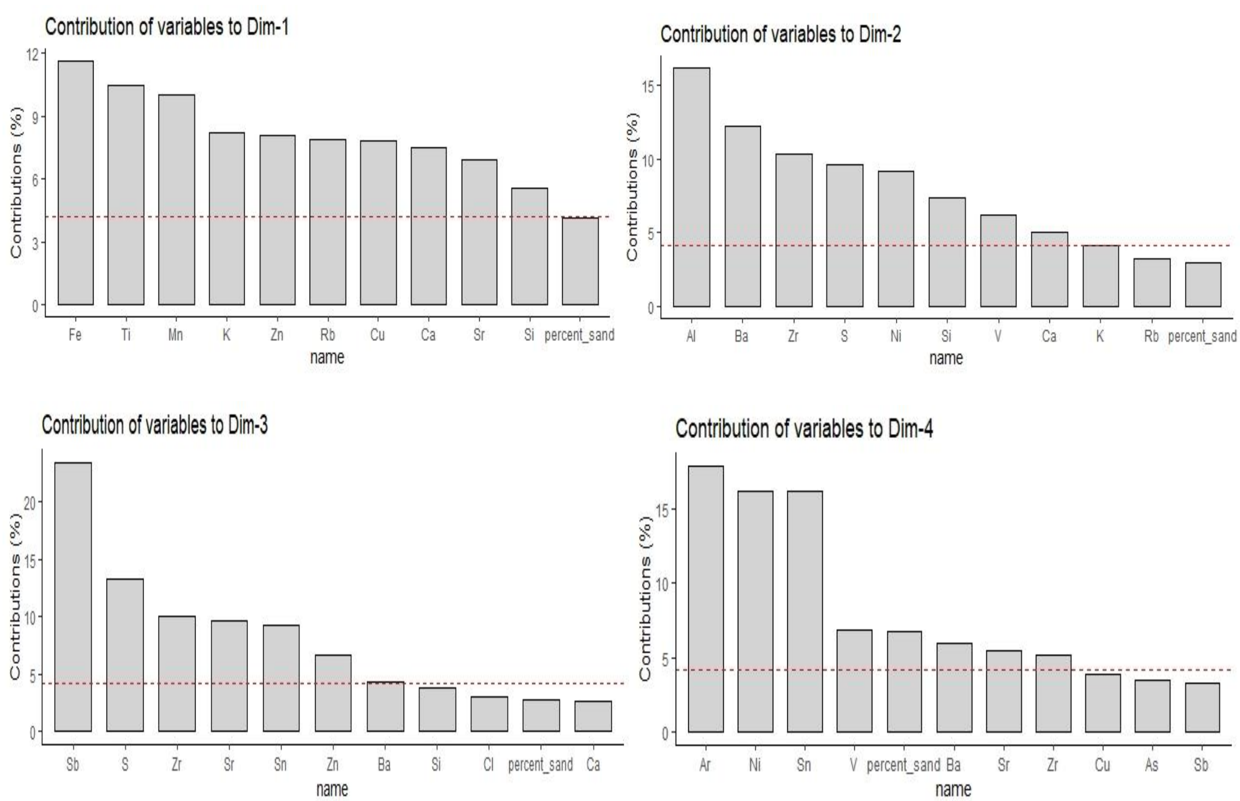

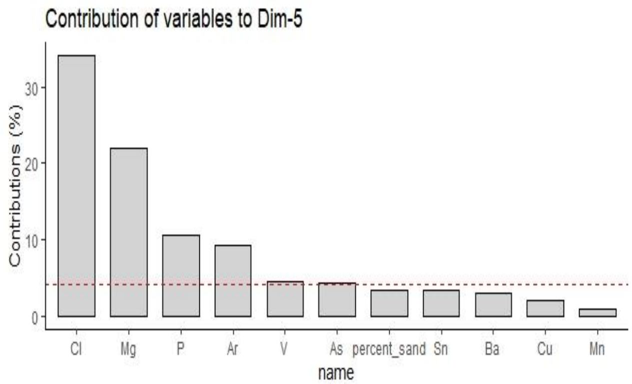

B5: Biplot of PC1 and PC2 of PCA of full core (mm scale).

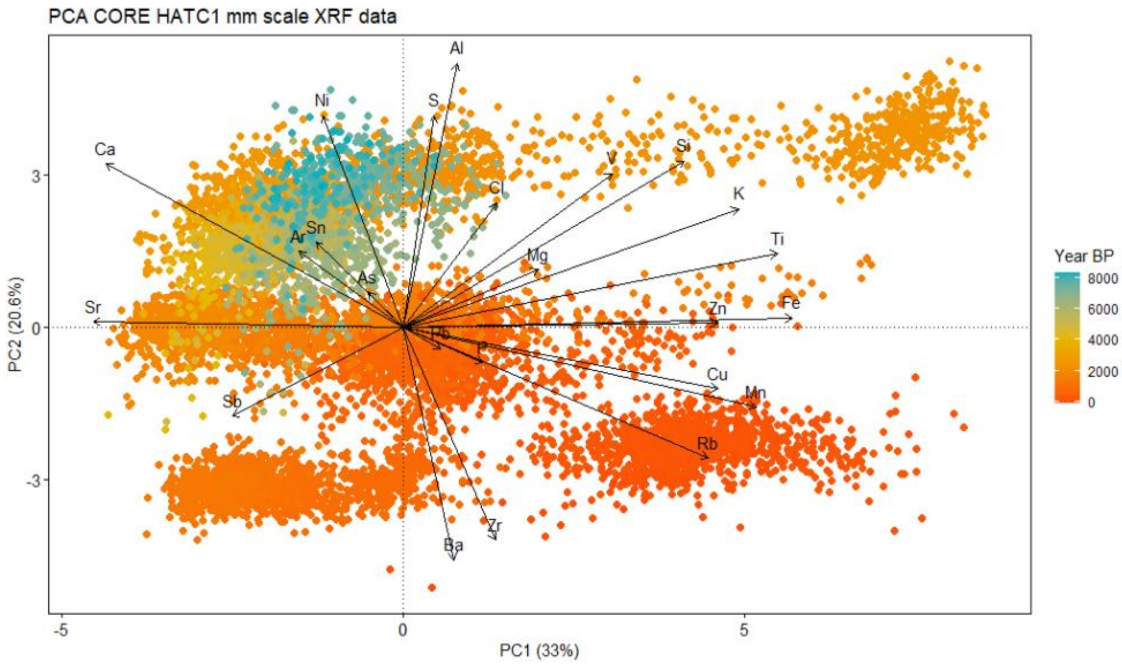

B6: PC1-5 over time from PCA of full core (mm scale).

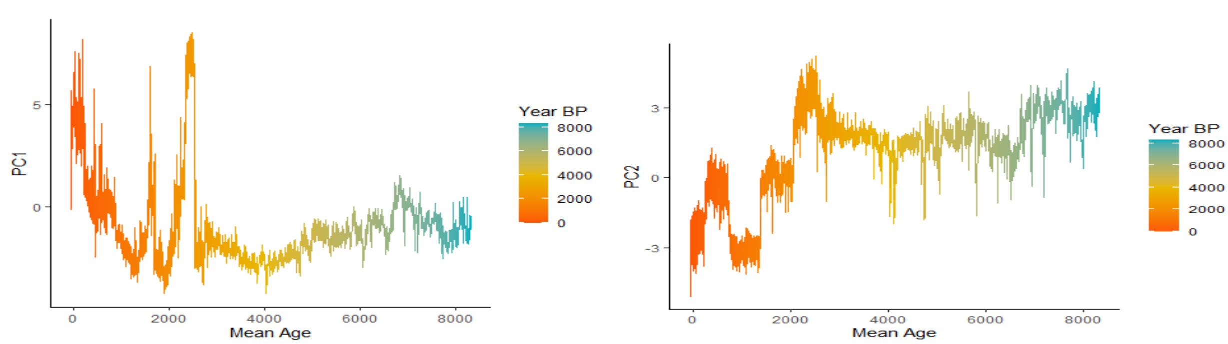

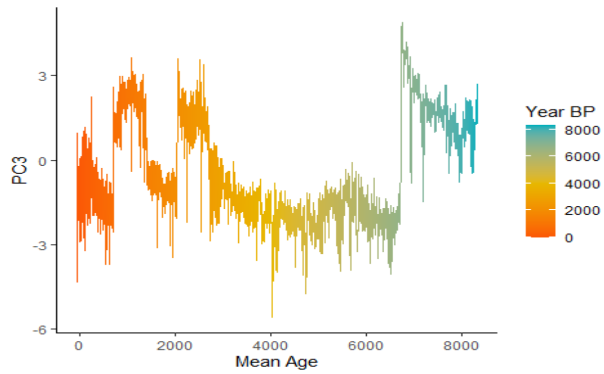

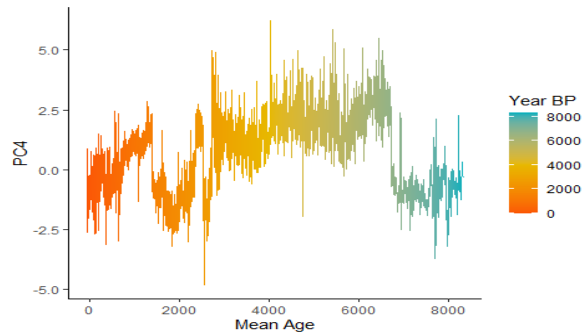

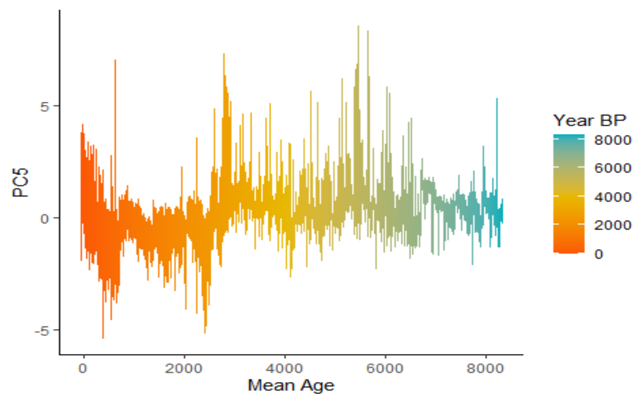

B7: Scree plot for PCA of full core (mm scale). The first 5 principle components explain 76.6% of the variance.

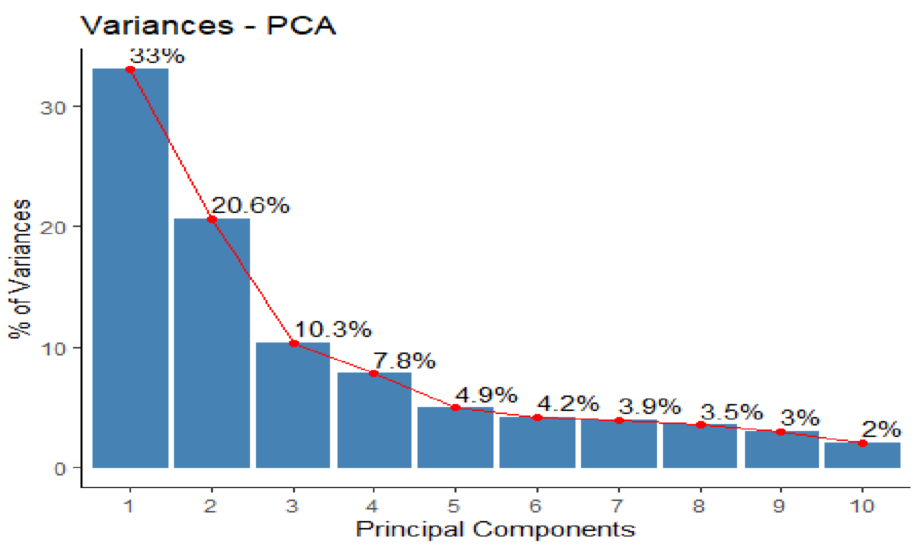

B8: Bar plot of variable contributions to the first five dimensions of PCA of the full core (mm scale).

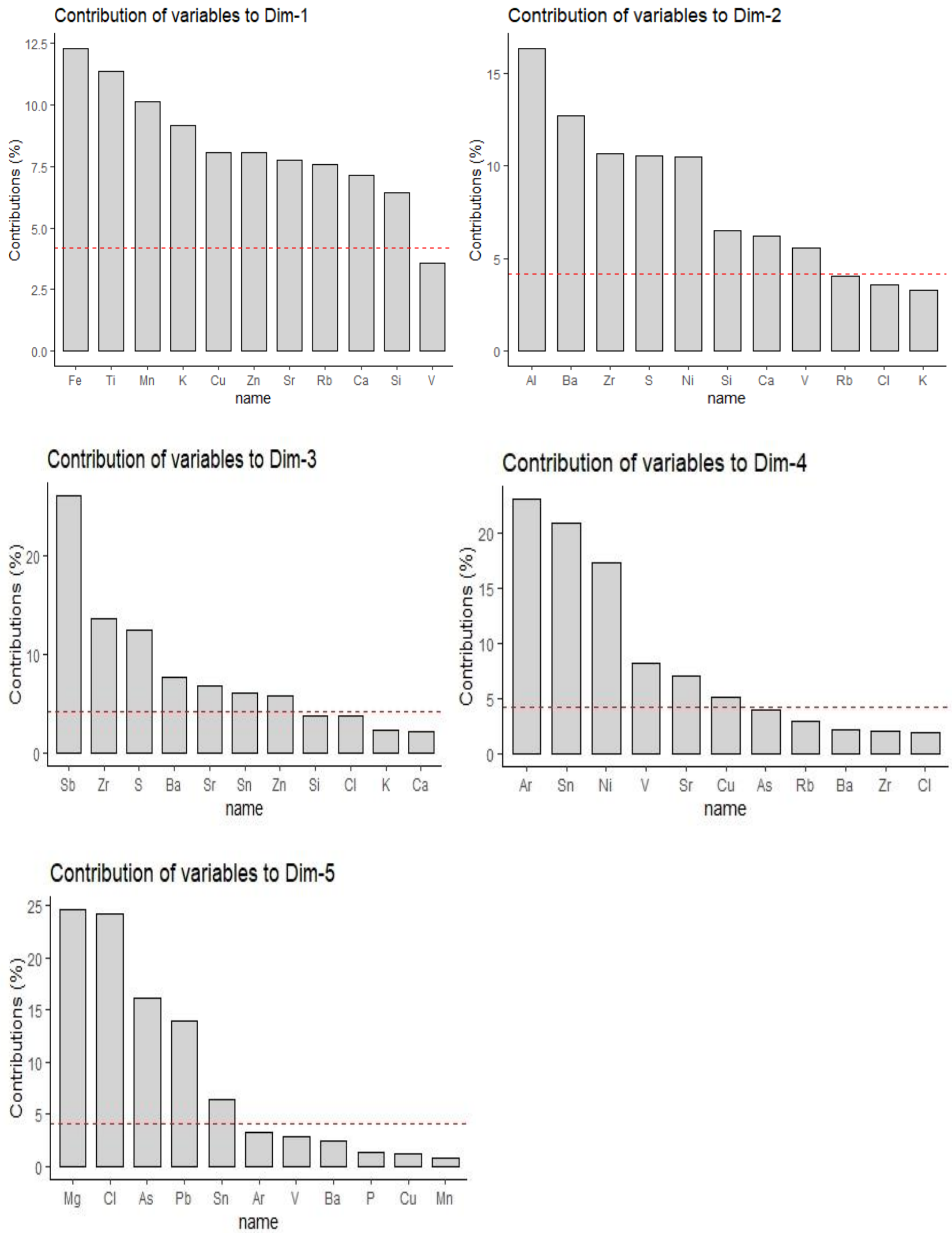

B9: Biplot of PC1 and PC2 of PCA of 3000 to -66 cal BP (cm scale)

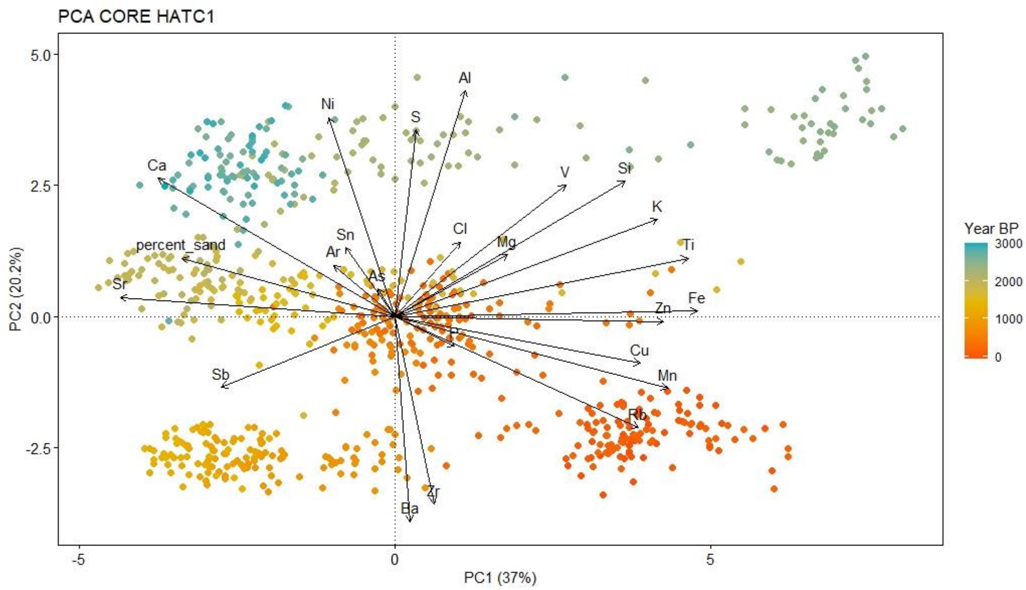

B10: PC1-5 over time for PCA from 3000 to -66 cal BP (cm scale)

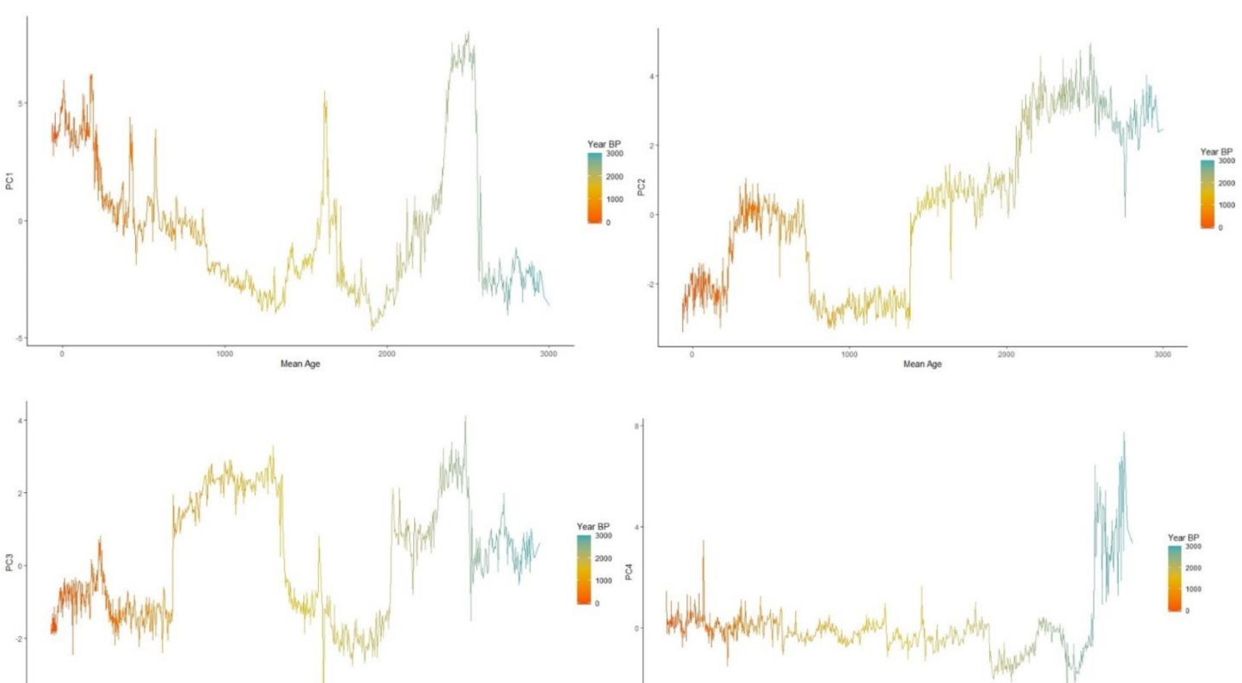

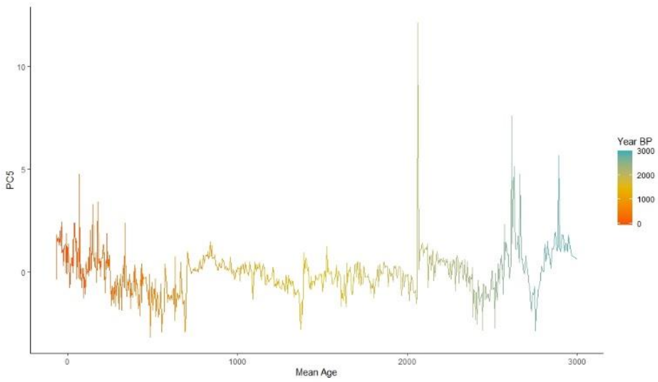

B11: Scree plot for PCA from 3000 to -66 cal BP (cm scale). The first 5 principle components explain 79% of the variance.

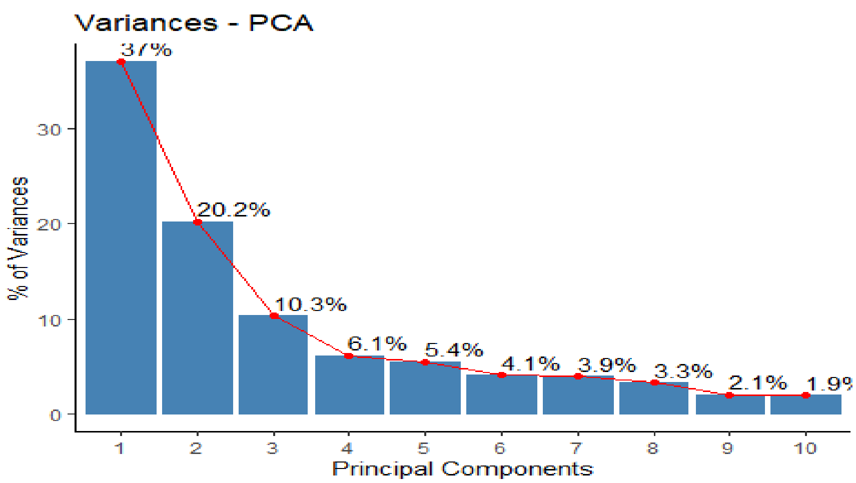

B12: Bar plot of variable contributions to the first five dimensions of PCA from 3000 to -66 cal BP (cm scale).

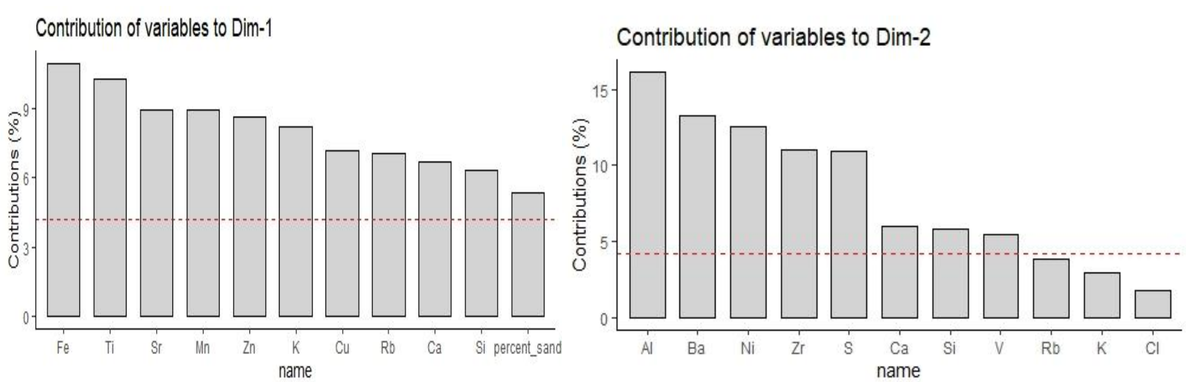

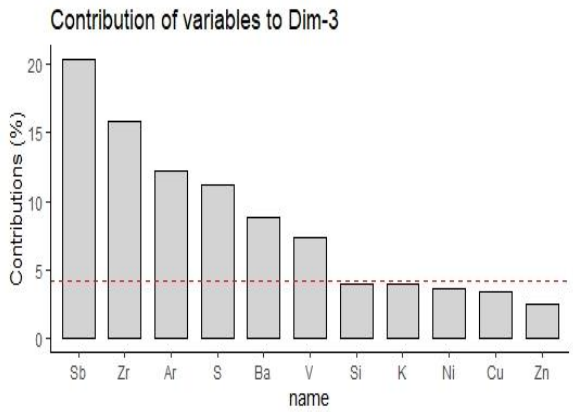

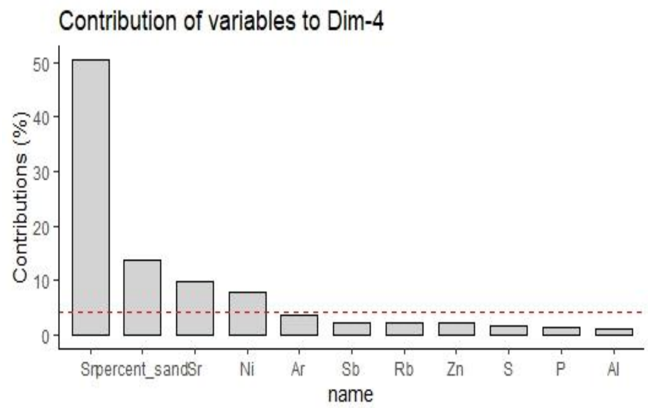

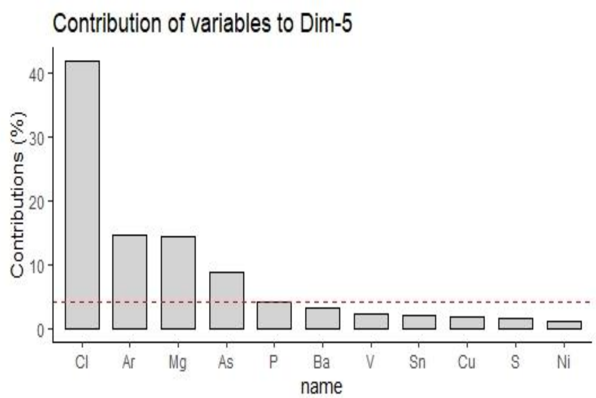

B13: Biplot of PC1 and PC2 of PCA of 3000 to -66 cal BP (mm scale)

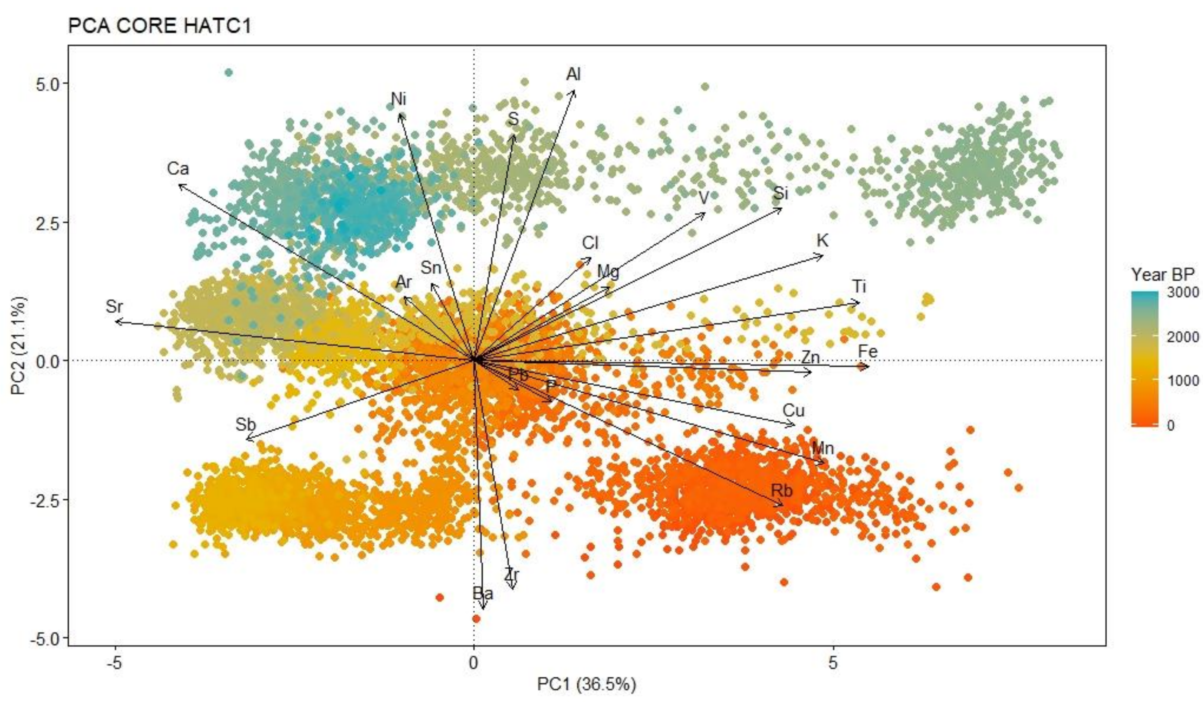

B14: PC1-5 over time for PCA from 3000 to -66 cal BP (mm scale)

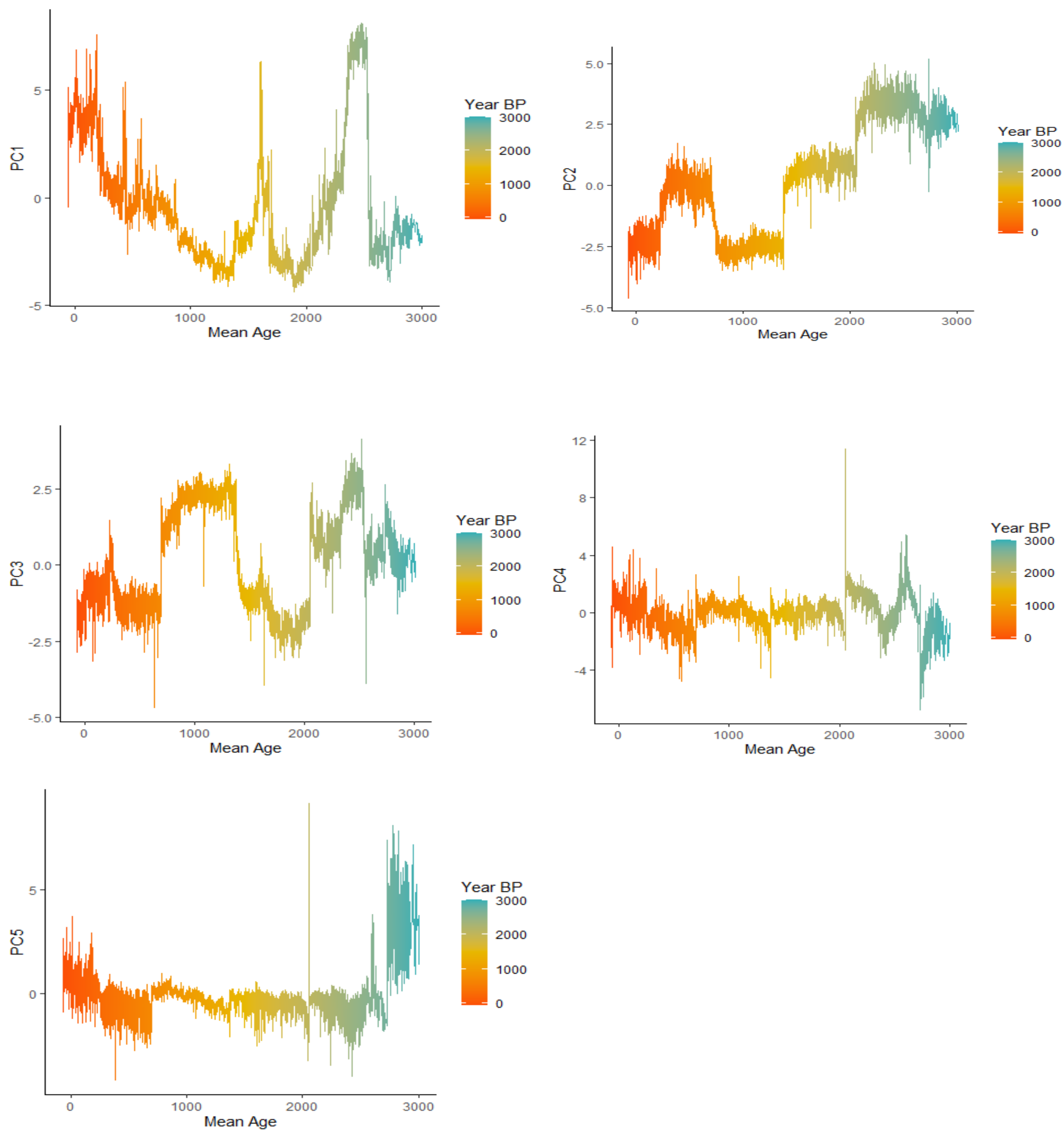

B15: Scree plot for PCA from 3000 to -66 cal BP (mm scale). The first 5 principle components explain 76.7% of the variance.

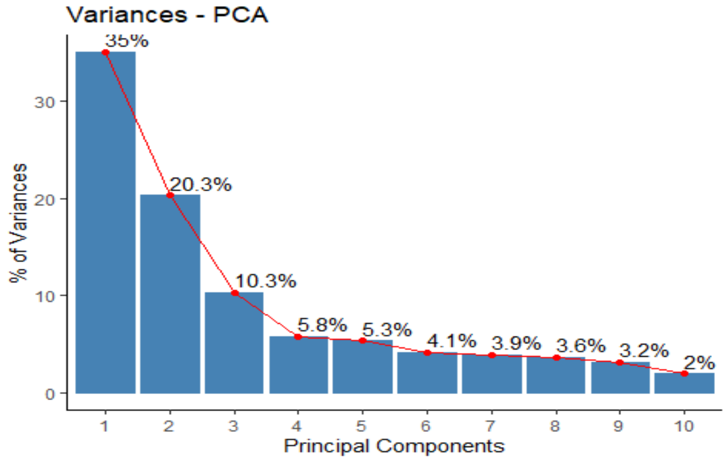

B16: Bar plot of variable contributions to the first five dimensions of PCA from 3000 to -66 cal BP (mm scale).

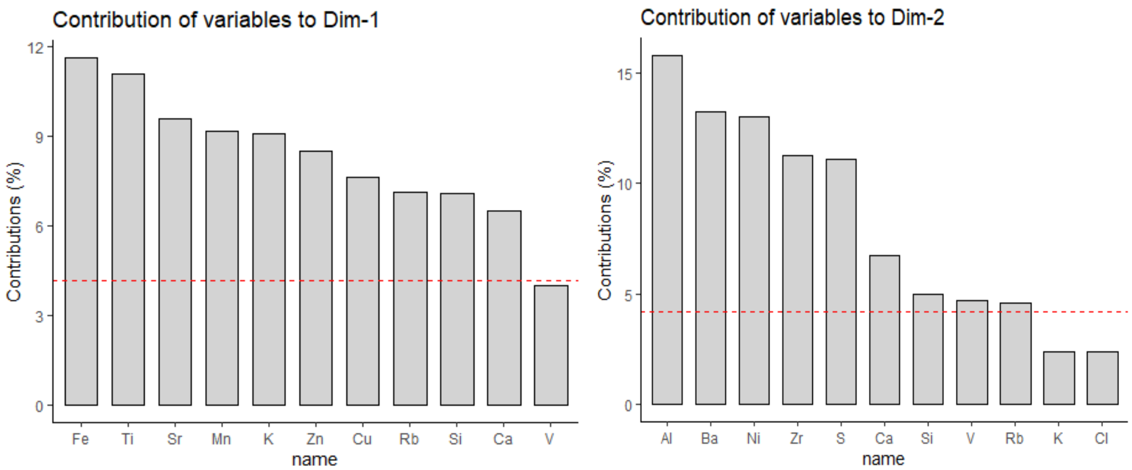

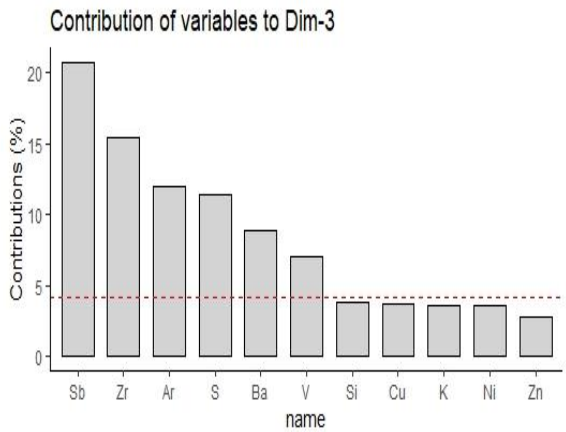

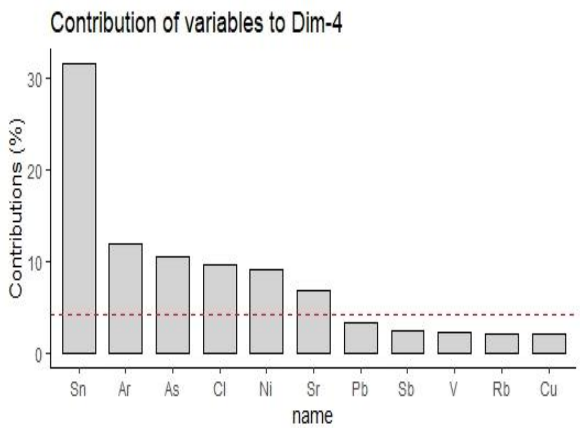

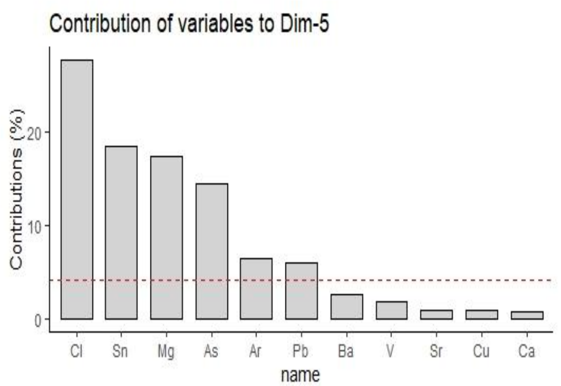

Appendix C: Microscopic pictures of sand samples throughout the core

<u>C1: 60-61 cm downcore</u>

D1 1:1, 60-61 cm (60-61 cm)

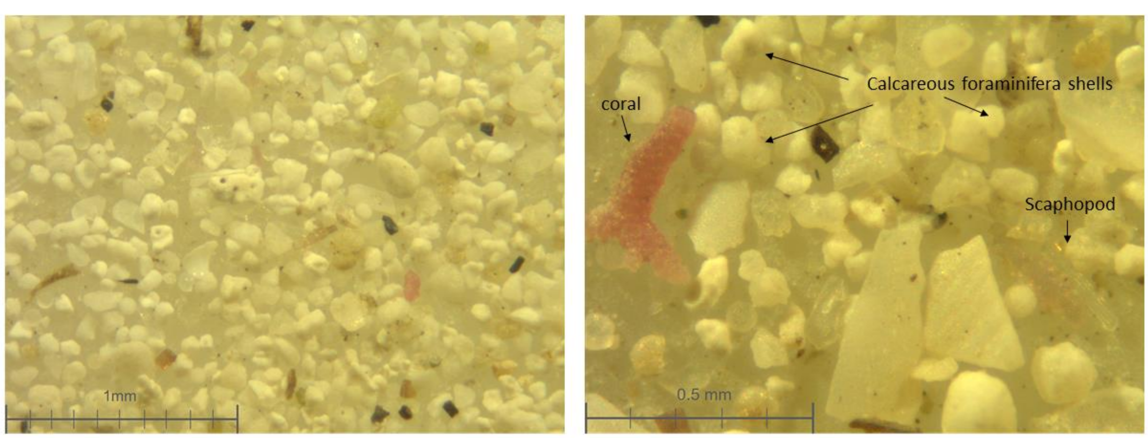

<u>C2: 205-206 cm downcore</u>

D2 2:7, 81-82 cm (205-206 cm)

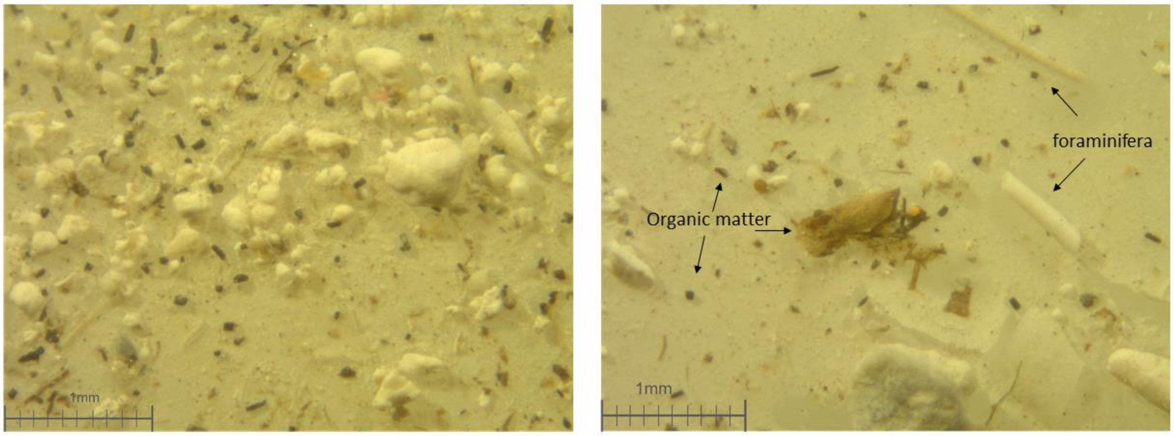

<u>C3: 358-359 cm downcore</u>

D2 3:7, 89-90 cm (358-359 cm)

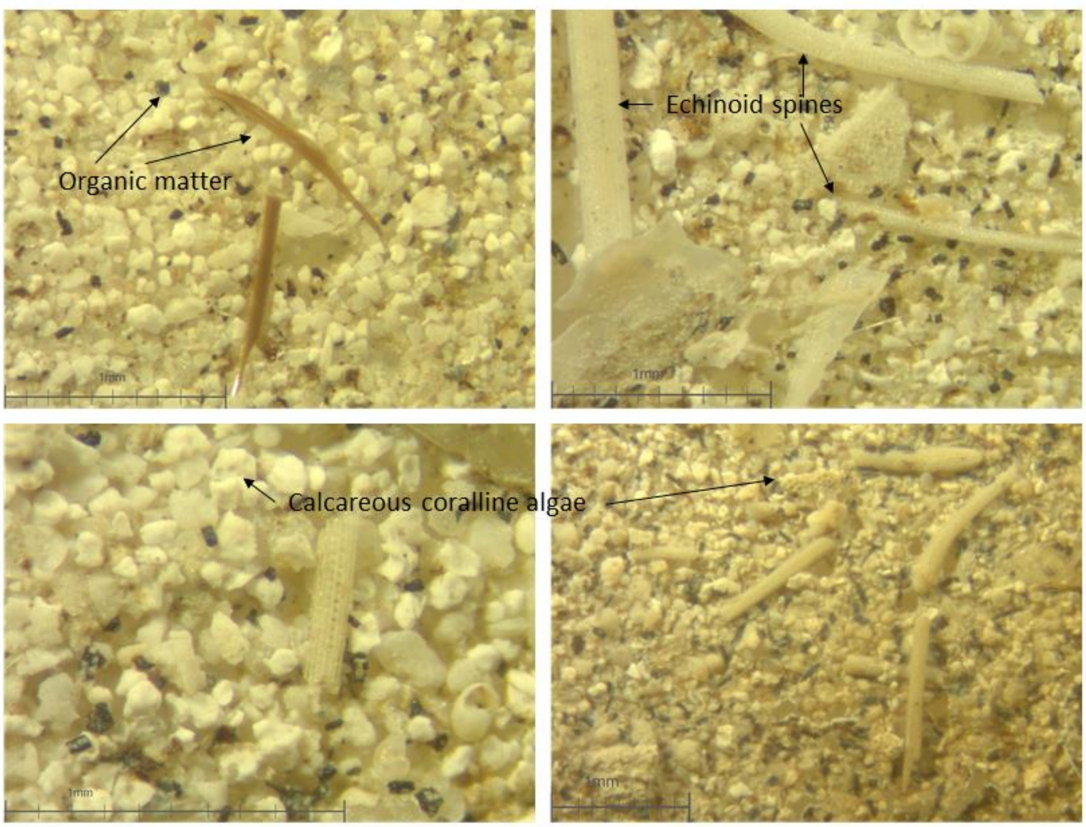

<u>C4: 509-510 cm downcore</u>

D2 4:7, 95-96 cm (509-510 cm)

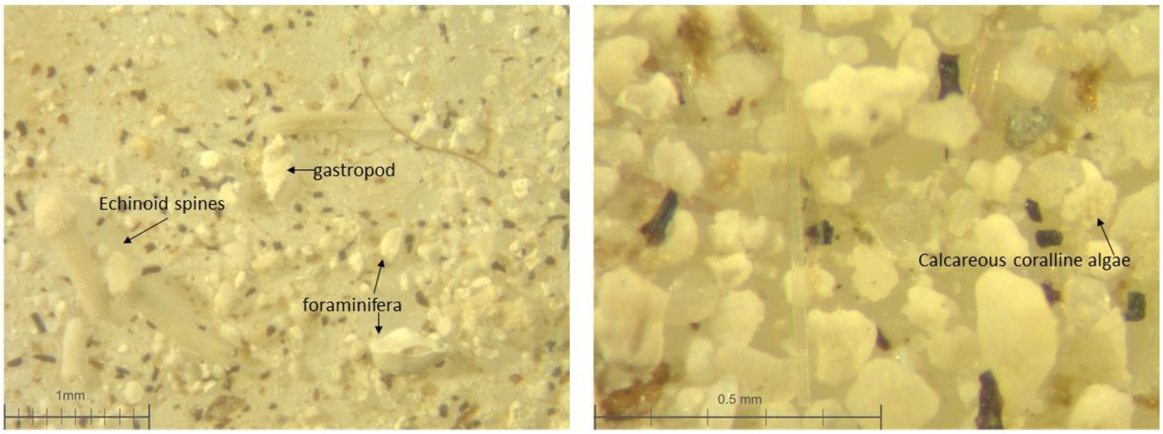

<u>C5: 661-662 cm downcore</u>

D2 5:7, 102-103 cm (661-662 cm)

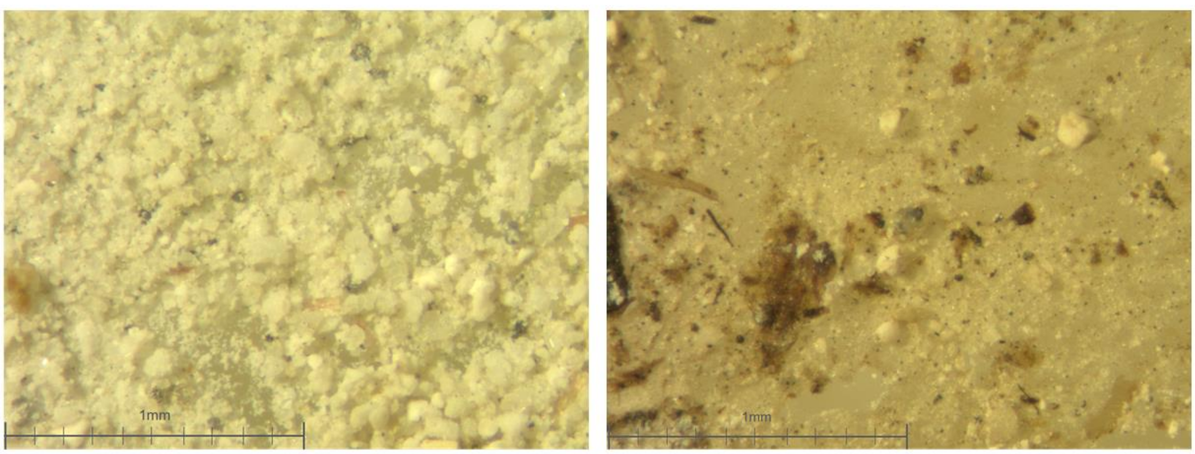

<u>C6: 664-665 cm downcore</u>

D2 5:7, 105-106 cm (664-665 cm)

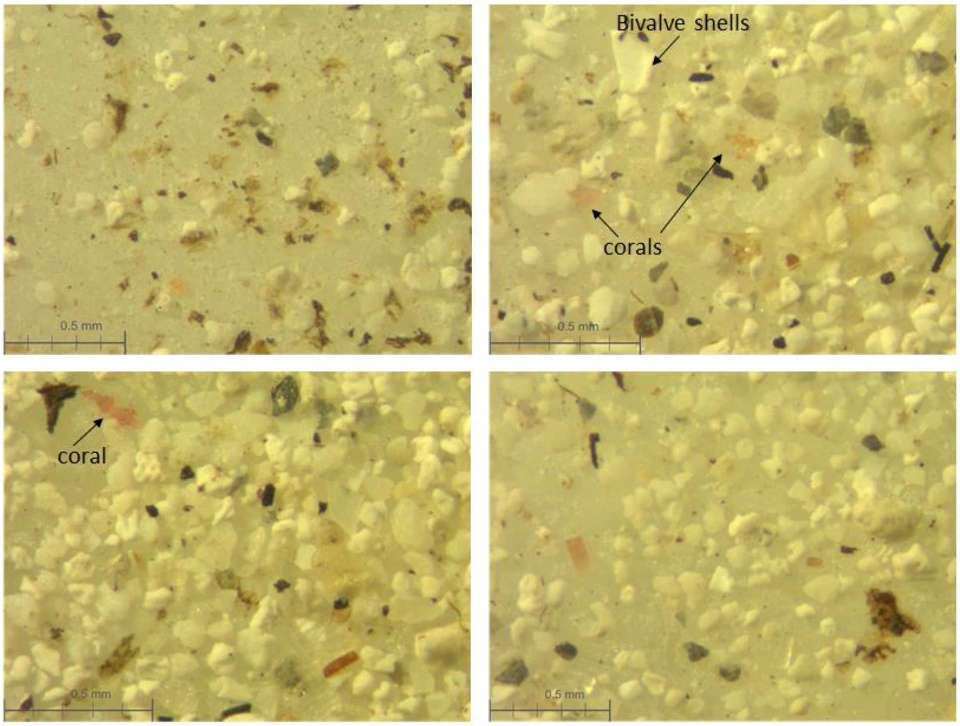

<u>C7: 769-770 cm downcore</u>

D2 6:7, 65-66 cm (769-770 cm)

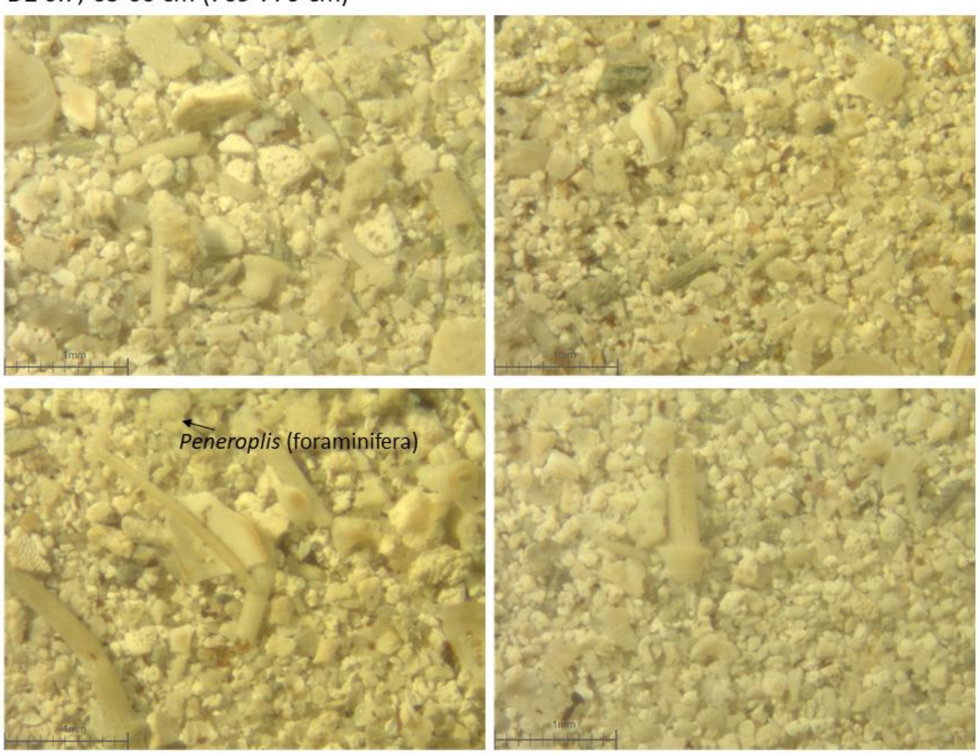

C8: 857-858 cm downcore

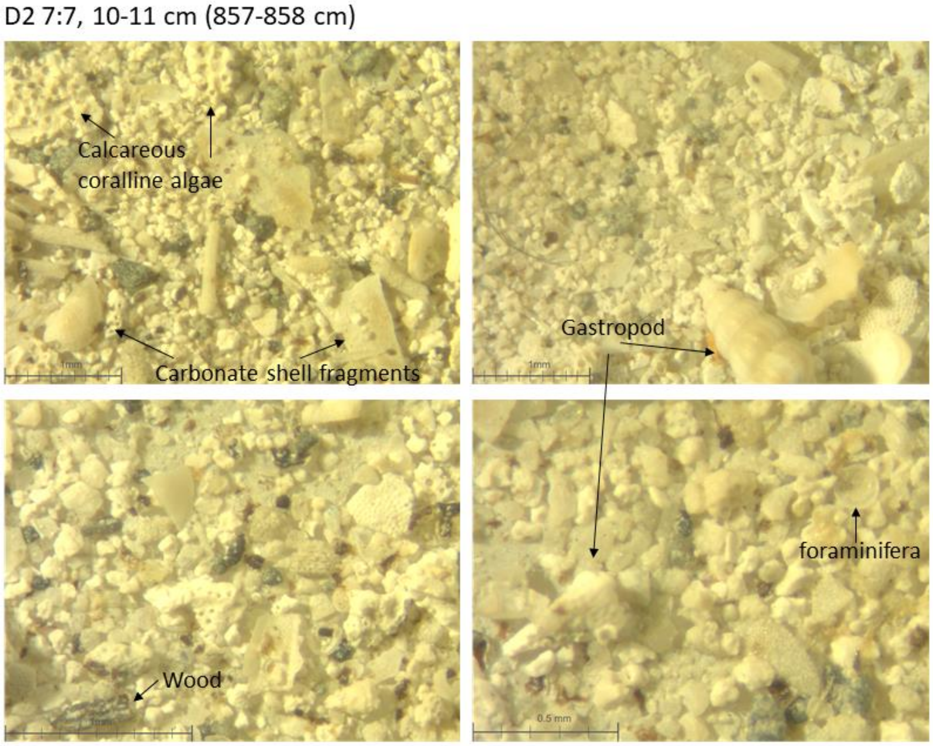

Appendix D: Samples of Rcode used in this study

D1: PCA code

```
pcainput <- read.csv("XRF_GS_PCA.csv")
pcadata <- pcainput[c(3:26)]
cpca <- PCA(pcadata, scale.unit=TRUE, graph=TRUE)

# Biplot: PC1 and PC2
col.ind=pcainput$mean_Age
gradient.cols=c("#FC4E07", "#E7B800", "#00AFBB")

fviz_pca_biplot(cpca, geom.ind="point",col.var="black",
        pointsize=2, xlab="PC1 (34.5%)",ylab="PC2 (20.9%)",
        col.ind=pcainput$mean_Age,
```

```
            gradient.cols=c("#FC4E07", "#E7B800", "#00AFBB"),
            axes.linetype="dotted", title="PCA CORE HATC1",
            legend.title="Year BP") +
  theme(panel.grid.minor=element_blank())+
  theme(panel.grid.major=element_blank())+
  theme(panel.border=element_rect(colour="black", fill=NA))+
  theme(axis.text = element_text(size=11)) +
  theme(axis.text = element_text(colour="black"))

  # Scores
  cpca$ind$coord

  # Loadings
  cpca$var$coord

  # Importance of components
  cpca$eig

#Visualize variance of the dimensions:
  fviz_eig(cpca,
        addlabels=TRUE,
        linecolor= "red",
        x = "Principal Components",
        y = "% of Variances",
        title = "Variances - PCA") +
    theme_classic()

#Visualize contribution of variables to dim1:
  fviz_contrib(cpca,
           choice="var",
```

```
            addlabels=TRUE,
            axes = 1,
            top = 11,
            fill = "lightgrey",
            color= "black") +
   theme_classic()


#plot PC1 over time
  PC1 <- read.csv("scores.csv")
   ggplot(PC1, aes(x=mean_Age, y=Dim.1,
          colour=pcainput$mean_Age)) +
     geom_line() +
     theme_classic()+
     labs(color="Year BP", x="Mean Age", y="PC1") +
     scale_color_gradient2(low="#FC4E07", mid = "#E7B800", high = "#00AFBB", midpoint =
4000)
```

D2: Cluster analysis, dendograms code

```
input <- read.csv("10cm_scale_-66-2900.csv")


elements <- input[c(4:46)]
rownames(elements)<-input$Age


#calculate clusters with appropriate df
diss <- dist(elements)
#cluster data
clust <- chclust(diss)


#Plot dendrogram
dend<-fviz_dend(clust, cex=0.4, k=9, k_colors = "aaas", color_labels_by_k = F,
                 ggtheme = theme_classic(), rect = TRUE, rect_border = c("uchicago"),
```

```
        rect_fill = TRUE, label_cols = "black", lwd = 1, main="")
plot(dend)
dev.off()
```

D3: age-depth model code

```
install.packages('rbacon')
library('rbacon')
#set working directory
setwd("C:/Users/moser/Thesis/Bacon_runs")
Bacon(
  core = "HATC1",
  #if you have a depth file you want to get specific ages for:
  depths.file = TRUE,
  #if you want ages at certain intervals:
  d.min = NA,
  d.max = NA,
  d.by=100000,
  slump=NA,
  thick = 5,
  cc1 = "IntCal20",
  cc2 = "Marine20",
  suggest = FALSE,
  verbose = TRUE,
  normal = TRUE,
  coredir = ".",
  acc.mean = 11,
  acc.shape = 3,
  accept.suggestions = TRUE,
  mem.strength = 8,
```

```
  mem.mean = 0.4,
  add.bottom = TRUE,
  prob = 0.95,
  plot.pdf=TRUE
)
```

Appendix E: Ages from age-depth model inferred for each cm of core HATC1

depth	min	max	median	mean
0	-68	-64	-66	-66
0.5	-67	-62	-65	-65
1.5	-67	-55	-63	-62
2.5	-66	-47	-61	-60
3.5	-66	-40	-59	-58
4.5	-66	-32	-57	-55
5.5	-65	-27	-55	-53
6.5	-64	-25	-53	-51
7.5	-63	-21	-50	-48
8.5	-62	-17	-48	-46
9.5	-62	-12	-46	-43
10.5	-60	-8	-44	-41
11.5	-58	-6	-41	-39
12.5	-57	-3	-39	-36
13.5	-56	0	-36	-34
14.5	-55	5	-34	-32
15.5	-54	9	-32	-29
16.5	-52	11	-29	-27
17.5	-51	14	-27	-24
18.5	-50	18	-24	-22
19.5	-49	22	-22	-20
20.5	-47	26	-20	-17
21.5	-45	28	-17	-15
22.5	-44	30	-14	-12
23.5	-43	33	-12	-10
24.5	-41	36	-10	-8
25.5	-40	39	-7	-5
26.5	-38	41	-5	-3
27.5	-36	44	-2	-1
28.5	-35	47	0	2
29.5	-34	51	2	4
30.5	-32	54	5	7
31.5	-29	57	7	9
32.5	-28	59	9	11
33.5	-26	62	12	14
34.5	-24	65	14	16
35.5	-22	69	16	18
36.5	-21	71	19	21
37.5	-19	74	21	23
38.5	-17	77	23	25
39.5	-16	81	26	28

40.5	-14	84	28	30
41.5	-11	87	31	32
42.5	-10	90	33	35
43.5	-8	93	36	37
44.5	-6	97	38	40
45.5	-4	99	40	42
46.5	-2	101	43	45
47.5	0	103	45	47
48.5	2	106	47	49
49.5	3	109	50	52
50.5	5	112	52	54
51.5	8	115	54	56
52.5	10	118	57	59
53.5	11	120	59	61
54.5	13	124	62	64
55.5	15	127	64	66
56.5	18	129	67	68
57.5	20	131	70	71
58.5	22	134	72	73
59.5	23	137	74	76
60.5	25	140	77	78
61.5	27	143	79	81
62.5	30	146	82	83
63.5	32	148	84	85
64.5	34	151	87	88
65.5	36	153	89	90
66.5	39	155	91	93
67.5	41	157	94	95
68.5	43	160	96	97
69.5	45	163	99	100
70.5	47	166	101	102
71.5	49	167	104	105
72.5	51	170	106	107
73.5	53	173	109	109
74.5	55	175	111	112
75.5	57	178	113	114
76.5	59	180	116	116
77.5	61	183	118	119
78.5	63	185	121	121
79.5	65	188	123	124
80.5	67	191	125	126
81.5	69	193	128	128
82.5	71	195	130	131
83.5	73	197	133	133
84.5	74	200	135	136
85.5	76	203	138	138
86.5	79	205	140	140
87.5	81	207	142	143
88.5	84	210	145	145
89.5	86	213	147	147
90.5	88	216	149	150
91.5	91	218	152	152
92.5	94	220	155	155
93.5	96	223	157	157
94.5	98	226	159	159
95.5	100	228	161	162
96.5	102	231	164	164
97.5	104	232	166	167
98.5	105	234	169	169
99.5	107	237	171	171
100.5	110	240	173	174
101.5	112	241	176	176

102.5	115	244	179	178
103.5	117	246	181	181
104.5	119	249	184	183
105.5	121	252	186	186
106.5	124	253	188	188
107.5	126	256	190	191
108.5	128	258	193	193
109.5	130	261	195	195
110.5	133	263	197	198
111.5	135	264	200	200
112.5	138	267	202	202
113.5	140	269	204	205
114.5	143	272	207	207
115.5	145	275	209	209
116.5	148	277	211	212
117.5	150	279	214	214
118.5	152	281	216	216
119.5	155	284	218	219
120.5	157	286	221	221
121.5	160	288	223	223
122.5	162	290	226	226
123.5	165	293	228	228
124.5	166	295	231	231
125.5	169	297	233	233
126.5	171	299	236	235
127.5	173	301	238	238
128.5	175	303	240	240
129.5	177	305	243	242
130.5	180	307	245	245
131.5	183	310	247	247
132.5	186	311	250	250
133.5	188	314	252	252
134.5	190	317	255	254
135.5	193	319	257	257
136.5	196	321	259	259
137.5	198	323	262	261
138.5	200	326	264	264
139.5	202	329	266	266
140.5	204	331	269	268
141.5	206	333	271	271
142.5	208	335	274	273
143.5	210	337	276	275
144.5	213	339	278	278
145.5	215	341	281	280
146.5	219	343	283	283
147.5	222	345	286	285
148.5	224	347	288	287
149.5	226	349	290	290
150.5	228	352	293	292
151.5	231	354	295	294
152.5	233	356	297	297
153.5	235	358	300	299
154.5	238	361	302	302
155.5	241	363	305	304
156.5	243	365	307	306
157.5	246	367	310	309
158.5	248	369	312	311
159.5	250	371	315	314
160.5	253	373	317	316
161.5	255	375	320	319
162.5	258	377	322	321
163.5	261	378	324	323

164.5	263	381	327	326
165.5	266	383	329	328
166.5	269	385	332	330
167.5	271	387	334	333
168.5	273	388	336	335
169.5	275	391	339	337
170.5	278	393	341	340
171.5	281	395	344	342
172.5	283	396	346	345
173.5	285	399	349	347
174.5	287	402	351	349
175.5	290	404	353	352
176.5	293	406	356	354
177.5	296	408	358	356
178.5	298	410	361	359
179.5	301	412	363	361
180.5	304	414	365	363
181.5	308	416	368	366
182.5	311	418	370	368
183.5	314	420	372	371
184.5	316	423	375	373
185.5	318	425	377	376
186.5	322	426	380	378
187.5	324	428	382	380
188.5	327	430	384	383
189.5	329	432	387	385
190.5	332	434	389	388
191.5	336	436	392	390
192.5	339	437	394	392
193.5	342	439	396	395
194.5	344	441	399	397
195.5	347	442	401	400
196.5	350	444	404	402
197.5	353	446	406	404
198.5	356	448	409	407
199.5	358	450	411	409
200.5	360	452	413	412
201.5	363	453	416	414
202.5	366	455	418	416
203.5	369	457	420	419
204.5	372	459	422	421
205.5	375	460	425	423
206.5	379	462	427	426
207.5	381	463	429	428
208.5	384	465	432	431
209.5	385	467	434	433
210.5	389	469	437	436
211.5	393	470	439	438
212.5	396	471	441	441
213.5	399	473	444	443
214.5	401	475	447	446
215.5	405	480	450	449
216.5	409	489	455	454
217.5	414	498	459	459
218.5	416	511	464	464
219.5	420	524	467	468
220.5	423	533	472	473
221.5	427	539	476	478
222.5	430	546	481	483
223.5	433	555	485	488
224.5	436	566	489	493
225.5	439	575	494	498

226.5	442	580	499	502
227.5	445	586	503	507
228.5	448	593	508	512
229.5	451	600	512	517
230.5	454	606	517	521
231.5	458	611	522	526
232.5	462	616	527	531
233.5	465	624	532	535
234.5	468	631	536	540
235.5	472	638	541	545
236.5	476	644	546	550
237.5	480	650	550	554
238.5	483	658	555	559
239.5	485	664	559	564
240.5	489	670	564	568
241.5	493	676	569	573
242.5	495	682	574	578
243.5	498	691	579	583
244.5	500	699	583	588
245.5	504	705	588	592
246.5	508	709	592	597
247.5	513	715	597	602
248.5	515	721	602	606
249.5	518	727	607	611
250.5	522	733	611	615
251.5	526	738	615	620
252.5	529	745	620	625
253.5	533	752	625	630
254.5	536	759	629	634
255.5	540	765	634	639
256.5	545	770	639	644
257.5	548	775	643	648
258.5	552	783	648	653
259.5	555	790	652	658
260.5	560	797	657	662
261.5	563	802	661	667
262.5	566	806	666	672
263.5	568	810	671	676
264.5	571	816	675	681
265.5	575	822	680	685
266.5	579	827	685	690
267.5	584	834	690	695
268.5	587	840	694	699
269.5	591	847	699	704
270.5	596	853	704	709
271.5	601	858	708	713
272.5	603	862	712	718
273.5	607	867	717	723
274.5	610	875	722	727
275.5	614	881	726	732
276.5	619	887	731	737
277.5	623	892	736	742
278.5	626	899	740	746
279.5	630	905	746	751
280.5	633	910	750	756
281.5	638	916	755	761
282.5	641	921	760	765
283.5	645	926	765	770
284.5	649	932	769	775
285.5	653	937	774	780
286.5	657	942	779	785
287.5	662	948	784	789

288.5	665	954	788	794
289.5	668	961	793	799
290.5	672	967	798	804
291.5	677	971	803	808
292.5	682	975	808	813
293.5	686	981	812	818
294.5	690	986	817	822
295.5	695	992	821	827
296.5	699	998	826	832
297.5	703	1003	831	836
298.5	706	1008	835	841
299.5	710	1014	840	845
300.5	713	1019	844	850
301.5	717	1023	848	855
302.5	721	1028	853	859
303.5	724	1033	858	864
304.5	727	1039	863	869
305.5	731	1045	868	873
306.5	736	1050	873	878
307.5	739	1053	877	883
308.5	743	1059	882	888
309.5	747	1066	886	892
310.5	751	1071	891	897
311.5	755	1076	896	902
312.5	757	1083	901	906
313.5	760	1089	905	911
314.5	763	1096	910	916
315.5	767	1101	915	921
316.5	772	1107	919	925
317.5	775	1112	924	930
318.5	778	1116	929	935
319.5	782	1121	933	940
320.5	786	1126	938	944
321.5	792	1131	942	949
322.5	797	1134	947	954
323.5	800	1140	952	959
324.5	804	1146	957	963
325.5	808	1152	961	968
326.5	812	1158	966	973
327.5	816	1164	971	977
328.5	820	1170	976	982
329.5	824	1177	981	987
330.5	828	1182	987	992
331.5	833	1186	991	996
332.5	838	1190	996	1001
333.5	841	1195	1000	1006
334.5	844	1202	1005	1011
335.5	848	1208	1010	1015
336.5	853	1212	1015	1020
337.5	858	1217	1019	1025
338.5	861	1224	1025	1029
339.5	864	1231	1029	1034
340.5	868	1236	1034	1039
341.5	873	1240	1039	1043
342.5	877	1246	1043	1048
343.5	880	1251	1048	1053
344.5	883	1258	1053	1057
345.5	886	1264	1057	1062
346.5	891	1269	1062	1067
347.5	896	1273	1067	1072
348.5	899	1279	1072	1076
349.5	903	1285	1077	1081

350.5	908	1289	1081	1086
351.5	911	1293	1086	1091
352.5	915	1301	1091	1095
353.5	918	1309	1095	1100
354.5	921	1315	1100	1105
355.5	927	1319	1104	1110
356.5	932	1324	1109	1114
357.5	935	1327	1114	1119
358.5	937	1333	1119	1124
359.5	942	1339	1124	1129
360.5	945	1346	1128	1133
361.5	950	1351	1133	1138
362.5	953	1356	1138	1143
363.5	956	1360	1142	1148
364.5	960	1368	1147	1152
365.5	964	1374	1152	1157
366.5	968	1377	1156	1162
367.5	974	1383	1161	1166
368.5	979	1388	1166	1171
369.5	983	1394	1171	1176
370.5	987	1400	1175	1181
371.5	993	1404	1180	1185
372.5	998	1410	1185	1190
373.5	1003	1417	1190	1195
374.5	1006	1422	1195	1199
375.5	1010	1427	1199	1204
376.5	1016	1431	1204	1209
377.5	1018	1436	1209	1214
378.5	1022	1441	1213	1218
379.5	1028	1447	1218	1223
380.5	1032	1454	1223	1228
381.5	1037	1457	1228	1233
382.5	1041	1461	1233	1237
383.5	1044	1466	1237	1242
384.5	1047	1471	1241	1246
385.5	1051	1477	1246	1251
386.5	1056	1482	1251	1256
387.5	1060	1487	1256	1261
388.5	1064	1494	1261	1266
389.5	1067	1500	1266	1271
390.5	1072	1506	1271	1276
391.5	1076	1514	1276	1280
392.5	1080	1520	1281	1285
393.5	1084	1526	1286	1290
394.5	1087	1532	1290	1295
395.5	1091	1537	1295	1300
396.5	1096	1541	1300	1305
397.5	1100	1545	1305	1309
398.5	1105	1551	1311	1314
399.5	1109	1556	1315	1319
400.5	1112	1562	1320	1324
401.5	1117	1568	1325	1328
402.5	1121	1573	1330	1333
403.5	1125	1579	1335	1338
404.5	1129	1584	1339	1343
405.5	1134	1589	1344	1348
406.5	1138	1594	1348	1352
407.5	1143	1598	1353	1357
408.5	1146	1603	1358	1361
409.5	1150	1608	1362	1366
410.5	1154	1612	1367	1371
411.5	1158	1616	1371	1375

412.5	1165	1620	1375	1380
413.5	1169	1627	1380	1385
414.5	1173	1632	1384	1390
415.5	1177	1639	1389	1394
416.5	1181	1643	1394	1399
417.5	1185	1649	1398	1404
418.5	1188	1654	1402	1409
419.5	1191	1658	1407	1414
420.5	1195	1666	1413	1418
421.5	1200	1670	1418	1423
422.5	1205	1674	1422	1428
423.5	1208	1680	1426	1432
424.5	1212	1683	1431	1437
425.5	1217	1688	1436	1442
426.5	1221	1692	1441	1447
427.5	1227	1698	1446	1451
428.5	1230	1702	1451	1456
429.5	1233	1708	1456	1461
430.5	1237	1713	1462	1466
431.5	1242	1717	1466	1470
432.5	1246	1721	1471	1475
433.5	1249	1727	1475	1480
434.5	1254	1734	1480	1484
435.5	1259	1740	1485	1489
436.5	1263	1746	1489	1494
437.5	1266	1751	1494	1498
438.5	1270	1756	1498	1503
439.5	1275	1763	1502	1508
440.5	1279	1769	1508	1513
441.5	1285	1773	1513	1517
442.5	1289	1777	1518	1522
443.5	1293	1783	1522	1527
444.5	1298	1788	1527	1531
445.5	1303	1794	1531	1536
446.5	1308	1798	1536	1541
447.5	1314	1802	1541	1546
448.5	1318	1808	1545	1550
449.5	1322	1814	1550	1555
450.5	1326	1820	1554	1560
451.5	1331	1826	1559	1564
452.5	1335	1829	1564	1569
453.5	1340	1832	1568	1574
454.5	1344	1837	1573	1578
455.5	1347	1842	1578	1583
456.5	1353	1846	1583	1588
457.5	1357	1851	1588	1593
458.5	1360	1856	1594	1597
459.5	1365	1861	1599	1602
460.5	1369	1865	1603	1607
461.5	1375	1869	1608	1611
462.5	1379	1874	1612	1616
463.5	1384	1879	1618	1621
464.5	1387	1884	1622	1626
465.5	1392	1889	1628	1630
466.5	1398	1896	1632	1635
467.5	1403	1900	1637	1640
468.5	1408	1905	1642	1645
469.5	1413	1912	1646	1650
470.5	1416	1918	1652	1654
471.5	1421	1924	1656	1659
472.5	1425	1929	1660	1664
473.5	1430	1935	1665	1669

474.5	1433	1940	1670	1674
475.5	1437	1946	1674	1678
476.5	1442	1950	1679	1683
477.5	1446	1954	1684	1687
478.5	1450	1960	1689	1692
479.5	1453	1965	1694	1697
480.5	1457	1969	1698	1701
481.5	1462	1974	1703	1706
482.5	1466	1978	1708	1711
483.5	1470	1981	1713	1716
484.5	1474	1986	1717	1720
485.5	1480	1991	1722	1725
486.5	1484	1996	1726	1730
487.5	1489	2001	1731	1734
488.5	1492	2006	1736	1739
489.5	1495	2011	1741	1744
490.5	1500	2017	1746	1748
491.5	1506	2022	1751	1753
492.5	1511	2029	1755	1758
493.5	1514	2035	1760	1763
494.5	1517	2039	1764	1767
495.5	1522	2044	1768	1772
496.5	1526	2049	1773	1777
497.5	1531	2054	1777	1782
498.5	1536	2058	1782	1786
499.5	1540	2062	1787	1791
500.5	1544	2067	1792	1796
501.5	1548	2071	1796	1800
502.5	1552	2077	1801	1805
503.5	1556	2083	1806	1809
504.5	1559	2088	1810	1814
505.5	1563	2092	1815	1818
506.5	1568	2097	1820	1823
507.5	1574	2102	1825	1828
508.5	1579	2108	1830	1832
509.5	1584	2114	1835	1837
510.5	1589	2119	1839	1842
511.5	1592	2124	1844	1846
512.5	1596	2129	1848	1851
513.5	1601	2134	1852	1856
514.5	1604	2141	1857	1860
515.5	1607	2148	1861	1865
516.5	1612	2151	1866	1870
517.5	1618	2154	1871	1875
518.5	1621	2161	1876	1880
519.5	1625	2165	1881	1884
520.5	1629	2171	1886	1889
521.5	1634	2173	1891	1894
522.5	1639	2178	1895	1898
523.5	1643	2183	1900	1903
524.5	1645	2189	1903	1908
525.5	1650	2195	1908	1912
526.5	1654	2200	1912	1917
527.5	1658	2205	1917	1921
528.5	1663	2209	1921	1926
529.5	1665	2213	1927	1931
530.5	1670	2217	1932	1935
531.5	1674	2222	1937	1940
532.5	1679	2226	1942	1945
533.5	1682	2232	1946	1949
534.5	1687	2237	1950	1954
535.5	1692	2242	1956	1958

536.5	1695	2249	1960	1963
537.5	1699	2255	1965	1968
538.5	1703	2262	1969	1973
539.5	1707	2266	1974	1977
540.5	1712	2271	1979	1982
541.5	1718	2276	1985	1987
542.5	1724	2280	1990	1992
543.5	1730	2285	1995	1997
544.5	1734	2290	2000	2002
545.5	1738	2295	2005	2006
546.5	1743	2299	2009	2011
547.5	1749	2303	2014	2016
548.5	1752	2309	2018	2021
549.5	1757	2315	2023	2025
550.5	1762	2319	2028	2030
551.5	1767	2323	2033	2035
552.5	1771	2327	2038	2040
553.5	1774	2333	2042	2044
554.5	1779	2337	2046	2049
555.5	1783	2343	2051	2054
556.5	1788	2349	2055	2058
557.5	1794	2353	2060	2063
558.5	1799	2356	2064	2068
559.5	1803	2360	2069	2072
560.5	1808	2364	2074	2077
561.5	1814	2368	2079	2082
562.5	1819	2372	2084	2087
563.5	1825	2376	2089	2091
564.5	1826	2381	2094	2096
565.5	1832	2388	2098	2101
566.5	1837	2392	2103	2105
567.5	1840	2398	2107	2110
568.5	1843	2403	2112	2115
569.5	1847	2408	2117	2119
570.5	1851	2412	2121	2124
571.5	1857	2414	2126	2129
572.5	1862	2421	2131	2133
573.5	1865	2426	2135	2138
574.5	1872	2431	2140	2143
575.5	1876	2437	2144	2148
576.5	1880	2439	2150	2152
577.5	1885	2446	2154	2157
578.5	1887	2450	2159	2162
579.5	1894	2454	2163	2166
580.5	1897	2459	2168	2171
581.5	1900	2464	2172	2176
582.5	1904	2468	2177	2181
583.5	1908	2472	2183	2185
584.5	1912	2479	2187	2190
585.5	1916	2484	2192	2195
586.5	1921	2487	2196	2200
587.5	1925	2489	2200	2204
588.5	1930	2495	2205	2209
589.5	1934	2499	2210	2214
590.5	1938	2504	2214	2218
591.5	1942	2509	2219	2223
592.5	1946	2513	2223	2228
593.5	1952	2519	2228	2232
594.5	1956	2526	2233	2237
595.5	1960	2530	2238	2241
596.5	1964	2533	2243	2246
597.5	1970	2538	2249	2251

598.5	1974	2545	2253	2256
599.5	1979	2552	2258	2260
600.5	1984	2556	2263	2265
601.5	1991	2561	2268	2270
602.5	1994	2566	2272	2275
603.5	1999	2570	2276	2279
604.5	2003	2578	2281	2284
605.5	2007	2584	2286	2289
606.5	2013	2589	2291	2294
607.5	2016	2595	2296	2299
608.5	2020	2599	2301	2303
609.5	2024	2603	2306	2308
610.5	2028	2608	2310	2313
611.5	2034	2612	2315	2318
612.5	2038	2616	2320	2322
613.5	2044	2620	2325	2327
614.5	2049	2624	2330	2332
615.5	2053	2629	2334	2337
616.5	2056	2634	2338	2341
617.5	2060	2638	2344	2346
618.5	2066	2641	2348	2351
619.5	2072	2645	2353	2355
620.5	2075	2649	2358	2360
621.5	2079	2654	2362	2365
622.5	2085	2659	2367	2369
623.5	2092	2665	2371	2374
624.5	2097	2670	2375	2379
625.5	2102	2674	2380	2384
626.5	2106	2679	2385	2388
627.5	2110	2684	2390	2393
628.5	2114	2690	2394	2398
629.5	2118	2695	2399	2402
630.5	2123	2700	2403	2407
631.5	2127	2703	2408	2412
632.5	2132	2710	2413	2417
633.5	2138	2715	2418	2421
634.5	2141	2721	2423	2426
635.5	2146	2727	2428	2431
636.5	2149	2730	2433	2436
637.5	2155	2735	2438	2440
638.5	2158	2740	2443	2445
639.5	2162	2745	2447	2450
640.5	2167	2749	2452	2455
641.5	2172	2753	2455	2459
642.5	2176	2759	2460	2464
643.5	2181	2765	2465	2469
644.5	2187	2770	2470	2473
645.5	2192	2776	2474	2478
646.5	2195	2781	2478	2483
647.5	2200	2787	2483	2487
648.5	2206	2793	2488	2492
649.5	2209	2797	2492	2497
650.5	2214	2802	2498	2502
651.5	2219	2805	2504	2506
652.5	2225	2811	2509	2511
653.5	2229	2817	2514	2516
654.5	2233	2826	2519	2521
655.5	2237	2830	2524	2525
656.5	2242	2834	2529	2530
657.5	2248	2837	2533	2534
658.5	2251	2840	2537	2539
659.5	2254	2846	2540	2543

660.5	2259	2850	2545	2548
661.5	2264	2856	2550	2553
662.5	2270	2862	2555	2558
663.5	2276	2869	2560	2563
664.5	2282	2875	2565	2567
665.5	2287	2879	2569	2572
666.5	2291	2883	2573	2577
667.5	2297	2889	2578	2582
668.5	2302	2894	2582	2586
669.5	2307	2899	2587	2591
670.5	2312	2902	2591	2596
671.5	2317	2906	2596	2601
672.5	2322	2910	2600	2605
673.5	2326	2914	2606	2610
674.5	2330	2920	2610	2615
675.5	2334	2924	2615	2619
676.5	2340	2928	2619	2624
677.5	2343	2932	2623	2629
678.5	2348	2938	2628	2633
679.5	2354	2943	2633	2638
680.5	2359	2949	2638	2643
681.5	2364	2953	2642	2648
682.5	2369	2957	2647	2652
683.5	2374	2962	2652	2657
684.5	2378	2967	2657	2661
685.5	2383	2971	2661	2666
686.5	2388	2976	2666	2671
687.5	2396	2980	2671	2675
688.5	2401	2987	2676	2680
689.5	2405	2992	2681	2685
690.5	2410	2997	2685	2689
691.5	2414	3000	2691	2694
692.5	2418	3006	2696	2699
693.5	2421	3011	2700	2703
694.5	2424	3016	2704	2708
695.5	2428	3020	2709	2712
696.5	2434	3026	2714	2717
697.5	2440	3031	2718	2722
698.5	2444	3034	2722	2727
699.5	2449	3039	2727	2731
700.5	2454	3044	2732	2736
701.5	2459	3050	2736	2741
702.5	2464	3055	2741	2745
703.5	2468	3061	2746	2750
704.5	2472	3065	2750	2755
705.5	2476	3070	2755	2760
706.5	2481	3077	2760	2765
707.5	2487	3083	2765	2769
708.5	2492	3088	2770	2774
709.5	2495	3092	2774	2779
710.5	2500	3096	2779	2784
711.5	2505	3099	2786	2789
712.5	2511	3104	2790	2793
713.5	2517	3112	2795	2798
714.5	2521	3120	2799	2803
715.5	2526	3126	2805	2807
716.5	2532	3133	2809	2812
717.5	2538	3141	2814	2817
718.5	2543	3145	2818	2822
719.5	2548	3151	2824	2827
720.5	2553	3155	2829	2831
721.5	2557	3163	2834	2836

722.5	2563	3165	2838	2841
723.5	2568	3169	2843	2846
724.5	2572	3174	2847	2850
725.5	2576	3180	2851	2855
726.5	2582	3187	2856	2860
727.5	2587	3194	2862	2865
728.5	2591	3201	2867	2869
729.5	2597	3207	2872	2874
730.5	2602	3211	2877	2879
731.5	2608	3216	2882	2884
732.5	2613	3221	2886	2889
733.5	2618	3226	2891	2893
734.5	2623	3233	2895	2898
735.5	2628	3241	2899	2903
736.5	2634	3253	2903	2908
737.5	2640	3260	2907	2912
738.5	2646	3269	2912	2917
739.5	2652	3276	2917	2922
740.5	2657	3281	2921	2927
741.5	2664	3288	2925	2932
742.5	2672	3295	2930	2937
743.5	2677	3302	2935	2943
744.5	2682	3310	2941	2948
745.5	2699	3323	2960	2968
746.5	2717	3343	2995	3002
747.5	2728	3383	3036	3037
748.5	2738	3449	3077	3072
749.5	2747	3526	3109	3106
750.5	2770	3588	3149	3142
751.5	2798	3629	3183	3179
752.5	2820	3685	3215	3217
753.5	2837	3742	3249	3254
754.5	2853	3803	3278	3291
755.5	2883	3858	3314	3327
756.5	2913	3893	3352	3363
757.5	2936	3939	3387	3399
758.5	2962	3995	3418	3435
759.5	2980	4054	3454	3470
760.5	3005	4098	3489	3506
761.5	3036	4129	3527	3543
762.5	3068	4167	3566	3579
763.5	3088	4228	3603	3615
764.5	3110	4284	3639	3652
765.5	3142	4329	3673	3688
766.5	3177	4371	3710	3725
767.5	3208	4411	3748	3762
768.5	3235	4458	3784	3799
769.5	3259	4516	3819	3836
770.5	3288	4569	3856	3873
771.5	3325	4598	3893	3909
772.5	3355	4644	3930	3946
773.5	3383	4685	3968	3982
774.5	3413	4738	4004	4019
775.5	3439	4775	4043	4056
776.5	3479	4809	4083	4095
777.5	3509	4844	4120	4134
778.5	3533	4882	4159	4173
779.5	3559	4928	4195	4212
780.5	3593	4974	4231	4249
781.5	3631	5011	4271	4285
782.5	3659	5052	4306	4322
783.5	3692	5094	4343	4358

784.5	3726	5146	4382	4394
785.5	3757	5188	4416	4431
786.5	3792	5223	4453	4467
787.5	3820	5263	4486	4503
788.5	3851	5300	4523	4539
789.5	3874	5339	4561	4575
790.5	3902	5382	4598	4612
791.5	3945	5424	4633	4648
792.5	3980	5465	4669	4684
793.5	4013	5518	4702	4721
794.5	4046	5554	4739	4757
795.5	4079	5599	4778	4795
796.5	4124	5635	4821	4834
797.5	4157	5675	4859	4873
798.5	4193	5721	4895	4912
799.5	4225	5769	4934	4951
800.5	4265	5808	4972	4988
801.5	4298	5841	5007	5023
802.5	4325	5871	5040	5059
803.5	4359	5911	5075	5094
804.5	4379	5953	5109	5130
805.5	4408	5985	5144	5166
806.5	4450	6018	5183	5203
807.5	4482	6057	5219	5239
808.5	4512	6096	5257	5276
809.5	4537	6144	5298	5313
810.5	4576	6183	5337	5352
811.5	4625	6202	5382	5392
812.5	4655	6230	5425	5432
813.5	4691	6263	5467	5472
814.5	4714	6308	5508	5512
815.5	4758	6349	5548	5549
816.5	4793	6380	5581	5584
817.5	4828	6407	5617	5619
818.5	4863	6441	5652	5654
819.5	4884	6472	5684	5689
820.5	4918	6511	5719	5724
821.5	4963	6537	5756	5760
822.5	4997	6563	5793	5797
823.5	5035	6603	5832	5833
824.5	5076	6646	5872	5869
825.5	5110	6678	5908	5905
826.5	5141	6709	5944	5940
827.5	5175	6747	5980	5975
828.5	5205	6792	6015	6010
829.5	5235	6839	6049	6045
830.5	5265	6878	6084	6080
831.5	5309	6903	6123	6117
832.5	5344	6929	6160	6154
833.5	5373	6961	6197	6191
834.5	5405	6996	6235	6227
835.5	5448	7025	6272	6265
836.5	5515	7053	6308	6303
837.5	5560	7080	6347	6341
838.5	5602	7113	6386	6379
839.5	5632	7147	6423	6417
840.5	5678	7177	6457	6454
841.5	5734	7212	6497	6491
842.5	5781	7247	6537	6529
843.5	5824	7290	6575	6566
844.5	5850	7330	6610	6603
845.5	5887	7366	6646	6641

846.5	5930	7389	6686	6678
847.5	5971	7410	6725	6716
848.5	6012	7429	6765	6753
849.5	6042	7465	6803	6791
850.5	6084	7499	6839	6828
851.5	6123	7524	6875	6865
852.5	6163	7548	6913	6903
853.5	6195	7580	6952	6940
854.5	6225	7618	6990	6977
855.5	6274	7644	7029	7015
856.5	6322	7664	7066	7052
857.5	6362	7690	7103	7090
858.5	6408	7721	7142	7128
859.5	6442	7762	7184	7165
860.5	6478	7801	7221	7202
861.5	6527	7823	7257	7238
862.5	6579	7851	7295	7274
863.5	6624	7877	7332	7310
864.5	6658	7910	7369	7347
865.5	6703	7934	7405	7383
866.5	6748	7952	7443	7421
867.5	6781	7974	7482	7458
868.5	6815	8005	7521	7495
869.5	6845	8037	7560	7533
870.5	6906	8070	7596	7570
871.5	6972	8084	7635	7608
872.5	7035	8109	7673	7646
873.5	7089	8137	7712	7684
874.5	7126	8170	7749	7722
875.5	7159	8200	7785	7757
876.5	7204	8214	7818	7791
877.5	7248	8235	7853	7825
878.5	7290	8259	7887	7858
879.5	7317	8291	7921	7892
880.5	7365	8311	7957	7927
881.5	7421	8326	7995	7963
882.5	7470	8340	8032	8000
883.5	7522	8358	8070	8036
884.5	7549	8384	8109	8073
885.5	7622	8405	8146	8111
886.5	7723	8416	8179	8150
887.5	7808	8428	8215	8189
888.5	7880	8445	8254	8228
889.5	7926	8466	8295	8267
890.5	8003	8488	8331	8305
891.5	8101	8496	8360	8342
892.5	8203	8506	8389	8379
893.5	8300	8520	8418	8416
894.5	8388	8539	8449	8452
895.5	8424	8560	8470	8476
896.5	8432	8574	8481	8487